

DESIGN OF POLYMER ARCHITECTURES FOR CATALYSIS

A Dissertation
Presented to
The Academic Faculty

by

Caroline B. Hoyt

In Partial Fulfillment
of the Requirements for the Degree
Doctor in Philosophy in the
School of Chemistry and Biochemistry

Georgia Institute of Technology
December 2017

COPYRIGHT © 2017 BY CAROLINE B. HOYT

DESIGN OF POLYMER ARCHITECTURES FOR CATALYSIS

Approved by:

Dr. Christopher W. Jones, Advisor
School of Chemical & Biomolecular
Engineering
Georgia Institute of Technology

Dr. Stefan France
School of Chemistry and Biochemistry
Georgia Institute of Technology

Dr. David Bucknall
School of Materials Science and
Engineering
Georgia Institute of Technology

Dr. Joseph Sadighi
School of Chemistry and Biochemistry
Georgia Institute of Technology

Dr. David Collard
School of Chemistry and Biochemistry
Georgia Institute of Technology

Date Approved: November 6, 2017

To My Family

ACKNOWLEDGEMENTS

I never thought I would be in graduate school, especially completing my Ph.D. in Chemistry at a place like Georgia Tech. I finished my B.S. in Chemistry from University of Florida, and I was prepared to go and find “a job.” I attribute my path to graduate school to my mentor, Dr. Pete Silks, who gave me a shot (lucky break #1) at Los Alamos National Laboratory and the wonderful people I worked with: Dr. Dave Kimball, Marvin Shorty, Marc Alvarez, and Dr. Ruilian Wu. From there, I realized I wanted to pursue a job where I could apply my chemistry knowledge to impactful problems, and I landed at Georgia Tech (lucky break #2).

My “graduate school experience” has been a truly humbling five-and-a-half-year path of intellectual and personal growth. I know I will forget so many people that have helped me along the way, and my words will not be able to express how incredibly grateful and thankful I am for every single person, so I will keep it short:

My adviser Dr. Jones (whom it took 3+ years to finally call “Chris”)

My committee members- Dr. Collard, Dr. France, Dr. Bucknall, Dr. Sadighi

The Jones Group (both past and present)- especially Li-Chen Lee, Simon Pang, Miles Sakwa-Novak, and Chunjae Yoo

My collaborators- Aaron Cohen, the Weck group at NYU and Dr. Marcus Weck

My roommate and close friends- Lucy Barksdale, Lucia Constantine, J.T. Wynn, Antonio Charvarria

My Georgia Tech sanity- Erin Gawron, Alex Hyla, and Abraham Jordan

My boyfriend and complete calm at home- Jeff Anderson (and compadre Homer)

And last but absolutely not least, my family

Thank you from the bottom of my heart!

TABLE OF CONTENTS

ACKNOWLEDGEMENTS	iv
LIST OF TABLES	x
LIST OF FIGURES	xii
LIST OF SYMBOLS AND ABBREVIATIONS	xvii
SUMMARY	xxii
CHAPTER 1: INTRODUCTION TO POLYMER STRUCTURES AND APPLICATIONS IN CATALYSIS	1
1.1 Introduction and Motivation	1
1.2 Linear polymer catalysts	3
1.2.1 Cooperative catalysis with heterogeneous supports	5
1.2.2 Hydroboration chemistry with homogeneous catalysts	8
1.2.3 Hydroboration chemistry with heterogeneous supports	9
1.3 Polymer brush catalysts	10
1.3.1 Cascade Catalysis	11
1.4 Polymer micelle catalysts	13
1.5 Micellar applications	14
1.6 Outlook	15
CHAPTER 2: ACID-BASE COOPERATIVE CATALYSIS USING LINEAR POLYMER SUPPORTS	16
2.1 Background	16
2.2 Experiments	18
2.2.1 General Aldol Condensation procedure	18
2.3 Materials Synthesis	19
2.3.1 Boc-deprotection for copolymer catalysts	20
2.3.2 Phthalimide deprotection of copolymer catalysts	20
2.3.3 Porous Organic Polymer Synthesis	20
2.4 Materials Characterization	21
2.5 Results and Discussion	25
2.5.1 Homogeneous Catalytic Pairs	25
2.5.2 Catalyst Loading and Characterization	30
2.5.3 Solvent effects on catalyst activity	33
2.5.4 Catalyst Architecture effects on reactivity	36
2.5.4.1 Random sequence polymer catalyst structure effects	36
2.5.4.2 Block sequence polymer catalyst structure effects	39
2.5.4.3 Overall catalyst structure effects	40
2.5.4.3.1 Porous Organic Polymers	40

2.6 Conclusions	41
CHAPTER 3: HYDROBORATION OF SUBSTITUTED ALKYNES USING A SOLID POLYMERIC CARBOXYLIC ACID CATALYST	43
3.1 Introduction	43
3.2 Experiments	45
3.2.1 Nuclear Magnetic Resonance studies of intermediates	45
3.2.1.1 Benzoic acid and pinacolborane	45
3.2.1.2 Poly(vinylbenzoic acid) and pinacolborane	46
3.2.1.3 Benzoic anhydride and pinacolborane	47
3.2.2 Experimental Reaction Order Determination using poly(vba) (Initial Rates Method)	48
3.2.3 Kinetic Isotope Effect Determination for the Hydroboration of Phenylacetylene and Phenylacetylene-d using poly(vba) (2 separate vessels)	50
3.2.4 Determination of Initial Rate of the Hydroboration of 1- ethynylcyclohexene with HBPIn in octane at 30 °C (up to 15 % yield)	52
3.2.5 Testing of alternative catalysts for the hydroboration of Phenylacetylene with HBPIn	52
3.2.6 General hydroboration procedure for alkyne substituent effects	53
3.2.6.1 Crude product NMR Shifts of substituted alkyne hydroboration	55
3.3 Materials Synthesis	60
3.3.1 Poly(vinylbenzoic acid) synthesis	60
3.4 Materials Characterization	61
3.4.1 Recycle Poly(vba) catalyst	62
3.5 Polymer catalyst optimization	63
3.6 Mechanistic studies of the the hydroboration of phenylacetylene with pinacolborane	65
3.6.1 NMR studies of intermediate species	67
3.6.2 Determination of Kinetic Isotop Effects	69
3.6.3 Determination of Reaction Orders through Methods of Initial Rates	71
3.7 Substituent scope of hydroboration of substituted alkynes with pinacolborane	78
3.8 Recycle studies of poly(vba)	79
3.9 Conclusions	80
CHAPTER 4: HYBRID PYRROLIDINE POLYMER BRUSH ON SILICA-SUPPORTED SULFONIC ACID MATERIAL AND ITS APPLICATION IN CASCADE CATALYSIS	81
4.1 Introduction	81
4.2 Experiments	83
4.2.1 Synthesis of co-condensed MCM-SH-CTAB	83
4.2.2 Thiol oxidation of MCM-SH-CTAB support	84

4.2.3 RAFT chain transfer agent silane synthesis	84
4.2.4 Synthesis of (S)-((1-Tert-Butoxycarbonyl)Pyrrolidin-2-yl)Methyl Acrylamide	85
4.2.4.1 (S)-2-Pyrrolidinemethanol (2)	85
4.2.4.2 (S)-1-(<i>Tert</i> -butoxycarbonyl)-2-pyrrolidinemethanol (3)	86
4.2.4.3 (S)-2-[(4-Toluenesulfonyloxy)methyl]pyrrolidine-1-carboxylic acid <i>tert</i> -butyl ester (4)	86
4.2.4.4 (S)-2-(Azidomethyl)pyrrolidine-1-carboxylic acid <i>tert</i> -butyl ester (5)	87
4.2.4.5 (S)-1-(<i>Tert</i> -butoxycarbonyl)-2-aminomethylpyrrolidine (6)	87
4.2.4.6 (S)-((1-(<i>Tert</i> -butoxycarbonyl)pyrrolidin-2-yl)methyl) Acrylamide (7)	88
4.2.5 Poly(boc-pyrrolidine acrylamide) polymer chain synthesis	88
4.2.6 General grafting procedure	89
4.2.7 General 2-step cascade reaction procedure	89
4.2.8 Optimization of acid-catalyzed deacetalization	90
4.2.9 Optimization of base-catalyzed Knoevenagel and Michael addition	90
4.3 Materials Characterization	91
4.4 Results and Discussion	94
4.4.1 Design of acid-base polymer brush catalyst	94
4.4.2 Catalyst structure effects on Acid-Base cascade reaction	101
4.5 Conclusions	104
 CHAPTER 5: C(SP³)-H MONOARYLATION CATALYZED BY A COVALENTLY CROSS-LINKED REVERSE MICELLE-SUPPORTED PALLADIUM CATALYST	 105
5.1 Background	105
5.2 Experiments	108
5.2.1 General preparation of cross-linked micelle (DM)	108
5.2.2 General immobilization of ligand in cross-linked micelle (DML)	109
5.2.3 General arylation procedure	109
5.2.4 General micelle recycling procedure	110
5.2.5 Initial Micelle loading optimization of Pd catalyzed C(sp ³)-H Monoarylation	111
5.2.6 Pd Catalyzed C(sp ³)-H Monoarylation Optimization	112
5.2.7 Solvent Screen of Pd catalyzed C(sp ³)-H Monoarylation	113
5.3 Results and Discussion	117
5.3.1 Micelle Design and Effects on C(sp ³)-H Monoarylation	117
5.3.2 Micelle-Ligand structure and impact on C(sp ³)-H Monoarylation	122
5.3.3 Substrate Scope of Pd-Catalyzed C(sp ³)-H arylation using DML-5	123
5.3.4 Recycling Studies of DML-5	127
5.4 Conclusions	129
 CHAPTER 6: SUMMARY AND FUTURE DIRECTIONS	 130
6.1 Summary	130
6.2 Future Directions	133

6.2.1 Polymeric Cooperative Catalysts	133
6.2.2 Extending Polymer Brush Catalysts for 3-Step Cascade Reactions	134
APPENDIX A. KINETIC EXPERIMENTS WITH POP-COOH IN HYDROBORATION OF PHENYLACETYLENE WITH PINACOLBORANE	134
A.1 Background on Porous Organic Polymers	134
A.1.1 Porous Organic Polymer Synthesis	134
A.1.2 Porous Organic Polymer Characterization	135
A.1.3 Porous Organic Polymer Catalyst Performance	136
APPENDIX B. CRUDE ¹H AND ¹³C SPECTRA FOR TABLE 3.7 SUBSTRATE SCOPE OF HYDROBORATION OF SUBSTITUTED ALKYNES USING PINACOLBORANE	140
REFERENCES	150

LIST OF TABLES

Table 2.1	Characterization of various copolymer catalysts	21
Table 2.2	Surface area and pore volume of POP- diol:ba	23
Table 2.3	Elemental analysis of POP- diol:ba	23
Table 2.4	Elemental analysis of phenylisothiocyanate coupled random 1:1 diol:ba copolymer catalyst	25
Table 2.5	Comparison of initial turnover frequencies (TOFs) for different solvent systems using the random 1:1 diol:ba catalyst	34
Table 2.6	Aldol condensation catalyzed by singly deprotected 1:1 diol:ba catalysts	37
Table 3.1	Hydroboration of phenylacetylene with pinacolborane using alternative catalyst	52
Table 3.2	Characterization of poly(vba)	60
Table 3.3	Solvent effects on hydroboration of phenylacetylene with poly(vba)	63
Table 3.4	KIE determination for the hydroboration of phenylacetylene using HBPIn in the presence of poly(vba) at 30 °C using octane as the solvent	69
Table 3.5	Determination of reaction orders of the hydroboration of phenylacetylene with HBPIn	70
Table 3.6	Determination of initial rate of the hydroboration of 1-ethynylcyclohexene with HBPIn in octane at 30 °C (up to 15% yield)	72
Table 3.7	Substituent effect of alkyne in hydroboration with pinacolborane	77
Table 3.8	Recycle studies of poly(vba) for the hydroboration of phenylacetylene	78
Table 4.1	Control reactions of sulfonic-acid catalyzed deprotection of 4-nitrobenzaldehyde dimethyl acetal	89

Table 4.2	Control reaction of base-catalyzed Knoevenagel and Michael addition	89
Table 4.3	Nitrogen physisorption of mesoporous silica catalysts	90
Table 4.4	Elemental analysis of mesoporous silica catalysts	90
Table 4.5	^1H NMR vinyl proton integration values derived from Figure 4.2 spectra	91
Table 4.6	2-step cascade reaction of 4-nitrobenzaldehyde dimethyl acetal to 2-benzylidenemalononitrile	101
Table 5.1	Initial Micelle Loading in Pd catalyzed $\text{C}(\text{sp}^3)\text{--H}$ Monoarylation	110
Table 5.2	Optimization of Pd catalyzed $\text{C}(\text{sp}^3)\text{--H}$ Monoarylation	111
Table 5.3	Solvent Optimization of Pd Catalyzed $\text{C}(\text{sp}^3)\text{--H}$ Monoarylation	112
Table 5.4	Elemental analysis of fresh and reused DML-5	115
Table 5.5	Micelle-supported ligands with various W_0 and micelle shell in Pd-catalyzed $\text{C}(\text{sp}^3)\text{--H}$ arylation	119
Table 5.6	Micelles with various pyridine-based ligands in Pd-catalyzed $\text{C}(\text{sp}^3)\text{--H}$ arylation	121
Table 5.7	Substrate scope of the Pd-catalyzed $\text{C}(\text{sp}^3)\text{--H}$ arylation using DML-5	123
Table 5.8	Recycling DML-5 in Pd-Catalyzed $\text{C}(\text{sp}^3)\text{--H}$ arylation	126
Table A.1	Catalytic Activity of the POP-COOH catalyst in the hydroboration of phenylacetylene with HPBin	137

LIST OF FIGURES

Figure 1.1	General cooperative catalysis cycles through transition state activation (A), sequential (B), dual (C), and self-activation (D).	5
Figure 1.2	General 2-Step cascade catalysis reaction.	11
Figure 2.1	Typical polymer synthesis by RAFT Polymerization.	19
Figure 2.2	^1H NMR spectra of in situ polymerization.	21
Figure 2.3	Integration ratio of the vinyl protons of monomer A (H_b) and monomer B (H_c) during in situ polymerization. The unchanging ratio demonstrates that the polymerization occurred in a random manner.	22
Figure 2.4	Nitrogen physisorption isotherm of POP- diol:ba .	23
Figure 2.5	IR spectra of the protected and deprotected random 1:1 diol:ba catalyst.	24
Figure 2.6	Amine coupling reaction used to quantify the accessible amines in the insoluble random 1:1 diol:ba copolymer catalyst.	24
Figure 2.7	Conversion (%) of various homogeneous acid and base pairs for the aldol condensation of 4-nitrobenzaldehyde and acetone at 50 °C under flowing Ar at 10 mol% of amine after 4 hours.	27
Figure 2.8	Synthesis of the weak-acid (diol) and amine-base (ba) styrene monomers, in protected form.	28
Figure 2.9	Illustration of various polymer catalyst sequence, (left) varying ratio of monomers, (center) various acid monomers and sequence, and (right) overall catalyst structure.	29
Figure 2.10	Titration curve of the 1:1 diol:ba random copolymer catalyst in DI H_2O in the presence of 0.010 M NaOH at 25 °C.	31
Figure 2.11	Conversion of 4-nitrobenzaldehyde with acetone at various 1:1 diol:ba catalyst loading based on CHN analysis at 50 °C over 24 hours. Catalyst loading at 100 mol% shown after 4 hour reaction time.	32

Figure 2.12	Kinetic curves of reactions using the random 1:1 diol:ba catalyst using different cosolvents in the aldol condensation with 100 mol% amine loading, as determined by elemental analysis. TOFs reported in Table 2.5 are determined through the initial linear region of the plot, and TON determined from final conversion determined by GC after 240 minutes.	34
Figure 2.13	Leaching test kinetic plot. Catalyst removed at 60 minute, and time point taken after 24 h. Hot filtration of catalyst to remove polymer, and reaction solution continued stirring at 50 °C.	35
Figure 2.14	Conversion of 4-nitrobenzaldehyde in the aldol condensation of 4-nitrobenzaldehyde with acetone in dichloromethane for copolymer catalysts that contain various ratios of acid and base sites at 50 °C using an apparent catalyst loading of 100 mol% amine.	36
Figure 2.15	Conversion of 4-nitrobenzaldehyde in the aldol condensation with acetone in dichloromethane for various copolymer catalysts containing different acid strength monomers and different monomer sequences at 50 °C using a catalyst loading of 100 mol% amine.	38
Figure 2.16	Conversion of 4-nitrobenzaldehyde in the aldol condensation with acetone in dichloromethane for various copolymer catalyst structures containing 1:1 diol:ba at 50 °C using a catalyst loading of 100 mol% amine.	40
Figure 3.1	Uncatalyzed hydroboration reaction with alkyne and pinacolborane.	42
Figure 3.2	¹ H NMR of benzoic acid with HBPIn in <i>d</i> -octane at 30 °C after 20 min.	44
Figure 3.3	¹¹ B NMR of poly(vba) and HBPIn in <i>d</i> -octane at 30 °C after 24 h.	45
Figure 3.4	¹¹ B NMR spectra of 1:1 ratio of benzoic anhydride with HBPIn in <i>d</i> -octane at 30 °C. The peak at 28.06 ppm corresponds to HPBin.	46
Figure 3.5	Plots of concentration of 2-styryl-BPin (M) vs. time (s) for Runs 1-4.	48
Figure 3.6	Plots of concentration of 2-styryl-BPin (M) vs. time (s) for Runs 5-8.	49

Figure 3.7	Plots of Concentration of 2-styryl-BPin (M) vs. time (s) for Runs 1-3.	50
Figure 3.8	Bromophenol blue catalyst structure.	52
Figure 3.9	Representative ^1H NMR crude product analysis for (E)-2-(4- <i>tert</i> -butyl)styryl)-4,4,5,5-tetramethyl-1,3,2-dioxaborolane in CDCl_3 . CH_2Br_2 used as internal standard at 4.93 ppm (s, 2H). Unreacted product appears at 3.03 ppm (s, 1H) and vinyl product peaks 6.12 ppm (d, 1H).	53
Figure 3.10	Polymer catalyst synthesis via RAFT polymerization.	59
Figure 3.11	GPC chromatogram of poly(vinylbenzoic acid) using THF as the eluent, with polystyrene calibrations.	60
Figure 3.12	^1H NMR recycled poly(vba) in MeOD.	61
Figure 3.13	^1H NMR 2 nd recycled poly(vba) in MeOD.	62
Figure 3.14	Possible scenarios for the generation of the activating species for the hydroboration of phenylacetylene with HBPPin as the boron source.	65
Figure 3.15	^{11}B NMR analysis of 1:1 ratio of benzoic acid with HBPin over 24 h in <i>d</i> -octane at 30 °C (20 min in red, 5 h in green, 24 h in blue). The peak at 28.13 ppm corresponds to HBPin.	66
Figure 3.16	^{11}B NMR analysis of 1:1 ratio of benzoic acid:HBPin:phenylacetylene over 24 h in <i>d</i> -octane at 30 °C (20 min blue, 5 h in green, 24 h in red).	67
Figure 3.17	Determination of the deuterium kinetic isotope effect for the hydroboration of phenylacetylene and phenylacetylene- <i>d</i> with HBPin as the boron source and poly(vba) as the catalyst.	69
Figure 3.18	Inverse first-order dependence on the initial rates for the formation of 2-styryl-BPin on the concentration of HBPin (A) and Phenylacetylene (B). First-order dependence on the initial rate for the formation of 2-styryl-BPin on the concentration of the acid catalyst (C).	71
Figure 3.19	Illustrative site inhibition due to over adsorption of species to active sites and steric site blocking, leading to inverse order dependence of the hydroboration of phenylacetylene with HBPin rate law.	73

Figure 3.20	Reaction profiles for the hydroboration of phenylacetylene with HBPIn using benzoic acid (black), benzoic anhydride (red), and poly(vba) (blue) as catalysts.	74
Figure 3.21	Proposed catalytic pathway for the hydroboration of phenylacetylene with HBPIn using poly(vba).	75
Figure 4.1	General synthesis of boc-pyrrolidine acrylamide monomer.	84
Figure 4.2	^1H NMR spectra of vinyl protons in RAFT-CTA polymerization of polymer brush-g.t. ($t = 0$, red; $t = 18$ h, blue).	91
Figure 4.3	TEM images of core-shell mesoporous silica catalyst MCM-SO ₃ H.	92
Figure 4.4	3-step cascade reaction catalyzed by a site-isolated acid-base polymer brush.	93
Figure 4.5	General syntheses of three hybrid sulfonic-acid pyrrolidine supported catalysts.	95
Figure 4.6	General preparation of protected MCM-SO ₃ H-pyrrol brush catalysts (with CTAB).	97
Figure 4.7	General preparation of MCM-SO ₃ H-pyrrol molecular catalyst.	99
Figure 5.1	Typical preparation of cross-linked micelle.	107
Figure 5.2	Immobilization of ligand in cross-linked micelle.	108
Figure 5.3	Absorption spectra of DM-5, DML-5, recycled DML-5, and homogeneous ligand in chloroform. $W_0 = [\text{H}_2\text{O}]/[\text{surfactant}] = 5$.	112
Figure 5.4	Hydrodynamic radius of DML-5 in various solvents using multiangle dynamic light scattering.	113
Figure 5.5	^1H NMR spectra of surfactant A (blue) and surfactant B (red) before irradiation in CDCl ₃ , and after irradiation to yield crude micelle (purple). After the micelle is formed, the solvent is removed by rotary evaporation and washed with cold MeOH, providing pure micelle (green).	114

Figure 5.6	¹ H NMR spectra of ligand immobilization within micelle core. Micelle DM in CDCl ₃ before ligand immobilization (blue). Next, ligand is immobilized leading to crude DML (red), and further washed with cold MeOH and pure DML is obtained (green).	114
Figure 5.7	¹ H NMR in CDCl ₃ of a) recycled and b) fresh DML-5 from first run Pd-catalyzed C(sp ³)–H monoarylation.	115
Figure 5.8	Pd-Catalyzed C(sp ³)–H Monoarylation.	116
Figure 5.9	General preparation of cross-linked micelle-supported ligand.	117
Figure A.1	XPS O1s scan of POP-COOH.	136
Figure A.2	Nitrogen physisorption isotherm of POP-COOH.	137

LIST OF SYMBOLS AND ABBREVIATIONS

9-BBN	9-Borabicyclo[3.3.1]nonane
A	surfactant A
AIBN	2,2'-Azobis(2-methylpropionitrile)
α	alpha
APTES	(3-aminopropyl)triethoxysilane
ATRP	Atom Transfer Radical Polymerization
B	Surfactant B
ba	benzylamine
BET	Brunauer-Emmett-Teller
β	beta
Boc	<i>Tert</i> -butyloxycarbonyl
ca	Carboxylic acid
[cat]	Concentration of catalyst
°C	Celsius
CDCl ₃	<i>d</i> -chloroform
cm ³	Centimeters cubed
cm ⁻¹	Inverse centimeters
-COOH	Carboxylic acid
CTA	Chain transfer agent
CTAB	Cetrimonium bromide
C wt%	Carbon weight percent
δ	Chemical shift

Đ	dispersity
d	doublet
DCE	dichloroethane
DINEA	N-diisopropylethylamine
DM	Double-tail micelle
DMAP	4-Dimethylaminopyridine
DML	Double-tail micelle with ligand
DML-5	Double-tail micelle with ligand, core size = 5
diol	3,4-dihydroxy styrene
DVB	Divinyl benzene
EA	Elemental analysis
EtOAc	Ethyl acetate
Eq.	equivalents
FID	Flame induced detector
FTIR	Fourier transform infrared spectroscopy
g	gram
GC	Gas chromatography
gf.	“grafting from”
GPC	Gel permeation chromatography
gt.	“grafting to”
H wt%	Hydrogen weight percent
h	hour
h ⁻¹	Inverse hours
HBPIn	pinacolborane
Hex	hexanes

Hz	hertz
J	Scalar coupling
kDa	kiladaltons
KIE	Kinetic isotope effect
KOtBu	Potassium <i>tert</i> -butoxide
M	Moles/liter
m	multiplet
-m.	molecular
MePPh ₃ Br	Methyltriphenylphosphonium bromide
mg	milligrams
min	minutes
mL	milliliter
mm	millimeter
mmol	millimole
mol %	Mole percent
M _n	Number average molecular weight
MOF	Metal organic framework
M _w	Weight Average molecular weight
MWCO	Molecular weight cut-off
-NH ₂	amine
N.D.	Not determined
NEt ₃	triethylamine
NHC	N-Heterocyclic carbene
nm	nanometer
NMP	Nitroxide-mediated radical polymerization

NMR	Nuclear magnetic resonance
N.R.	No reaction
N wt%	Nitrogen weight percent
-OH	alcohol
pa	aniline
Pd(TFA) ₂	Palladium(II) triflate
Ph-I	Phenyl iodide
Pht	Phthalimide
Poly(vba)	Poly(vinylbenzoic acid)
POP	Porous organic polymer
PPh ₃	triphenylphosphine
ppm	Parts per million
RAFT	Reverse addition-fragmentation chain-transfer
r.t.	Room temperature
s	singlet
sec	seconds
-SH	thiol
SiO _x	Silicon dioxide surface
SI-RAFT	Surface-initiated reverse addition-fragmentation chain-transfer
-SO ₃ H	Sulfonic acid
TEM	Transmission electron microscopy
TEOS	Tetraethyl orthosilicate
TFA	Trifluoroacetic acid
THF	tetrahydrofuran
TLC	Thin layer chromatography

TML	Triple-tail micelle with ligand
TOF	Turnover frequency
TON	Turnover number
TsCl	Toluenesulfonyl chloride
μL	microliter
μs	microsecond
W_0	Core size
wt %	Weight percent
XPS	X-ray photoelectron spectroscopy

SUMMARY

Polymer structures provide tunable platforms for catalyst design due to the high degree of structural control possible in their synthesis. Various polymeric structures such as micelles, brushes, as well as traditional linear chains and a recent emerging class of porous organic polymers (POPs) are available for numerous applications. In the field of catalysis, both transition-metal and metal-free catalysis have been demonstrated using catalytically active sites attached on polymer supports. In this study, several different molecular catalysts have been prepared on polymer supports targeting applications in organic synthesis, as well as demonstrating aspects of cooperative and cascade catalysis. An overall goal of this thesis was to demonstrate the benefits of various polymer catalyst architectures in a variety of catalytic reactions including cooperative and cascade catalysis using acid and base sites, acid catalyzed hydroboration reactions, and Pd catalyzed C–H arylation.

This thesis is organized into six chapters. The first chapter gives an overview of the use of polymer supported catalysts in organic synthesis, with a special emphasis on the use of polymer supports in organocatalysis. An introduction to key concepts explored in this thesis is also presented, including the applications of organocatalysts in cooperative and cascade reactions catalyzed by combinations of acid and base sites. Additionally, the organocatalytic hydroboration of alkynes is introduced as a target reaction, as well as the Pd catalyzed C–H activation to produce new C–C bonds. The second chapter explores the application of a linear polymer support in cooperative catalysis of the aldol reaction, which is a system that has been extensively studied on

mesoporous silica supports. The new linear polymer catalyst demonstrated comparable reactivity to the mesoporous silica supports, and the importance of monomer unit placement, strength of the acid and base, and the acid-base ratio are demonstrated.

The third chapter extends the concepts learned from the second chapter with regard to acid-base cooperative catalysis to polymer-silica hybrid catalysts in which the acid and base sites are confined into separate domains within the catalyst. In this chapter, the acid and base functionalities are incorporated into mesoporous silica and polymer brush domains to yield a polymer brush catalyst that targets a 3-step cascade reaction. The cascade is comprised of the 4-nitrobenzaldehyde dimethyl acetal acid-deprotection to 4-nitrobenzaldehyde which undergoes a base-catalyzed Knoevenagel and Michael addition to yield different chromenes. The polymer brush synthesis was designed based on the size of the substrates and resulting products, forming larger final products on the exterior of the brush through basic moieties on the polymer chains, while functionalizing the interior of the mesoporous silica support with a strong acid that converts the smallest substrates.

The next chapter is a fundamental kinetic and mechanistic study of the hydroboration of various alkynes with pinacolborane utilizing a carboxylic acid polymer catalyst. This project originated from chapter two as well, using a homopolymer from the acid-base cooperative study and applying it to hydroborations. The study elucidated the kinetic order of the reaction in catalyst and substrates, and a proposed mechanism was supported by a kinetic isotope effect and ^{11}B NMR studies. The linear polymer catalyst was the first example of an organocatalytic polymer catalyst for the hydroboration of functionalized alkynes, providing a platform for future organocatalyst designs.

Chapter five discusses the utility of a polymer micelle support for the Pd-catalyzed $C(sp^3) - H$ monoarylation. Using this micelle support, steric and electronic effects were invoked to direct the $C - H$ monoarylation of an unnatural amino acid with substituted aryl iodides. The support demonstrated high tolerance for substituted aryl iodide coupling partners, while also recycling the support. Because the support was functionalized with weakly binding amines, the palladium was unable to be recycled and reused. To that end, the proposed future directions of this project include the design and synthesis of bidentate ligands for $C(sp^3) - H$ monoarylation to mitigate this problem. The use of the polymer micelle was one of the first demonstrations of this support applied to $C - H$ activation, and the support has many tunable properties that can be adjusted in future applications.

Lastly, the final chapter outlines possible future directions for these different projects as well as summarizes the fundamental findings from each of these studies. Understanding the fundamental aspects that were tuned for each support and applied to these organocatalytic reactions provides a basis for future improvements on these supports as well as applications in synthetic organic chemistry.

CHAPTER 1.

INTRODUCTION TO POLYMER STRUCTURES AND THEIR APPLICATIONS IN CATALYSIS

1.1 Introduction and Motivation

Fundamental understanding of the structure of catalyst active sites has driven innovation by improving catalytic performance and catalyst design. Due to economic, environmental and sustainability factors, there has been a continual creation and evaluation of new catalysts for well over a century.¹ These demands can be met through the design and development of recyclable catalysts, which can be used to help achieve sustainable chemical processes. Often the recycling process is facilitated by use of a heterogeneous system, whereby the catalyst exists in a separate phase from the reaction media (e.g. solid catalyst in liquid media). In contrast, recovery and recycle of a catalyst that exists homogeneously in a single phase is more challenging. Often, homogeneous, molecular catalysts are attached to solid supports to facilitate recovery and recycle; however, this must be done without compromising activity and selectivity associated with the homogeneous catalyst.^{2,3} In effective designs of supported molecular catalysts, a firm understanding of the catalyst behavior in the homogenous reaction can lend insight into the design of a heterogeneous analogue. There are numerous classes of insoluble

(heterogeneous) supports, and one class of materials that has been widely used for equipping homogenous systems with a heterogeneous handle is polymer supports.^{4,5}

Polymer supports provide an incredibly tunable support architecture, standing out in the vast arena of alternative heterogeneous support structures which are typically less easily tuned.⁶ Depending on the requirements for specific reactions, polymer structures can be made to fit the needs of the reaction. Polymer architectures previously used as heterogeneous catalysts include but are not limited to linear and branched chains,^{7,8,9} brushes,^{10,11,12} dendrimers^{13,14} micelles,^{15,16,17,18} and polymer resins,^{19,20} among other structures. Large scale, industrialized processes have employed polymer resins most often, typically to provide an ease of recovery and reuse, though resins have been used in small scale productions of chemicals as well.^{21,22} For fundamental studies using polymer catalysts, the exact active site location and environment is critical for extending fundamental knowledge gained to the applied realm of catalysts. Linear polymers have a vast amount of applications, and within this class of polymers there are subdivided sequences of random, block, and alternating linear chains which possess utility in conjugated solar cells,^{23,24,25,26,27} electrolytic deposition for fuel cells,^{28,29,30,31} and electronics^{32,33,34} as a few examples.

Linear polymers have the benefit in catalysis of site placement on each monomer of the polymer chain, and typically serve as a soluble support for catalytic sites, with recovery requiring a few separation steps. Because single chain catalysis is a challenging system to define, the alternative system to examine are brushes. Polymer brush systems employ a solid support, with one end of a polymer chain tethered to the support. This

system extrapolates knowledge gained from a soluble linear system, and provides a heterogeneous support which can reduce recovery steps.

Brushes can be grown using various uses utilizing controlled polymerization techniques such as ATRP,^{35,36,37} RAFT,^{38,39,40} and NMP.^{41,42} By far, the most common support used for polymer brush synthesis is SiO_x. Brush structures have applications in stimuli-responsive surfaces^{43,44} and recently electronics⁴⁵ and catalysis.⁴⁶ Within catalysis, these supports have tethered both organic and inorganic moieties for cooperative and cascade catalysis.^{47,48}

The last structure discussed within this dissertation is a micelle. Micelles have served as a hybrid support with solubility in a system akin to a linear polymer, but size and microenvironment specifications like a brush. Micelles are effective structures for carrying out chemistry in aqueous media without compromising activity of both organic and inorganic catalysts through utilizing microenvironments.^{49,50,51} Micelles have served as ideal platforms for drug delivery through the dynamic nature of the structure in a aqueous environment,^{52,53} and as covalently-bound stable reverse micelle which perform catalysis in organic solvents.⁵⁴

1.2 Linear polymer catalysts

Linear polymer catalysts have served as supports for both organic and inorganic/organometallic active sites. The literature contains hundreds of examples using soluble polymers as supports in the liquid phase, with the materials acting as pseudo-heterogeneous catalysts. Alternatively, linear polymers, when insoluble, can form solid particles in solution that can be recovered by filtration from liquid media.

In this thesis, linear polymer chains functionalized with acidic and basic sites have been prepared to study the impact of polymer structure on cooperative acid-base catalysis in liquid media. Linear polymer chains in solution can take on some nebulous physical characteristics similar to enzymatic structures, which can be beneficial in catalysis, specifically cooperative catalysis, which utilizes the characteristics of site flexibility, cooperative interactions, and a controlled, typically close proximity of catalytic sites. Supporting inorganic/organometallic catalysts through the design of ligand-modified monomers can induce self-folding of the polymer-ligated active sites in solution due to chelation of the metal sites, reducing the distance between active sites.^{55,56} For reactions catalyzed by organic active sites, the self-folding to form nanoparticles requires tuning of the acid and base components because of the potential for quenching if the strong acid and base sites can self-assemble by numerous multidentate interactions. For acid-base cooperative catalysis using amine and weak acid sites such as silanols, mesoporous silica supports have been widely employed, where co-annihilation of the acid and base species is limited due to the fixed placement of moieties on a rigid, insoluble surface.

1.2.1 Cooperative catalysis with solid catalysts

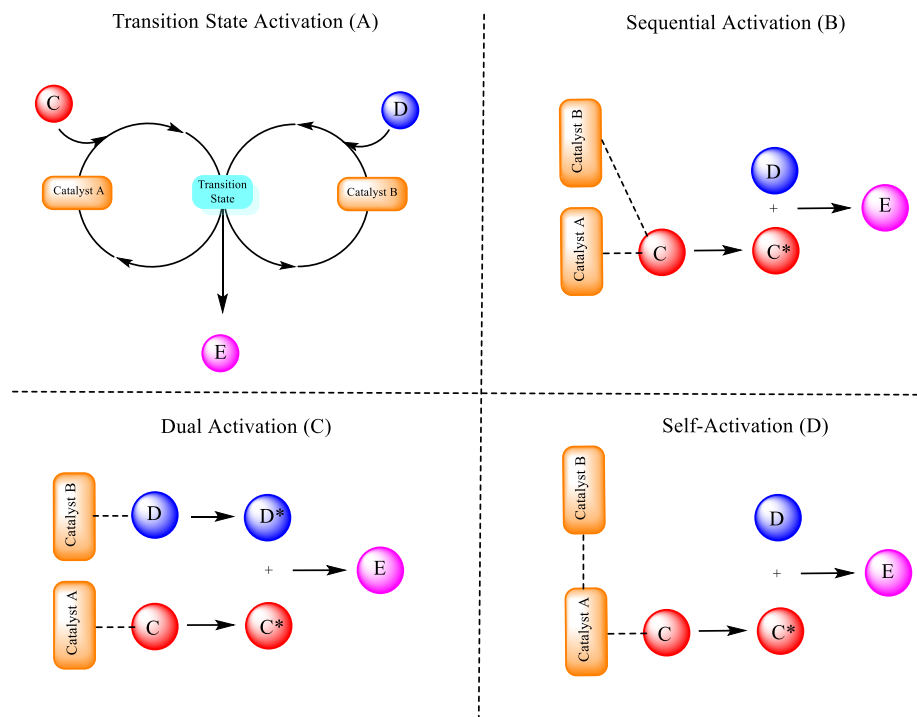


Figure 1.1: General cooperative catalysis cycles through transition state activation (A), sequential (B), dual (C), and self-activation (D).

Cooperative catalysis can occur in many different modes as depicted above in Figure 1.1. In cooperative, transition state activation, two separate catalytic sites activate two different reactants that ultimately produce the product in tandem.⁵⁷ Schematically, as seen above in Figure 1.1, catalyst A activates substrate C to C*, while Catalyst B activates substrate D to D* to form product E in transition state activation. In a second type of cooperative catalysis, referred to as sequential activation (B), Catalyst A and B interact with one substrate to prepare the compound for reactivity with the second, unactivated substrate (Figure 1.1). Dual activation involved Catalyst A interacts with C, and Catalyst B interacts with D to form E, and Self-Activation (D) involves Catalyst A and B forming

an activated complex to interact with C and unactivated substrate D. Each of these modes of cooperative activation have all reactants and catalysts present from the beginning of the reaction, which is critical for catalyst design when the incorporation of moieties that inherently quench one another are present.⁵⁸ The most well known examples of cooperative catalysts are enzymes. To this end, scientists have looked to enzymatic systems for inspiration regarding catalyst design, and many chemists have developed catalysts that seek to position the functional groups in an active pocket such that catalytic sites productively interact with the reactants. Biological systems have mastered complicated reactions under mild conditions using such designs, in many cases simultaneously incorporating functionalities that are inherently opposed, such as acids and bases.⁵⁹ Many times, enzymes utilize a hydrophobic binding pocket that contains organocatalytic or metallic species,⁶⁰ performing catalysis through cooperative interactions of each catalytic site with the reactants.

Cooperative acid-base catalysis has been thoroughly explored using mesoporous silica supports that have provided a fixed, rigid surface to tether active species to. Mesoporous silica supports such as MCM-41 and SBA-15 have a hexagonal array of pores, typically ranging from 2-200 nanometers in diameter, with large surface areas.^{61,62,63} The ordered support is suitable to be used for many reactions due to the stability of the matrix, as well as the ability for incorporation of multiple functional groups. The support inherently has an acidic silanol surface that is used to tether various organosilanes thorough grafting procedures to introduce specific functionalities. An alternative way to introduce specific functional groups is via the incorporation of specific

organosilanes during in the initial synthesis of the support, an approach known as co-condensation.⁶⁴

Cooperatively catalyzed acid-base reactions such as the aldol condensation,⁶⁵ nitroaldol condensation,⁶⁶ and Knoevenagel condensation⁶⁷ have demonstrated the importance of combining both acid and base sites in the catalysts to achieve significantly enhanced reaction rates. Several factors have been explored in various catalyst designs, including the role of base type (e.g. various amines), acid type and strength, as well as the proximity of the acid and base sites to each other. As an example, using the aldol condensation as the test reaction, the importance of acid strength in the cooperativity of acid and base sites was explored, showing that weaker acid sites led to more effective catalysts, with the idea that weaker acid sites were less likely to protonate and quench the base sites.⁶⁸ In a later study, the inherent acidity of the silanol surface was shown to be a highly effective acidic partner to grafted primary alkyl amine species for these coupling reactions.⁶⁹ Through the many years of research on cooperative catalysis utilizing mesoporous silica supports with various acids and bases, a few key characteristics have been identified for optimal cooperativity: flexibility in the acid and base partners,⁷⁰ choosing an appropriate acid and base strength,^{68,69} and the proximity of the cooperative partners.

As noted above, most studies of amine/acid cooperativity in aldol and related coupling reactions have employed rigid, porous silica supported active sites. In chapter 2, the use of linear polymeric supports containing acid and base sites of similar strengths to those explored in studies of cooperative catalysis with mesoporous silica is described. Specifically, a fundamental study of the key concepts noted above was completed using a

polystyrene support as one of the first comprehensive studies of this type of catalysis using a linear polymer. This study found that weakly acidic monomers were more effective cooperative partners with an amine base than a stronger acid. In a subsequent study employing polymer-supported catalysts, the stronger acid monomer was exploited further in a fundamental examination of the hydroboration of alkynes forming new C–B bonds while using a simple, low cost organocatalyst.

1.2.2 Hydroboration chemistry with homogenous catalysts

Hydroboration chemistry was discovered in the late 1950s by Herbert C. Brown, which placed an organoborane on an olefin as a useful synthetic intermediate.⁷¹ Since the genesis of this reaction, decades of investigations have been dedicated to honing this useful intermediate. Hydroborations have primarily been used in synthetic organic chemistry as a functional handle easily modified in further synthetic strategies.⁷² The borylated products are generally air-stable and easy to handle,⁷³ compounding the usefulness of this reaction. Commonly used hydroborating reagents are diborane,⁷¹ 9-BBN,⁷⁴ catecholborane,^{75,76} and pinacolborane.^{77,78} Producing the boron-containing products has been achieved through a wide array of transition-metal catalyzed reactions catalysed by metal complexes based on Ti,⁷⁹ Zr,^{80,81} Pd,^{82,83} and Rh,^{84,85,86} among others.

Hydroboration reactions over the years have been tuned to produce both the classic E-substituted alkyne or olefin with anti-Markovnikov placement, as well as Z-substituted unsaturated compounds. This reaction with transition metal catalysts can achieve the synthesis of Z-alkylboronates,^{87,88} activation of internal alkynes and olefins,^{89,90} as well as addition to heteroatom moieties. As fundamental studies of the

various mechanistic pathways using these various transition-metal catalysts have led to understanding of the catalytic cycles, researchers have most recently begun to turn toward less expensive transition metals such as Fe,^{91,92} Co,^{93,94,95,96} and Cu^{97,98} as well as transition-metal free systems. The use of less expensive catalysts in reactions that still maintain a high degree of regio- and stereoselectivity facilitates the more widespread use of this reaction in synthetic chemistry.

1.2.3 Hydroboration chemistry with heterogeneous catalysts

There are limited examples of solid catalysts in the literature for hydroboration reactions. Only a few different supports such as MOFs and mesoporous silica have been reported for hydroboration catalysis, typically being employed with the hopes of recycling the expensive metal and avoiding metal leaching. Transition metals, both particles and ions, supported on different solid structures have been shown to catalyze this reaction, but not all examples have demonstrated the ability to reuse the catalyst.^{99,100,101,102,103} One study used of macroporous polymer-supported rhodium catalyst that was reused for hydrogenation and hydroborations reactions, but displayed rhodium leaching.¹⁰⁴ Two reports have employed mesoporous silica supported rhodium and zirconium complexes.^{105,106} The recycle of zirconium hydride complexes on silica supports was demonstrated over 8 cycles without loss of activity, improving the reuse of an air and moisture-sensitive complex in the homogenous case. The ability to recycle and reuse expensive metals for this reaction has not been widely described in the literature. However, there has been an emergence of the use of organocatalysts for this chemistry in recent years, which offers the potential for simpler, less costly catalytic systems.

Recently, the use of a homogeneous, small molecule carboxylic acid catalyst was reported to catalyze the hydroboration of substituted alkynes using pinacolborane. With the ability to prepare carboxylic acid containing polymers developed in the work described in chapter 2, new polymeric catalysts for the hydroboration of alkynes were developed and explored. Through controlled polymerization techniques, the polymer chains can provide exact placement of active sites on each chain, and the elimination of transition metals may be a cost-efficient way of creating new solid catalysts while maintaining high activity. Understanding mechanistically how the catalyst performs the hydroboration can lead to improved catalyst design. To that end, Chapter 3 describes work that identified a carboxylic acid polymer catalyst that was deployed in a fundamental analysis of the hydroboration of substituted alkynes with pinacolborane as the boron source. Experiments targeting the elucidation of the mechanism with which this catalyst performs the hydroboration were completed. While an exact mechanism not fully identified, the kinetic isotope effect (KIE) in the reaction was identified and the kinetic orders in catalyst and substrate allowed for the identification of a proposed pathway for the reaction using the carboxylic acid organocatalyst.

1.3 Polymer brush catalysts

Hybrid organic-inorganic supported structures are ubiquitous in applications from materials to catalysis. Polymer brushes are a specific type of organic-inorganic hybrid material if a solid, inorganic surface is employed, with the polymer brush defined as a structure having one end of a polymer chain tethered to a solid surface. The support can be a myriad of materials, but is most often silica due to its highly modifiable surface. Generally, there are two approaches to synthesizing a polymer brush: “grafting to” and

“grafting from”.¹⁰⁷ The “grafting to” approach involves synthesizing the polymer chain with a modified end group that can be grafted to the surface. The “grafting from” approach typically deposits some form of an initiator or propagation agent on the surface of the support and grows the polymer from the surface.

Polymer brushes in catalysis have been used to support both transition metal complexes and organic species as active sites. Transition metals are most often supported through polymerizing ligands that chelate to the metal once it is introduced into the system. Examples of brush-supported transition-metal complex catalysts include Ag,¹⁰⁸ Au,¹⁰⁹ Pd,¹¹⁰ Cu,¹¹¹ and Ni.¹¹¹ These metals have been used to perform various types of catalysis, from single-site to cooperative,¹¹² and bifunctional reactions.⁹

1.3.1 Cascade Catalysis

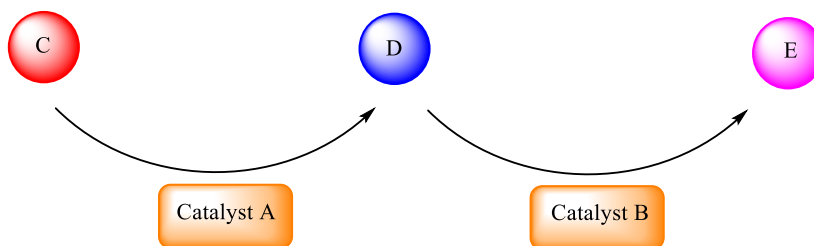


Figure 1.2: General 2-Step cascade catalysis reaction.

Cascade catalysis refers to a one-pot tandem or multi-step reaction where there is a domino of substrate C going to D going E, utilizing two separate catalysts A and B, as illustrated above in Figure 1.2. The concept of cascade catalysis is rooted in enzymatic behaviour where multiple transformations occur in tandem due to compartmentalization in biological systems. For this dissertation, a focus has been placed on extending the

cooperative acid-base chemistry developed in chapter 2 to these cascades. Whereas cooperative catalysis requires the creation of domains with acid and base sites situated in close proximity to each other, in cascade reactions that seek emulate biological systems, it can be desired to spatially separate the different types of active sites. In this work, it was sought to spatially isolate acid and base sites into separate domains. In the literature, there are a few classic cascade reactions, one class of which consists of an acid-catalyzed acetal-deprotection followed by some form of base-catalyzed addition. The supports used for this catalysis are expansive, and in recent literature examples using porous cross-linked networks,¹¹³ covalent organic frameworks,¹¹⁴ and metal-organic frameworks¹¹⁵ have been reported.

Polymer brushes provide a malleable support for the synthetic needs associated with designing catalysts for cascade reactions. Star polymers have served to encapsulate a sulfonic acid catalyst to perform an acid- deprotection of 4-nitrobenzaldehyde dimethyl acetal, coupled with dialkylamino pyridine to perform the Baylis-Hillman with methyl vinyl ketone.¹¹⁶ Bottle-brush polymer catalysts have also displayed high activity for the tandem acetal-deprotection-base-catalyzed Knoevenagel condensation, which incorporated a sulfonic acid and N-methylaminopyridine in the interior of separate brushes.⁴⁷

Cascade catalysis has mostly focused on two-step cascades, and the study performed in Chapter 4 has begun to extend knowledge from two-steps to three steps for an acid-base-catalyzed reaction with two base catalyzed steps. Due to the excess base necessary to perform a third step, a polymer brush incorporating basic moieties was designed, while maintaining acid functionalities in the support to give a useful

architecture. Exploration of different hybrid organic-inorganic architectures was carried out and catalytic studies were performed, with hopes of extending these concepts to larger platform chemical syntheses.

1.4 Polymer micelle catalysts

Polymer micelles are structures that take advantage of hydrophobic and hydrophilic compartmentalization for various applications like drug delivery⁵³ and in this study, catalysis.¹¹⁷ Often these micelles mimic biological systems, shuttling reactants and products through individual compartments in tandem to create complex molecules that are synthetically challenging.^{118,119} The various micelle structures available offer a tunable support for applications in catalysis.

Classic micelles employ hydrophobic and hydrophilic characteristics to dynamically form in aqueous conditions, while reverse micelles utilize the reverse process to form in organic solutions. The majority of polymer micelle syntheses are achieved through self-assembly of block copolymers or individual surfactant molecules composed of hydrophobic and hydrophilic zones.^{120,121} To increase stability of the micelles formed by individual surfactant molecules, cross-linking the head groups can eliminate exchange of core contents and fix the micelle structure to withstand higher temperatures.^{122,123} In this work, such an approach was undertaken to design micelle-supported Pd catalysts for C-H activation.

1.5 Micellar applications in catalysis

Micelles have served as a support to perform organic transition-metal catalyzed reactions carried out in organic solvents in an aqueous medium.^{124,125,126,127} Alternatively, these micelles can create an active pocket similar to an enzyme, with spatial configurations that facilitate cooperative interactions.¹²⁸ Another exploitation of the spatial confinements of the core can be to facilitate chelation of metals to ligands immobilized within the core.¹²⁹

The many microenvironments created by polymer micelles are tuned characteristics of these supports such as size of the core,^{130,123} polymer block synthesis,^{131,132} and functionalization of key organic species within the structure.^{133,134} Applying the various synthetic changes is specific to the role or application envisioned for each micellar system; however, the focus of micellar supports for catalysis within this thesis was to promote size selectivity to a C(sp³)–H monoarylation of an unnatural amino acid with substituted aryl iodides, while offering the potential for ligand, metal or catalyst recovery and reuse.

C – H functionalization has received tremendous attention in the synthetic organic chemistry community over the last two decades, with advances coming from both ligand coordination as well as catalyst design to promote the specificity and reactivity of the catalysis. Many groups have designed complex catalyst systems that promote various types of C–H functionalization, activating sp, sp², and sp³ bonds. In collaboration with Dr. Jin-Quan Yu's group, the first generation of micelle-supported ligands to promote Pd-catalyzed C(sp³)–H monoarylations was developed.

1.6 Outlook

With the overall target of applying various polymer structures to cater to different types of catalysis, the work in this thesis has employed linear polymers synthesized by controlled radical polymerization techniques, polymeric micelles and silica-supported polymer brushes to achieve an array of different functional catalytic materials. In each case, the polymer and catalyst design was targeted towards a specific application. For each polymer and catalytic target, fundamental insights into the catalytic process was obtained, yielding additional ideas about how the different polymer structures could be tuned for each reaction.

Applying concepts from the mesoporous silica literature to linear polymer supports for cooperative catalysis is described in Chapter 2. The polymer synthesized performed as well as silica catalysts, with the ability to tune both monomer design and polymer solubility offering opportunities to increase reaction rates further. Chapter 3 addresses completely different chemistry using a similar linear polymer supported benzoic acid, and new into organocatalyzed hydroborations have been obtained, a field where organocatalysts have not been explored thoroughly. Chapter 4 has extended concepts learned from cooperative catalysis in chapter 2, and presented the synthesis polymer brush structures suited to carry out a 3-step cascade, successfully catalyzing the first two steps in tandem. Lastly, utilizing a photoinitiated cross-linking micelle structure for a Pd-catalyzed $C(sp^3) - H$ monoarylation applied an entirely new support to this type of C-H activation chemistry, and fundamental steric implications associated with the micellar catalysis were discovered.

CHAPTER 2.

ACID-BASE COOPERATIVE CATALYSIS USING LINEAR POLYMER SUPPORTS

Parts of this chapter are reproduced from ‘Hoyt, C.B.; Chen, L. – C.; Cohen, A. E.; Weck, M.; Jones, C. W. Bifunctional Polymer Architectures for Cooperative Catalysis: Tunable Acid-Base Polymers for Aldol Condensation. *ChemCatChem*, **2017**, 9, 137-143.’

2.1 Background

As mentioned in chapter 1, many biological systems that utilize organic active sites to catalyze reactions under mild conditions through cooperative catalytic pathways, whereby two or more active sites work together to activate the reactant(s). An array of designed, chemical catalysts also catalyze reactions by employing cooperative effects, whether it be by metal/metal cooperativity using nanoclusters,¹³⁵ metal-ligand cooperativity,^{136,137,58} or via cooperative interactions in organocatalytic systems, akin to biological catalysts.^{138,139,140,141,142,143,144} Considering one specific example of chemical catalysts, many researchers have used the biological inspiration to develop cooperative catalysts based on amines and acidic groups functionalized on mesoporous silica supports.^{145,146,68} Although mesoporous silica supports are easy to prepare and functionalize with various functional groups via grafting of organosilanes, the rigidity of the supports differs substantially from the flexibility that biological macromolecular catalysts offer. Many silica supported bifunctional catalysts have focused on the aldol or nitroaldol reactions as tools to explore cooperative activation of aldehydes with

various coupling partners.^{147,68,148,149} The numerous studies on mesoporous silica supports have established amine-silanol interactions as the most useful acid-base pair for the cooperatively catalyzed aldol condensation⁶⁹ compared to related systems that utilize stronger acid sites. Initial studies on the use of different types of amines,^{150,151,70} as well as the role of amine linker length identified flexibility in the amine-functionalized silanes as an important factor that could be tuned to alter the cooperative interactions between the amines and silanols.^{70,152,153} One study looked at intramolecular interactions of secondary amines paired with varying acid strength pairs on the same alkyl chain, and found weakly acidic alcohols to be the best cooperative partners for catalyzing the aldol condensation.¹⁵²

While cooperative amine-acid catalysts based on silica supports are relatively well-studied, there are limitations in this system that can potentially be addressed by using other supports. As noted above, the silica surface is rigid and inflexible compared to enzymatic catalysts. Another constraint with the silica based systems is the difficulty in controlling amine placement on the silanol surface. Controlling the amine density grafted onto the silica surface has been manipulated through the use of bulky protecting groups,^{154,155} but this introduces more steps to a synthesis that utilizes simplicity as a key attraction. Another drawback to silica supports is the range of acidities that may exist on the silanol surface,¹⁵⁶ as well as the ability to control silanol number and location independently. Literature reports suggest that silanols on the silica surface can range in acidity, with an average pKa value of 7.^{151,157,158} The acidity of the silica surface can be further tuned to be more acidic through the incorporation of heteroatoms into the silica framework.^{148,159,160} A recent study exploring a variety of heteroatom substitutions into

the silica surface showed that the strongest Lewis acidic species, zirconium, decreased the conversion for the aldol condensation relative to the metal-free silica surface.¹⁶¹ This is consistent with the results discussed above, where weaker acidity led to improved reaction rates.^{69,152}

Building from the array of research conducted on silica supports, we have hypothesized that synthetic polymer systems can provide new design elements that are challenging to utilize with silica systems. A wide variety of monomers can be utilized, and these monomers can be copolymerized through controlled/living polymerization techniques that allow for a high degree of control over the polymerization and, potentially, the placement of specific monomers within the chain.^{162,125} To this end, in this initial investigation, we report here a series of polystyrene polymers containing amines and weakly acidic diols in their side-chains and explore their use as catalysts in the aldol condensation of 4-nitrobenzaldehyde and acetone. Our goal of this initial polymer-supported study is to compare and contrast the behavior of these polymer catalysts to the well-studied silica/amine systems.

2.2 Experiments

2.2.1 General Aldol Condensation procedure

Under flowing nitrogen in a 25 mL 2-neck round bottom flask, 1.0125 mL of 0.10 M aldol stock solution containing 4-nitrobenzaldehyde, dimethoxybenzene (internal standard), and acetone and 1.0125 mL dichloromethane was micropipetted into a 2-neck (25 mL) round-bottom flask and stirred at room temperature for 10 minutes. A 25 μ L aliquot was removed to determine the 0-minute time point, and then the polymer catalyst

was added (100 mol% N), measured in air. The reaction vessel was sealed and placed into 50 °C oil bath. Samples were removed over 4 hours and rinsed through a silica plug with acetone to remove catalyst. Conversion (%) was determined through GC with FID.

2.3 Materials Synthesis

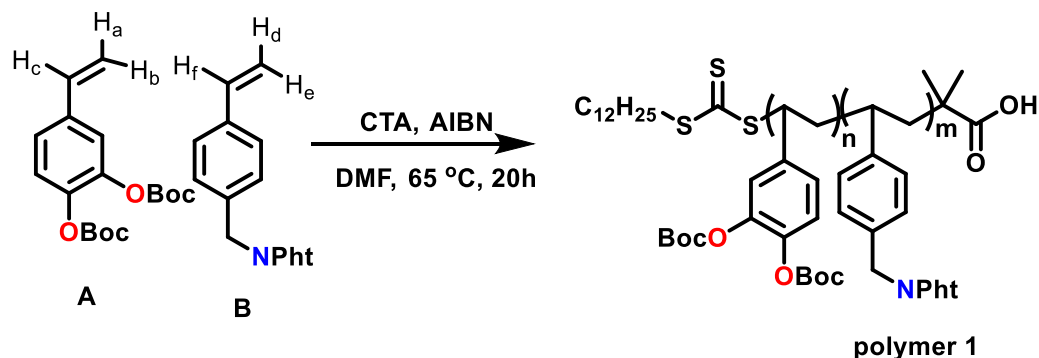


Figure 2.1: Typical polymer synthesis by RAFT polymerization.

Polymer 1: A typical procedure for RAFT polymerization was as follows: Monomer **A** (0.300 g; 0.892 mmol, 50 equivalents) and monomer **B** (0.235 g; 0.892 mmol, 50 equivalents) were dissolved in 1.4 mL of DMF. Then, dodecyl propionic acid chain transfer agent (0.0065 g; 0.0178 mmol, 1 equivalent) and AIBN (0.001 g; 0.00178 mmol, 0.1 equivalents) and 1,3,5-trioxane as the internal standard were dissolved. The reaction mixture underwent four cycles of freeze, pump, thawing. The line was purged with flowing argon three times, then the flask was backfilled with argon. The reaction was polymerized at 65 °C for 20 hours. Monomer conversion reached 55%, as determined through ¹H NMR analysis and the disappearance of peaks at 5.7 and 5.2 ppm (Figure 2.2). The reaction mixture was purified by dialysis in acetone with a 2 KDa MWCO (Spectrum Laboratories, CA, USA). Pure **polymer 1** was obtained by removal of

acetone through rotary evaporation, leaving a pale yellow solid. The number of repeat units in the polymer was determined through GPC using polystyrene standards. The molecular weight distributions determined by GPC using THF as the eluent were: $M_n = 6200$ g/mol, $D = 1.35$

2.3.1 *Boc-deprotection for copolymer catalysts*

Copolymer catalysts (200 mg) were dissolved in 10 mL of acetone with an excess of TFA and stirred at room temperature overnight. Acetone and TFA were removed by rotary evaporation and the residue was dissolved in methanol for the next deprotection step. The crude copolymer was a light yellow solid.

2.3.2 *Phthalimide deprotection of copolymer catalysts*

Crude copolymer from the boc-deprotection was dissolved in ethanol, and an excess of $\text{NH}_2\text{NH}_2 \cdot \text{H}_2\text{O}$ was added. The mixture was placed in an oil bath at 60 °C overnight. The deprotected copolymer was then filtered with 200 mL of ethanol, 100 mL of DI H_2O , and then 200 mL of ethanol. The final crude polymer was a lavender solid. The deprotection of the polymer was confirmed using FTIR by the lack of a carbonyl peak, suggesting boc deprotection, and appearance of amine stretch at 3360 cm^{-1} , associated with the primary amine.

2.3.3 *Porous Organic Polymer Synthesis*

The synthesis of the POP was adapted from previous literature.¹⁶³ In a 250 mL pressure tube, DVB (2.0 g) the vinyl **diol** (7.68 mmol) and **ba** (7.68 mmol) monomers were dissolved in THF (50 mL) with 0.2 g of AIBN. 1 mL of DI H_2O was added to the

solution, and stirred in a pressure flask at 100 °C for 24 h. The resulting white solid was filtered with excess THF, and dried overnight under reduced pressure.

2.4 Materials Characterization

Table 2.1: Characterization of various copolymer catalysts

Polymer	$M_{n, \text{NMR}}$ (g/mol)	$M_{n, \text{GPC}}$ (g/mol)	\bar{D}	Units	N wt%
Homo $-\text{NH}_2$	8,700	4,100	1.21	16	20.24
Random 1:1_ $-\text{OH}:\text{NH}_2$	16,500	6,200	1.35	21	5.00
Random 1:1_ $-\text{COOH}:\text{NH}_2$	13,000	4,000	1.22	21	4.68
Ratio 1:4_ $-\text{OH}:\text{NH}_2$	21,300	10,100	1.38	32	6.39
Ratio 4:1_ $-\text{OH}:\text{NH}_2$	14,100	6,900	1.27	25	2.68
Block $-\text{NH}_2$, OH	8,700, 22,200	5,100, 8100	1.35, 1.89	19, 40	5.95
Block $-\text{NH}_2$, COOH	8,700, 16,800	5,100, 8,200	1.35, 1.51	19, 40	5.95

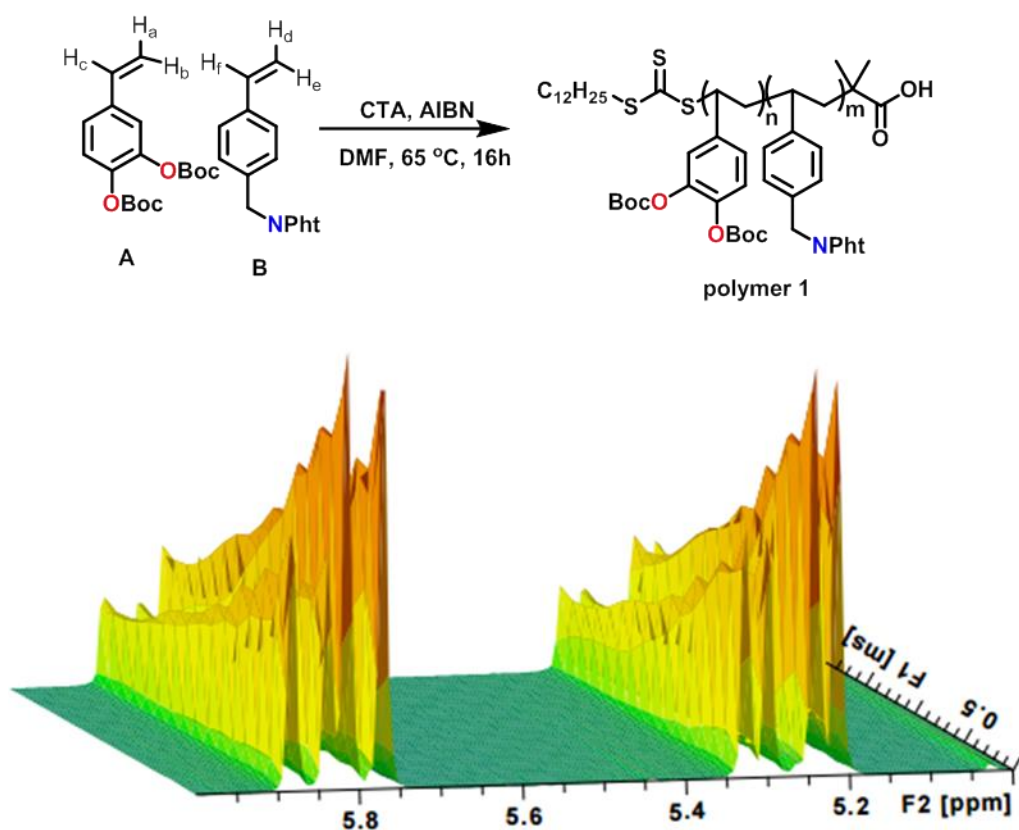


Figure 2.2: ¹H NMR spectra of in situ polymerization.

Monomer A (110 mg, 0.327 mmol) and monomer B (86 mg, 0.327 mmol), 2-(dodecylthiocarbonothioylthio)-2-methylpropionic acid (0.002 mg, 0.00654 mmol), Azobis(2-methylpropionitrile) (~1 mg, 0.00065 mmol) was added to DMF-*d*₇ (0.75 mL). The polymerization was carried out in a J. Young NMR tube. This reaction solution was freeze-pump-thawed five times to remove oxygen and was heated to 65 °C under argon for 16 h. The NMR data were collected *in situ* for each hour (relaxation time = 10 seconds).

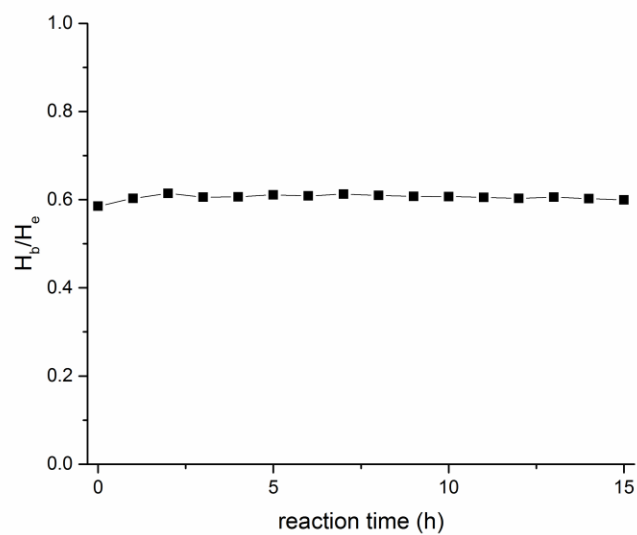


Figure 2.3: Integration ratio of the vinyl protons of monomer A (H_b) and monomer B (H_e) during in situ polymerization. The unchanging ratio demonstrates that the polymerization occurred in a random manner.

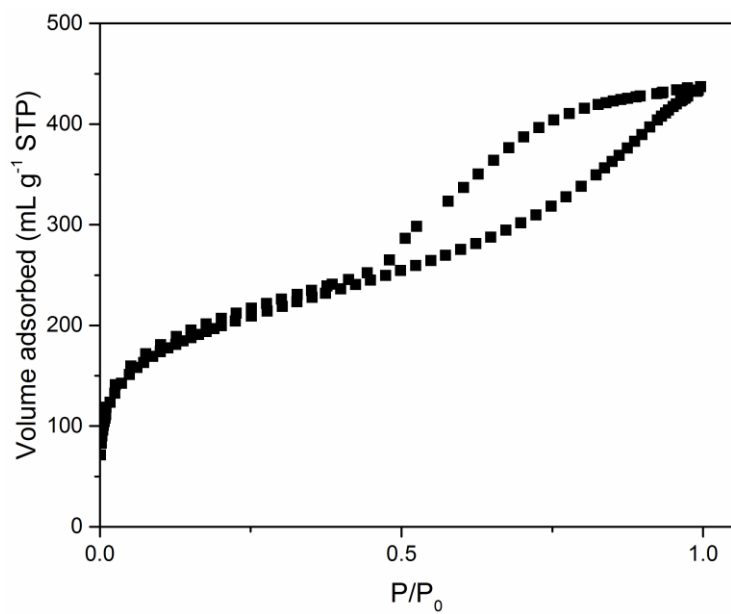


Figure 2.4: Nitrogen physisorption isotherm of POP-diol:ba.

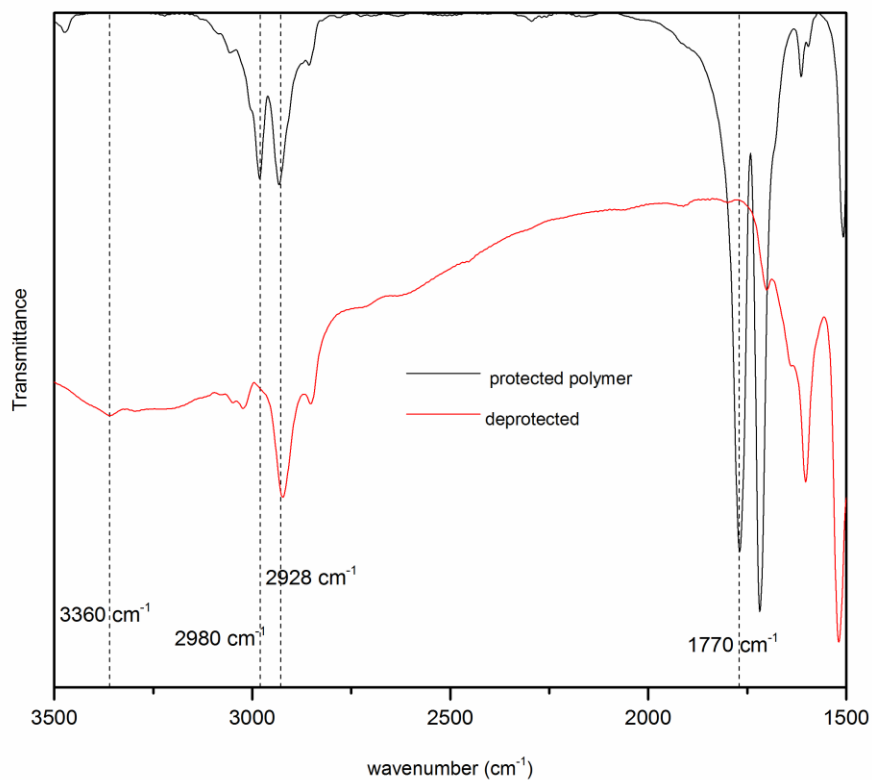
Table 2.2: Surface area and pore volume of POP-**diol:ba**

Sample	BET Surface Area (m ² /g)	Pore Volume (cm ³ /g)
POP- diol:ba	700	0.7

Table 2.3: Elemental analysis of POP-**diol:ba***

Catalyst	N wt%	C wt%	H wt%
POP-diol:ba	1.55	85.33	7.58

*remaining 5.5 wt% is oxygen from diol monomer incorporation

**Figure 2.5:** IR spectra of the protected and deprotected random 1:1 **diol:ba** catalyst.

Deprotection is evidenced by the loss of the carbonyl peak at 1770 cm^{-1} and 2980 cm^{-1} corresponding to the methyl, associated with the -Boc group, and appearance of the N-H stretches around 3360 cm^{-1} and remaining 2928 cm^{-1} methylene stretch of polymer backbone and benzylamine.

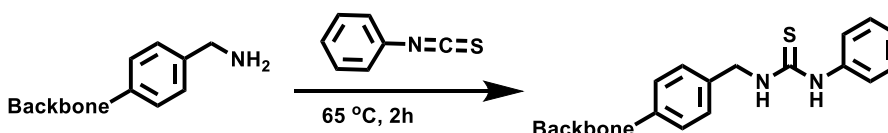


Figure 2.6: Amine coupling reaction used to quantify the accessible amines in the insoluble random 1:1 **diol:ba** copolymer catalyst.

Table 2.4: Elemental analysis of phenylisothiocyanate coupled random 1:1 **diol:ba** copolymer catalyst

Element	C	H	N	S
Initial	68.46	7.19	5.05	0
Final	73.93	7.78	5.42	0.88

2.5 Results and Discussion

2.5.1 Homogeneous Catalytic Pairs

For cooperatively catalyzed aldol and nitroaldol reactions using amine-modified silica catalysts, previous literature has shown that weak acids in tandem with a simple primary amine base have cooperatively catalyzed the reactions most efficiently, relative to primary amines paired with stronger acids. In early work, various acid-base pairs on functionalized mesoporous silica supports were investigated by pairing a phosphoric acid, an aromatic sulfonic acid, or a carboxylic acid with a primary amine group for a model

aldol condensation reaction between functionalized benzaldehydes and acetone.^{138,164,165} The results showed that the carboxylic acid with the primary amine catalyzed the aldol condensation most efficiently. Further extrapolating from this concept, Brunelli identified that surface silanols cooperatively interact with aminosilanes to catalyze the aldol condensation more effectively compared to the carboxylic acid.¹⁶⁴ To this end, we sought to identify a reactive olefinic organic monomer with similar acidity to the silanols of mesoporous silica with which to pair a primary amine base. A dihydroxy-functionalized styrene monomer was identified as a suitable functional monomer with appropriate acidity. The diol unit incorporates two alcohol functionalities, (loosely) akin to a silanol-laden silica surface, while maintaining an acidity similar to surface silanols.¹⁵⁷ Although carboxylic acids were shown to be less useful than silanols as amine partners on silica supports, we hypothesized that the ability to control the location of the acid and base sites to a degree via controlled polymer syntheses may allow these sites to be more useful in polymeric systems than they were in the silica catalysts. To this end, a carboxylic acid containing monomer was also employed.

Primary amines have been shown to be highly efficient in the aldol condensation. As they are the most well-studied amine species in the silica-supported cooperative catalysts, we chose to incorporate a primary amine into the basic monomer used in the bifunctional polymer synthesis. To screen the reactivity of the different potential active sites, benzylamine and phenylamine were chosen as candidate active sites with different base strengths, with resonance through the ring possible in phenylamine, decreasing basicity. The benzylamine base gives increased basicity and also incorporates a small degree of flexibility due to the methylene spacer, which was previously identified in the

mesoporous silica literature as a useful feature to enhance cooperative interactions of amines with the surface silanols.⁷⁰

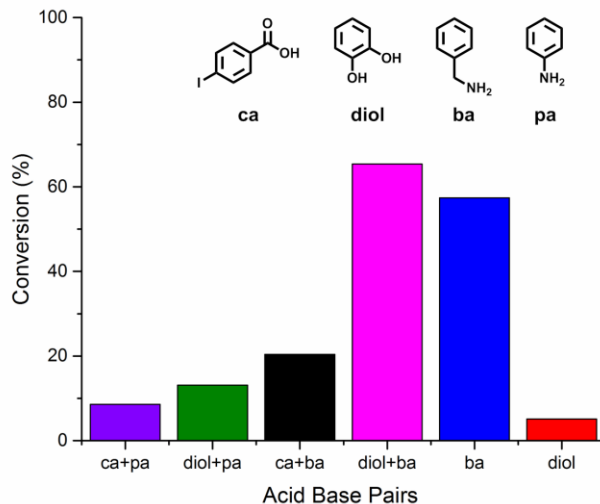


Figure 2.7: Conversion (%) of various homogenous acid and base pairs for the aldol condensation of 4-nitrobenzaldehyde and acetone at 50 °C under flowing Ar at 10 mol% of amine after 4 hours.

Figure 2.7 displays the catalytic performance of each homogenous, small molecule catalyst, and as expected from the trends derived from the porous silica systems studied, the stronger carboxylic acid (**ca**) paired with benzylamine (**ba**) showed diminished activity compared to the weakly acidic diol unit (**diol**) paired with benzylamine, likely due to an increased degree of neutralization with the larger pK_a difference between **ba** and **ca**. The degree of neutralization of relatively strong acid and base sites can potentially be reduced by heterogenizing the moieties on a surface such as silica,¹⁶⁴ or potentially on a polymer backbone. **Pa** paired with the acidic **diol** or **ca** showed minimal conversion of 4-nitrobenzaldehyde due to the reduced basicity of the amine in resonance with the aryl ring, showing that insufficient basicity leads to poor

catalytic activity.^{150,151,166} The conversion observed for **ba** alone corresponds to the aldol condensation being effectively catalyzed by a base only, though it is clear that the conversion can be enhanced through the addition of a weak acid such as the **diol**.^{69,150,151,70,152,153,158} Thus, the trend of enhanced reactivity from the pairing of a weaker acid with the primary amine with suitable basicity, as observed in the silica systems, was replicated with this simple study of small molecules. This forms the basis for the monomer design for use in polymer supported cooperative catalysts.

We next sought to test this cooperativity between the two acids (**diol**, **ca**) and optimal base (**ba**) sites using functional groups tethered to a polystyrene support. For this purpose, functionalized styrene monomers approximating the optimized homogeneous acid-base pair were prepared,^{167,168,169} as shown in Figure 2.8. Additionally, the commercially available 4-vinylbenzoic acid was utilized as the corresponding **ca** monomer.

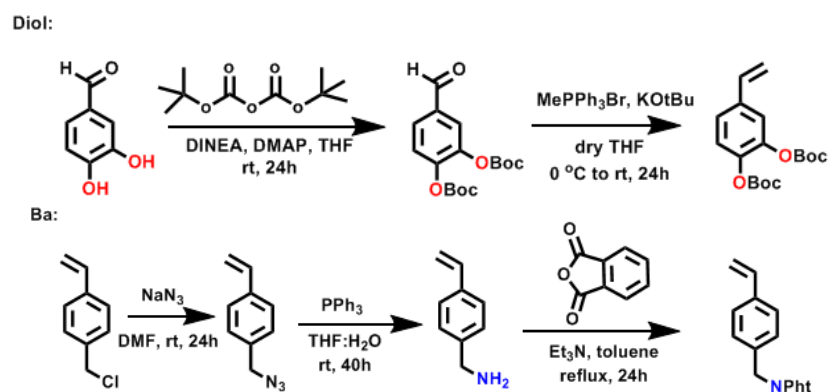


Figure 2.8: Synthesis of the weak-acid (**diol**) and amine-base (**ba**) styrene monomers, in protected form.

The protected **diol** and **ba** monomers were copolymerized through reverse addition-fragmentation chain-transfer (RAFT), producing polymers with low polydispersities and short chain lengths, to ensure the array of polymers with varying composition were similar in overall structure.¹⁷⁰ The polymerizations were monitored using ¹H NMR to follow the disappearance of the vinyl peaks associated with each monomer. The vinyl peaks of both the **diol** and **ba** monomers decreased at the same rate, indicative that the copolymerization was random (Figure 2.3).¹⁷¹¹⁷² Use of RAFT polymerization with protected monomers allowed access to random and block sequenced copolymer catalysts incorporating either **diol** and **ba** units, or **ca** and **ba** units, as well (Figure 2.9). All of these catalysts were synthesized as linear polymer chains containing between 20 and 30 repeat units (Table 2.1).

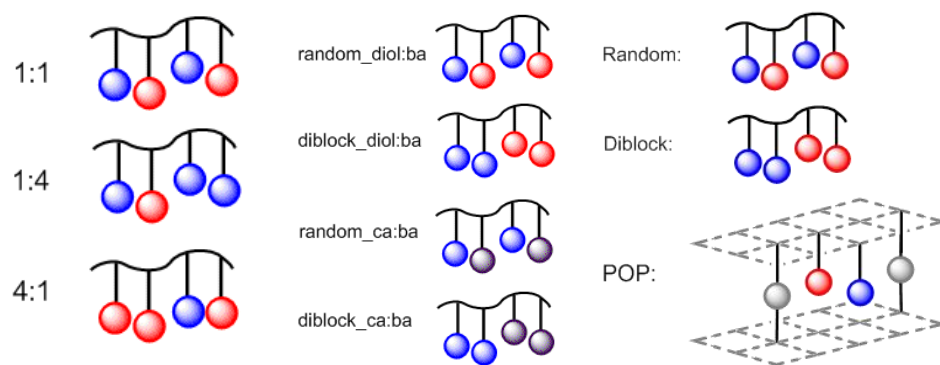


Figure 2.9: Illustration of various polymer catalyst sequence, (left) varying ratio of monomers, (center) various acid monomers and sequence, and (right) overall catalyst structure.

2.5.2 Catalyst Loading and Characterization

Once the polymers were fully deprotected through sequential deprotection steps, the polymers became insoluble in various solvents ranging from hexane to deionized water. Therefore, a range of techniques was used to characterize these polymers molecular weights, polydispersities, and active sites aside from classic solution state ^1H -NMR spectroscopy. A straightforward qualitative characterization was carried out using infrared spectroscopy, which was used to support the complete deprotection of both protecting groups on the polymer via the disappearance of the C=O stretch at approximately 1770 cm^{-1} and formation of a small peak around 3360 cm^{-1} that can be attributed to an aliphatic N-H stretch (Figure 2.5).

Initial catalytic studies began with the 1:1 **diol:ba** polymeric catalyst with a random distribution of acid and base sites at an amine loading of 10 mole %, conditions that allowed direct comparison to the silica catalysts widely described in the literature. Interestingly, the conversion of 4-nitrobenzaldehyde with acetone after 24 hours reached only 9.3 %. Under the same conditions, a typical aminopropyl-functionalized mesoporous silica catalyst achieved 65% conversion.¹⁷¹ Subsequently, increased catalyst loadings were explored, up to an apparent catalyst loading of 100 mole % (Figure 2.11). At an apparent 100% catalyst loading, the apparent initial TOF was 2.1 h^{-1} , which is slightly lower compared to aminosilica catalysts studied previously ($\sim 2.6\text{ h}^{-1}$).⁶⁹ These data may appear to suggest that the base and acid sites attached to the polymer backbone are inherently less active than those associated with the aminosilica catalysts. However, the apparent catalyst loading does not necessarily equal the amount of available active sites for catalysis. As noted above, the polymers were not fully soluble under the reaction

conditions employed (the polymers were not soluble in most solvents, see above, and only a small number of sites may be accessible to the reactants). Indeed, we hypothesized that the apparent catalytic activity may be associated with only sites on the external surface of the collapsed polymer chains, meaning there may be few accessible diol and benzylamine groups.

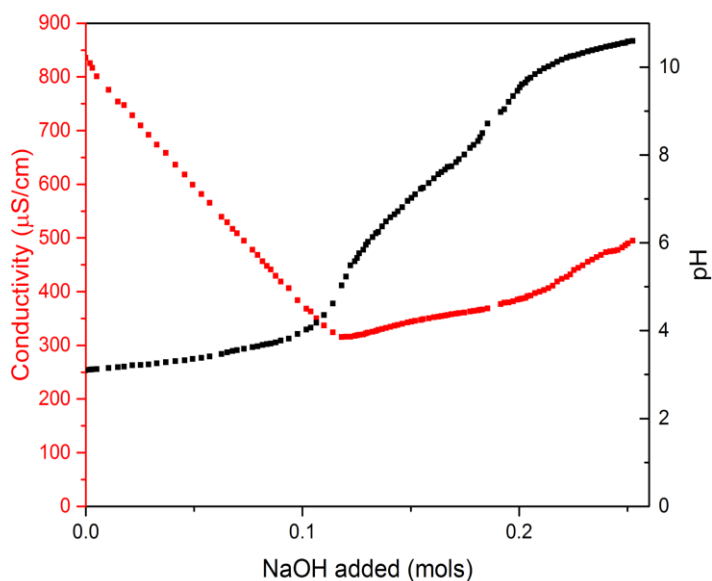


Figure 2.10: Titration curve of the 1:1 **diol:ba** random copolymer catalyst in DI water in the presence of 0.010 M NaOH at 25 °C.

To probe the amount of accessible acid sites, the random 1:1 **diol:ba** copolymer was titrated using sodium hydroxide. The titration curves display diprotic acid characteristics; the first equilibrium point was attributed to neutralization of excess HCl and occurred at approximately pH ~7, while the second equilibrium point was the conversion of accessible **diol** units to ketones around a pH ~9 . Based on the titration results, approximately 8 mol % of diols were accessible, indicating that only a small

fraction of the diol units on the exterior of the polymer chains were accessible for catalysis. Further, a coupling reaction was carried out using phenylisothiocyanate to titrate the number of accessible primary amines on the external surface of the polymer. Elemental analysis of the recovered, reacted polymer showed a sulfur content of 0.88 wt %, corresponding to 8.5 mole % of amine reacted (Figure 2.6), in good agreement with the titration value of 8 % accessible diols (Figure 2.10). Through these two methods, similar amounts of both diol and benzylamine were available for cooperative catalysis. Based on these results, the actual TOF for the 1:1 **diol:ba** copolymer catalyst was 25 h^{-1} , which is well above the initial TOF observed for the aminosilica catalyst discussed above.

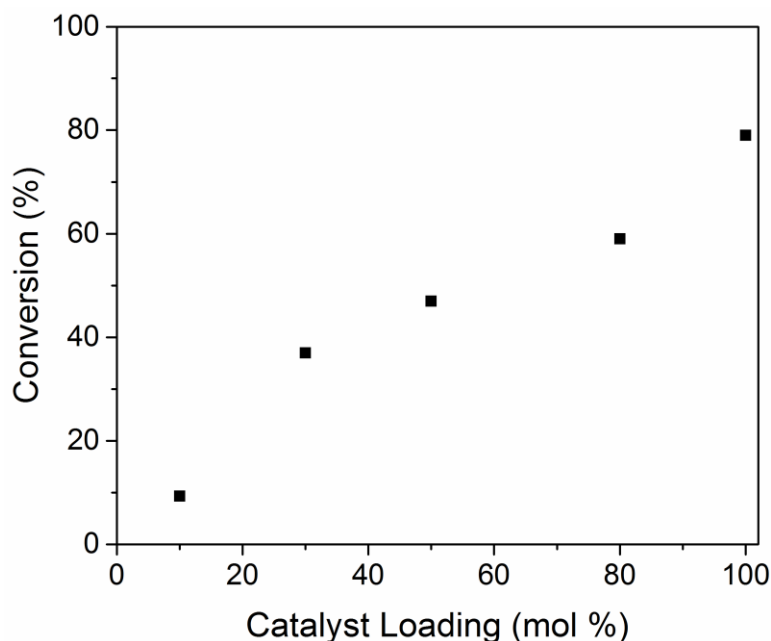


Figure 2.11: Conversion of 4-nitrobenzaldehyde with acetone at various 1:1 **diol:ba** catalyst loading based on CHN analysis at 50 °C over 24 hours. Catalyst loading at 100 mol% shown after 4 hour reaction time.

2.5.3 *Solvent effects on catalyst activity*

Due to the insolubility in the array of solvents explored, a range of cosolvents was examined in pursuit of partially or fully solubilizing the linear polymer catalysts. Because acetone was used as a solvent as well as reactant, each reaction co-solvent was in a 50:50 volume ratio of acetone:cosolvent. In a range of polarities, from hexane to water, the linear chains did not fully solubilize. This is attributed to the highly functionalized chains and high degree of hydrogen-bonding that is possible within the monomer units, as well as intermolecularly with neighboring chains.¹⁷³ Lastly, the polymer is a styrene based system, which is poorly solubilized in acetone. These data suggest that spacer monomers are needed in next generation polymer catalysts, better separating the acid and base sites as well as a different ketone coupling partner.

The observed catalytic activity associated with the array of solvent mixtures is given in Table 2.5. For the random 1:1 **diol:ba** polymer system, more useful reaction co-solvents appeared to have moderate polarity, such as dichloromethane. In nonpolar solvents, such as hexane, reports have shown the promotion of the low activity imine pathway with primary amine catalysts.^{174,166} A recent study that explored the effect of water on an amine-functionalized silica based catalyst in the aldol condensation showed that water pushed conversion to quantitative yield over the course of one hour. The reaction rate increased 10 fold in that study with the replacement of hexane with water using aminopropyl functionalized silica nanoparticles.¹⁷⁴ These results are consistent with the observed trends here, with toluene offering the slowest rate and water the highest, different by about a factor of 10. The enhanced rate in water has been suggested to be due to a reduced likelihood of imine formation in the aldol mechanism, a non-productive

pathway that inhibits product formation.^{149,59} Similar effects of enhanced product yields and selectivities in the presence of water have been reported with homogeneous proline catalyzed aldol condensations as well.^{175,176} Acetone offered a higher initial rate than other solvents of intermediate polarity, likely due to the fact that acetone was both a solvent and a reactant, with the reaction being kinetically positive order in acetone.

Table 2.5: Comparison of initial turnover frequencies (TOFs) for different solvent systems using the random 1:1 **diol:ba** catalyst^a

Solvent system	Dielectric Constant	Initial TOF(h⁻¹)
Toluene	2.38	4.7
Dichloromethane	8.93	13
Acetone	20.7	25
Acetonitrile	36.6	10
H ₂ O	80.1	47

^{a)} TOFs reported are determined through the initial linear region of the plot in Figure 2.12

A noteworthy trend that can be gleaned from the conversion/time profiles plotted in Figure 2.12 is the plateau in conversion observed when using water/acetone and acetone solvent systems.

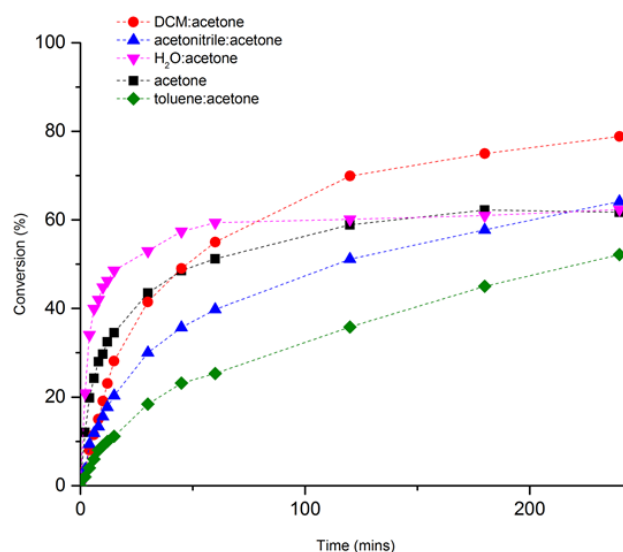


Figure 2.12: Kinetic curves of reactions using the random 1:1 **diol:ba** catalyst using different cosolvents in the aldol condensation with 100 mol% amine loading, as determined by elemental analysis. TOFs reported in Table 2.5 are determined through the initial linear region of the plot, and TON determined from final conversion determined by GC after 240 minutes.

A fundamental understanding of this plateau is not available at this stage, though it should be noted that equilibrium constants for many ketone-aldehyde aldol condensations lie only slightly on the side of products and excess water may limit the final equilibrium conversion.¹⁷⁷ Also, this system could also undergo an unfavorable catalyst transformation that limits catalytic activity, such as oxidation of the diol moieties. Proton transfer from the diol monomer, a hypothesized part of the catalytic mechanism, might promote oxidation of the diol to a benzoquinone species, thus removing the acidic species needed for cooperative catalysis with neighboring amines.^{178,179} As noted below, the diols have been observed to oxidize after extended use or storage. As further conviction of catalytic activity, a leaching test was performed and activity of the reaction was terminated upon removal of the cooperative polymer catalyst

demonstrating no free small chain polymer present or leaching of active species off the polymer chain.

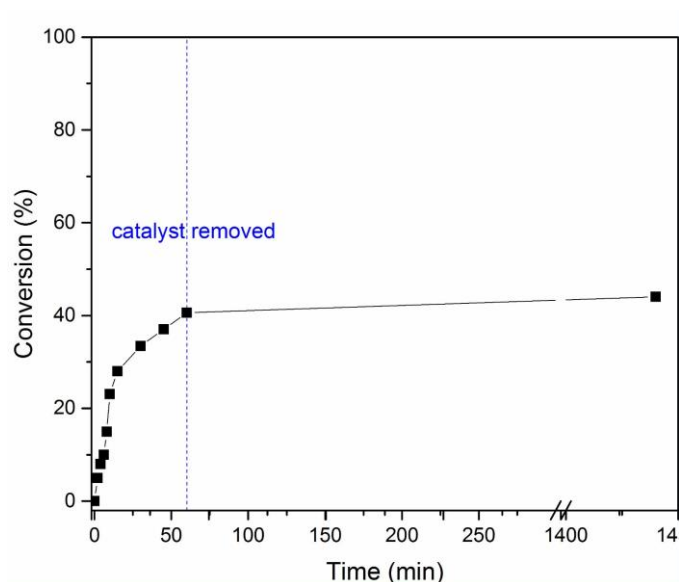


Figure 2.13: Leaching test kinetic plot. Catalyst removed at 60 minute, and time point taken after 24h. Hot filtration of catalyst to remove polymer, and reaction solution continued stirring at 50 °C.

2.5.4 Catalyst Architecture effects on reactivity

2.5.4.1 Random sequence polymer catalyst structure effects

Building from these initial studies with the random 1:1 **diol:ba** copolymer and an appropriate solvent system, further elucidation of catalytic cooperativity was investigated using a series of random copolymers with different ratios of monomers and with diblock copolymers, containing each active site segregated into separate domains.

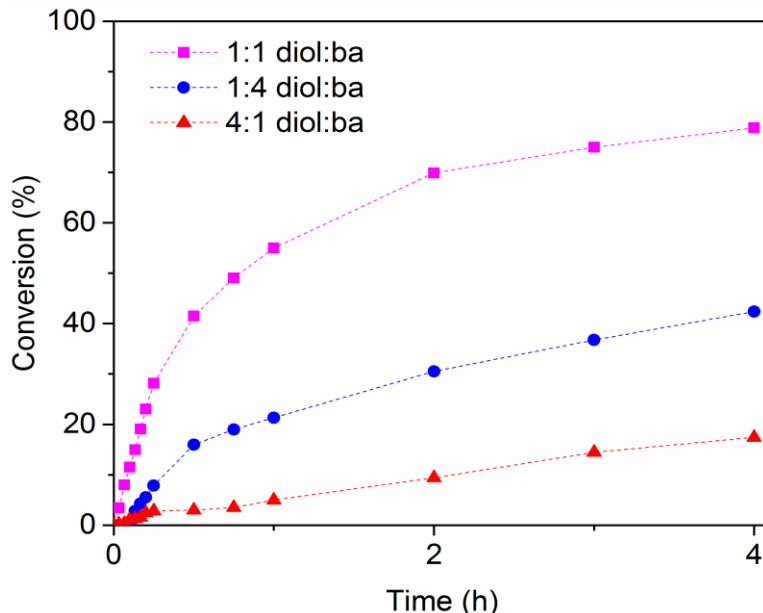


Figure 2.14: Conversion of 4-nitrobenzaldehyde in the aldol condensation of 4-nitrobenzaldehyde with acetone in dichloromethane for copolymer catalysts that contain various ratios of acid and base sites at 50 °C using an apparent catalyst loading of 100 mol % amine.

The random 1:1 **diol:ba** copolymer catalyst exhibited the highest reaction rate, suggesting a high degree of cooperativity in a catalyst with an equal number of acid and base sites (Figure 2.14, pink). The importance of the amine base sites as the primary active sites and the supporting role of the weak acids is evident in comparing the kinetics of the random 1:4 **diol:ba** catalyst (Figure 2.14, blue) and the random 4:1 **diol:ba** (Figure 2.14, red). The amine rich catalyst (1:4 **diol:ba**) was more active than the amine poor catalyst (1:4 **diol:ba**). This may be associated with a higher number of accessible base sites on the external surface of the collapsed polymer owing to the larger fraction of amine sites in the polymer. The lower activity of the amine poor catalyst may be associated with too few primary active sites. The higher activity of the catalyst with an

approximately equal number of acid and base sites is consistent with enhanced rates due to cooperative catalysis.

Table 2.6: Aldol condensation catalyzed by singly deprotected 1:1 **diol:ba** catalysts

Entry	Catalyst	Yield of 1 [%]
1	None	N.R.
2	Protected copolymer	N.R.
3	Copolymer-OH	10
4	Copolymer-NH ₂	18

Cooperative catalytic activity was highest with freshly deprotected 1:1 **diol:ba** catalysts exposing both **diol** and **ba** units. In Table 2.6, catalytic activity is displayed with singly deprotected materials. Activity was severely decreased with roughly 10% conversion with exposed **diol** and 20% with deprotected **ba**. Upon observation of the catalyst after the reaction, the catalyst color had darkened somewhat. Further, when the catalysts were intentionally aged in air before reaction, the color also darkened. These materials were then tested for catalytic activity. The activity of the catalyst was reduced down to the activity of a singly deprotected **ba** catalyst, likely attributed to aerobic oxidation of the **diol** monomer.^{178,179} This observation supports the necessity of the presence of both weak acid and base for optimal catalytic activity, as well as future catalyst design opportunities with alternative weak acids.

2.5.4.2 Block sequence polymer catalyst structure effects

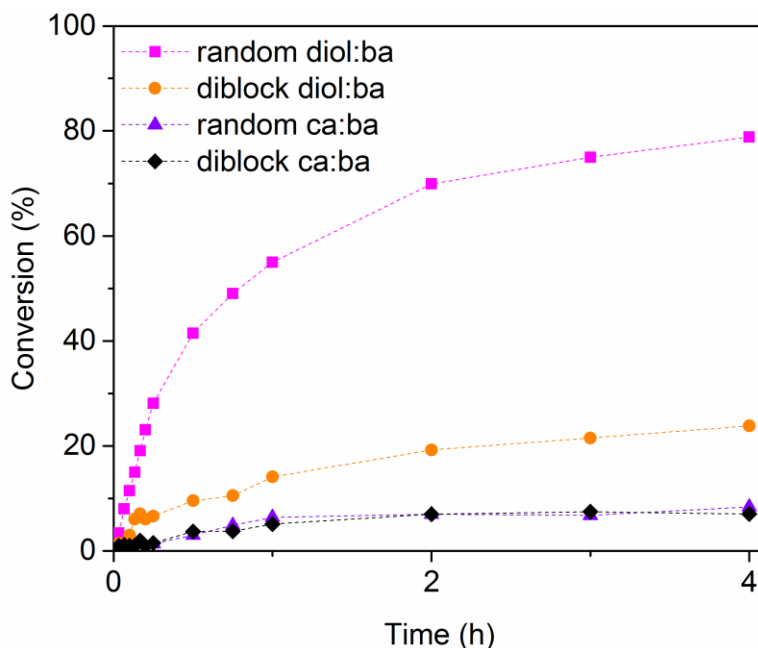


Figure 2.15: Conversion of 4-nitrobenzaldehyde in the aldol condensation with acetone in dichloromethane for various copolymer catalysts containing different acid strength monomers and different monomer sequences at 50 °C using a catalyst loading of 100 mol % amine.

The impact of acid strength and monomer sequence distribution (1:1 acid: amine ratio) was also explored at the standard, apparent 100% amine loading. Two copolymers were synthesized using 4-vinylbenzoic acid (**ca**) and benzylamine (**ba**) in random and block structures. Both of these copolymers were relatively poor catalysts, with an initial TOF of 0.7 h^{-1} and minimal conversion after 4 h (Figure 2.15). Amongst the 1:1 **diol:ba** catalysts, the random copolymer proved to be far more active than the block copolymer. This observation supports the notion that distribution of the amine sites amongst the weak acid sites, as in a random copolymer, leads to more effective cooperativity than isolation of the amines and acid sites in separate domains.

2.5.4.3 Overall catalyst structure effects

2.5.4.3.1 Porous Organic Polymers

Porous organic polymers (POP) are an emerging class of supports that create mesoporous networks with divinyl benzene as the main component of the structure. This support has a simple synthesis, and creates a porous support that classic polymer resins with divinyl benzene lack. Tuning the pore size of the mesopores benefits different types of catalysis, while functionalization of the aryl rings of the support are another route to incorporating catalytic sites.^{180,163} Alternatively, the incorporation of polymerizable ligands have been utilized in these structures.¹⁸¹

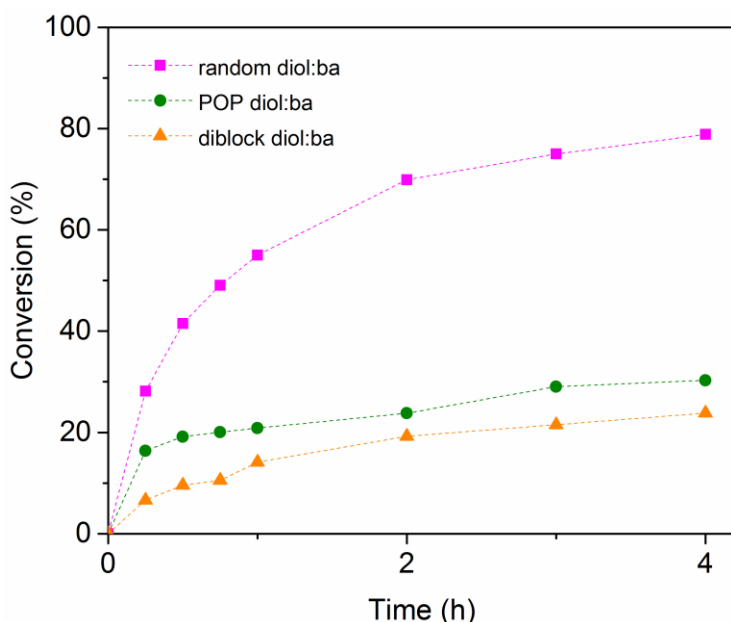


Figure 2.16: Conversion of 4-nitrobenzaldehyde in the aldol condensation with acetone in dichloromethane for various copolymer catalyst structures containing 1:1 diol:ba at 50 °C using a catalyst loading of 100 mol % amine.

The impact of overall polymer architecture effects the rate of product formation greatly. POP **diol:ba** is representative of a porous organic polymer that is made from the copolymerization of **diol**, **ba**, and divinylbenzene monomers in THF with water as a coporogen and AIBN as the initiator.¹⁶³ The overall structure of this support is rigid and analogous to the mesoporous silica supports previous used in literature, but eliminates the effects of the acidic silanol surface. However, due to the randomness of the polymerization, it can be assumed that active monomers are not in proximity to cooperatively interact. Again, the block copolymer has isolated the cooperative species so this sequence of polymer is not ideal for cooperativity. The random **diol:ba** copolymer was the superior support structure for cooperatively catalyzing the aldol condensation of 4-nitrobenzaldehyde in acetone.

2.6 Conclusions

Most prior catalyst design work using amine/acid hybrid catalysts for aldol reactions has focused on silica supported catalysts. In this work, an array of polymer catalysts was developed for the aldol condensation, demonstrating cooperativity with a diol and benzylamine functionality. The use of polymeric catalyst offers the catalyst designer different, and perhaps more, degrees of freedom in the design of cooperative acid/base catalysts. RAFT polymerization provided linear polymer chains that were insoluble heterogeneous catalysts that, at high apparent catalyst loadings, efficiently catalyzed the aldol condensation. This first generation of linear polymer catalysts provides a highly tunable platform to further build cooperative catalysts and begin to explore fundamental concepts such as monomer placement within overall linear

polymeric architectures. With a low accessible catalyst loading in this work (ca. 8%), revised polymer designs are expected to allow for enhanced cooperativity and activity.

CHAPTER 3.

HYDROBORATION OF SUBSTITUTED ALKYNES USING A SOLID POLYMERIC CARBOXYLIC ACID CATALYST

3.1 Introduction

Transition metal-catalyzed addition reactions with boron-containing compounds with alkynes (or olefins) to form carbon-carbon bonds remains a vital tool in organic synthesis.^{182,85} The resulting alkynylboronic ester product of these additions are air and thermally stable, and easy to handle for further transformations.⁸⁴ In recent years, there has been a push for metal-free alternative catalytic routes for these hydroborations without compromising yields or substrate scope. Early examples of uncatalyzed hydroborations were reported in 1959 by Brown, showing the first uncatalyzed hydroboration of unsaturated olefins using elevated temperatures.⁷¹

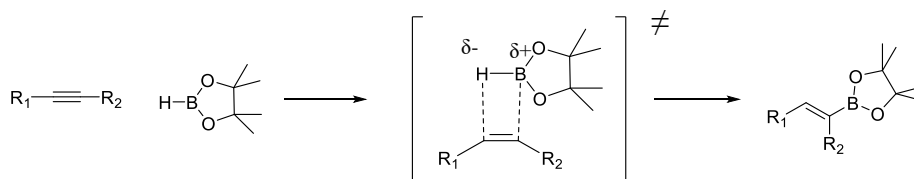


Figure 3.1: Uncatalyzed hydroboration reaction with alkyne and pinacolborane.

Over the years, the work was expanded to include base-catalyzed hydroborations using alkali metals,^{183,184} frustrated Lewis pairs,^{185,186,187,188} amides,¹⁸⁹ NHCs¹⁹⁰ and an acid¹⁹¹ as examples of metal-free alternative catalysts for hydroboration reactions using a variety of boron sources and unsaturated compounds.¹⁹²

Many times high performing, and expensive, transition metal catalysts do not have the ability to be recycled. Heterogenizing a highly reactive zirconium hydride complex improved recycle and reuse of the typically water sensitive complex when supported on silica.¹⁰⁶ One of the few examples using a polymer support catalyzed the borylation of α,β -unsaturated acceptors with $\text{Cu}(\text{OH})_2$ and recycled the catalyst 6 times, which would otherwise not be possible.¹⁰⁰ To date, organocatalytic polymers have yet to be examined for this reaction, which provide a tunable platform for immobilizing catalytic species, and provides a recyclable handle.

Herein we demonstrate the use of a linear polymer support with acidic functionalities that performs as well as the soluble acid catalyst. Quantitative yields of various substituted alkynes were reached, and the polymer catalyst was facily separated from the reaction solution and reused at least 3 times without loss of yield. Moreover, a mechanistic understanding of this reaction can facilitate the future design of organocatalysts for hydroborations. Kinetic isotope effect (KIE) determination indicates the rate limiting step is a rehybridization of the alkyne, while the experimental rate orders determined an inverse first-order dependence on both reactants and first-order dependence on the catalyst concentration. Further NMR studies were conducted to assign intermediate structures throughout the reaction, with the identification of a nonactive

acid-boron adduct formation, which temporarily occupies active sites throughout the reaction.

3.2 Experiments

3.2.1 *Nuclear Magnetic Resonance studies of intermediates*

3.2.1.1 Benzoic acid and pinacolborane

In a nitrogen-filled glove box, a Norell standard series 5 mm NMR tube was charged with 1:1 equivalent of benzoic acid and pinacolborane (HBPin) and 0.7 mL of *d*-octane. ^1H NMR and ^{11}B NMR spectra were recorded at 30 °C on a Bruker AVIII-400 spectrometers. All chemical shifts were recorded in parts per million (ppm) with reference to residual solvent peaks. The reaction was monitored over 24 h, until complete consumption of HBPin. In a glove box, 1 equivalent of phenylacetylene was added to the NMR tube.

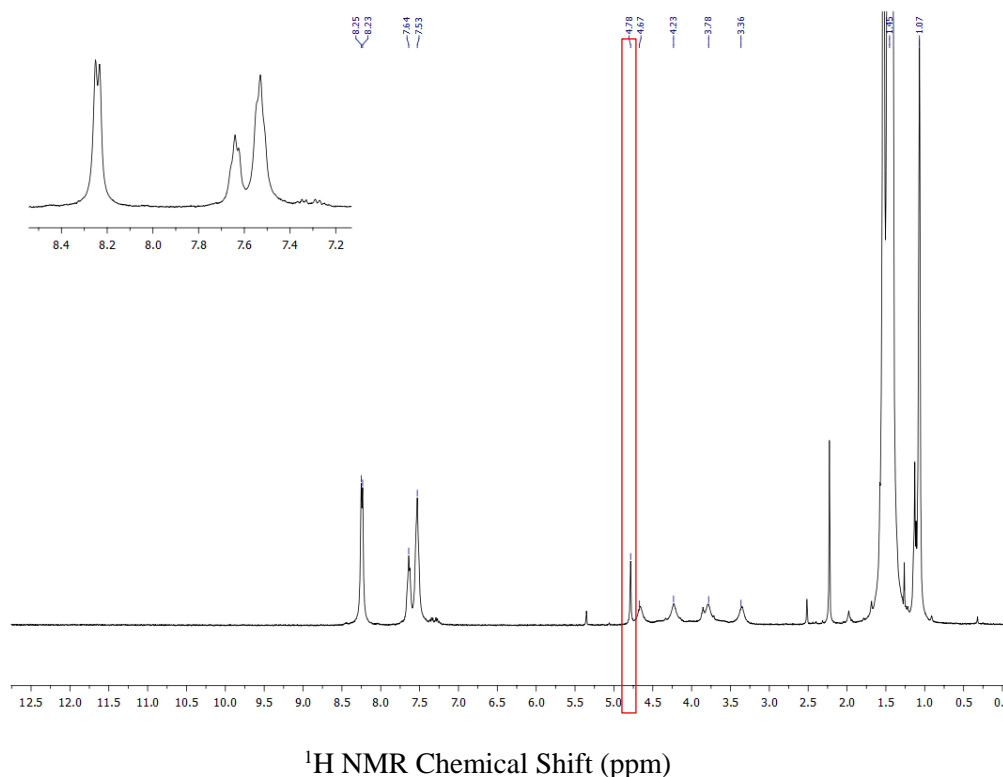


Figure 3.2: ^1H NMR of benzoic acid and HBPin in *d*-octane at 30 °C after 20 min. H_2 evolution at 4.78 ppm (red).

3.2.1.2 Poly(vinylbenzoic acid) and pinacolborane

In a nitrogen-filled glove box, a Norell standard series 5 mm NMR tube was charged with 1:1 equivalent of poly(vinylbenzoic acid) [poly(vba)] and pinacolborane (HBPin) and 0.7 mL of *d*-octane. ^1H NMR and ^{11}B NMR spectra were recorded at 30 °C on a Bruker AVIII-400 spectrometers. All chemical shifts were recorded in parts per million (ppm) with reference to residual solvent peaks.

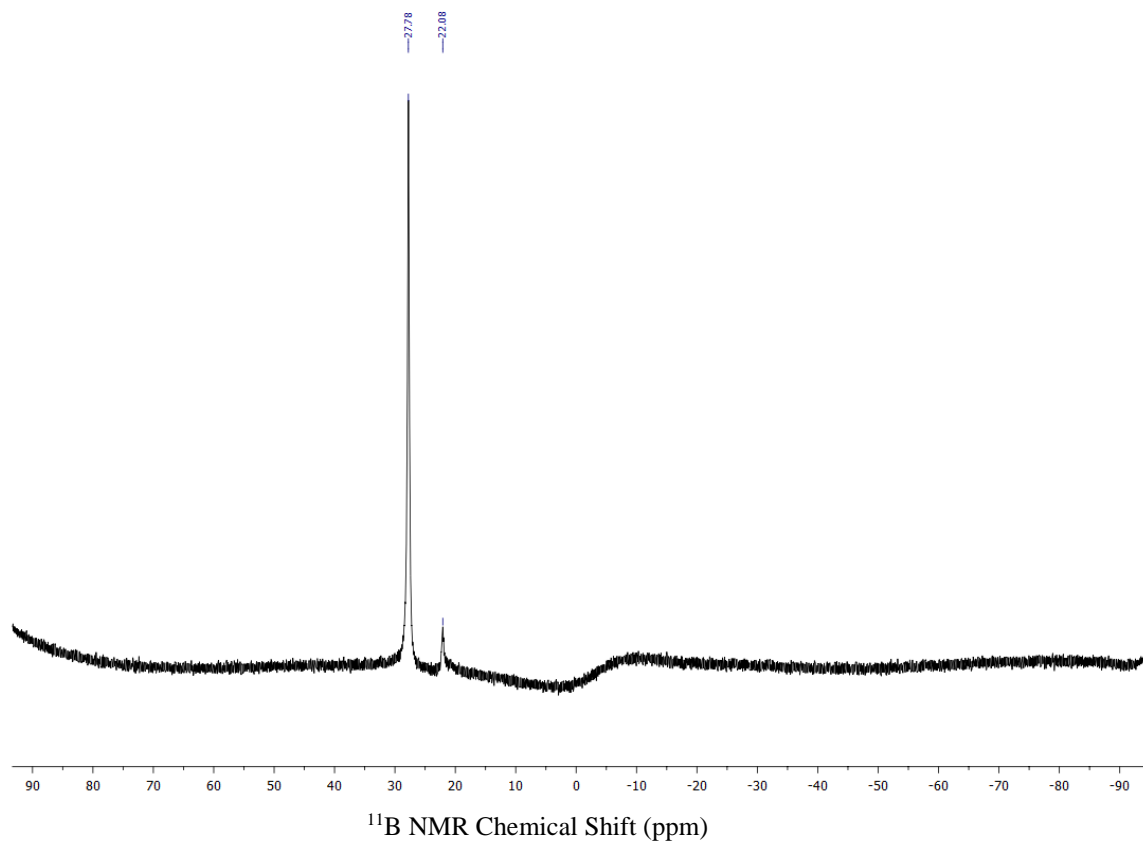


Figure 3.3: ^{11}B NMR of poly(vba) and HBPIn in *d*-octane at 30 °C after 24 h.

3.2.1.3 Benzoic anhydride and pinacolborane

In a nitrogen-filled glove box, a Norell standard series 5 mm NMR tube was charged with 1:1 equivalent of benzoic anhydride and pinacolborane (HBPIn) and 0.7 mL of *d*-octane. ^1H NMR and ^{11}B NMR spectra were recorded at 30 °C on a Bruker AVIII-400 spectrometers. All chemical shifts were recorded in parts per million (ppm) with reference to residual solvent peaks.

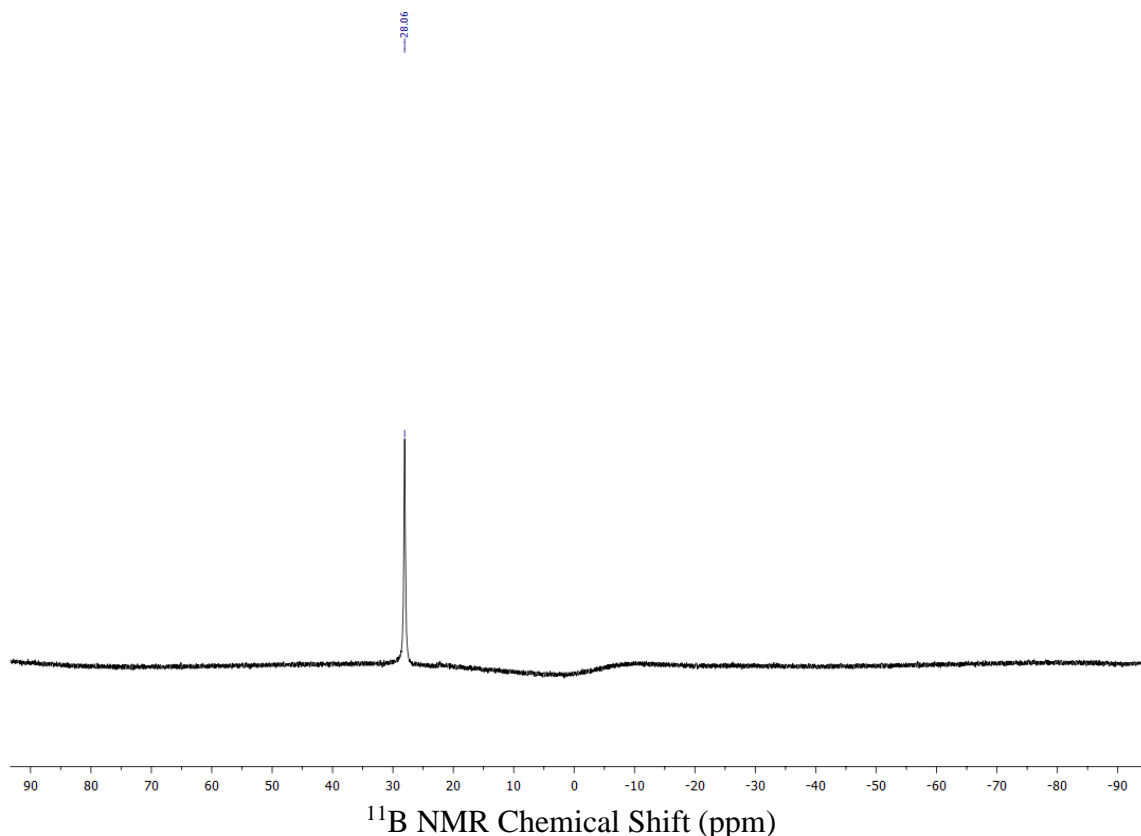


Figure 3.4: ^{11}B NMR spectra of 1:1 ratio of benzoic anhydride with HBPIn in *d*-octane at 30 °C. The peak at 28.06 ppm corresponds to HBPIn.

3.2.2 Experimental Rate Law Determination using poly(vba) (Initial Rates Method).

In a nitrogen-filled glove box, a 3.5 mL vial was charged with a stir bar and appropriate amounts of phenylacetylene, HBPIn, octane and poly(vba) (weighed in air) using mesitylene as the internal standard. The vial was sealed with a rubber septum and stirred at 30 °C. The reaction was monitored by gas chromatography using small aliquots of the reaction mixture, and passing the aliquot through a pad of silica gel rinsing with hexane. The rate law was determined using the initial rates method (up to 15 % yield).

The rates of the reaction correspond to the rate of formation of 2-styryl-BPin (Figure 3.5 and Table 3.5).

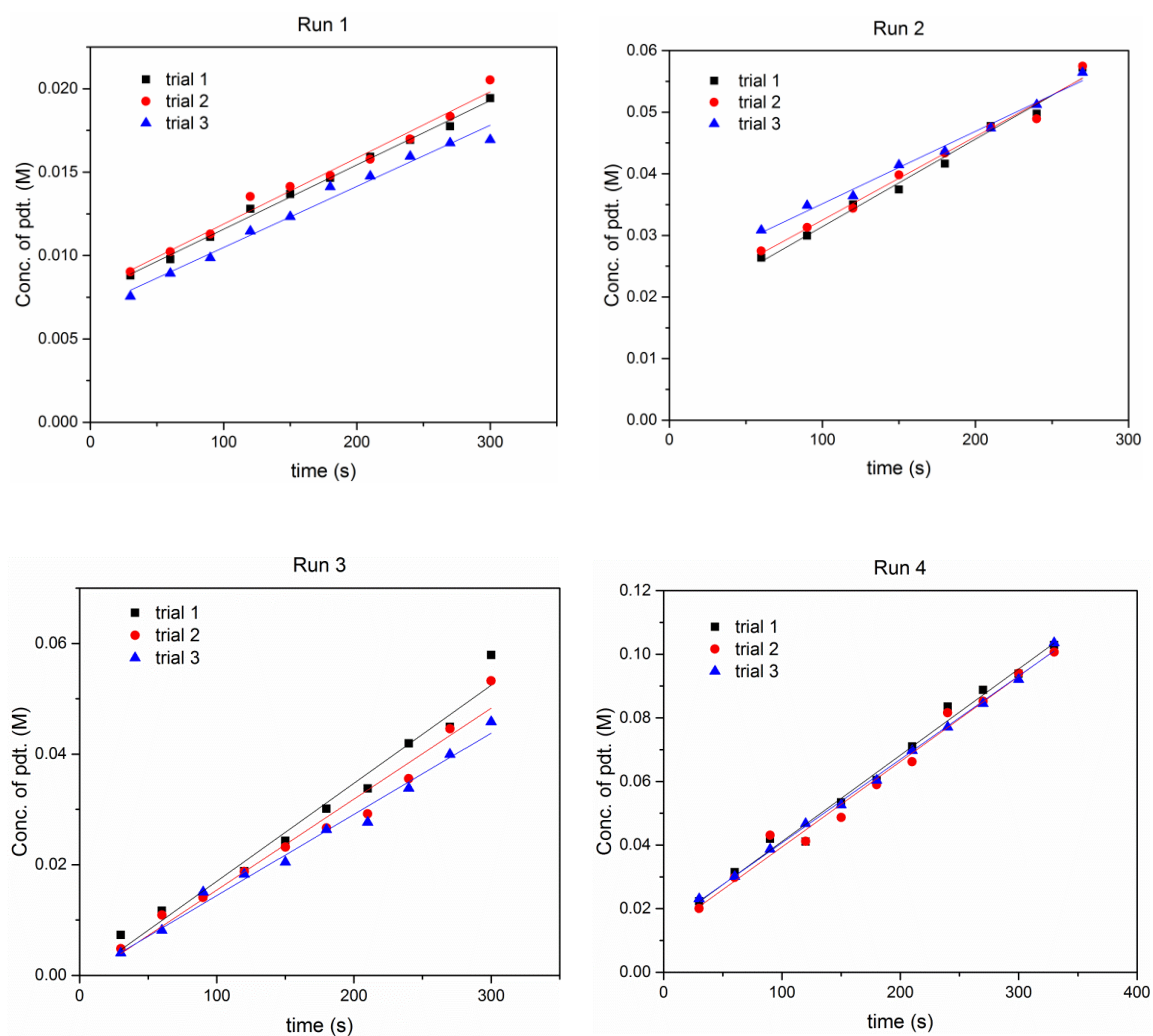


Figure 3.5: Plots of concentration of 2-styryl-BPin (M) vs. time (s) for Runs 1-4.

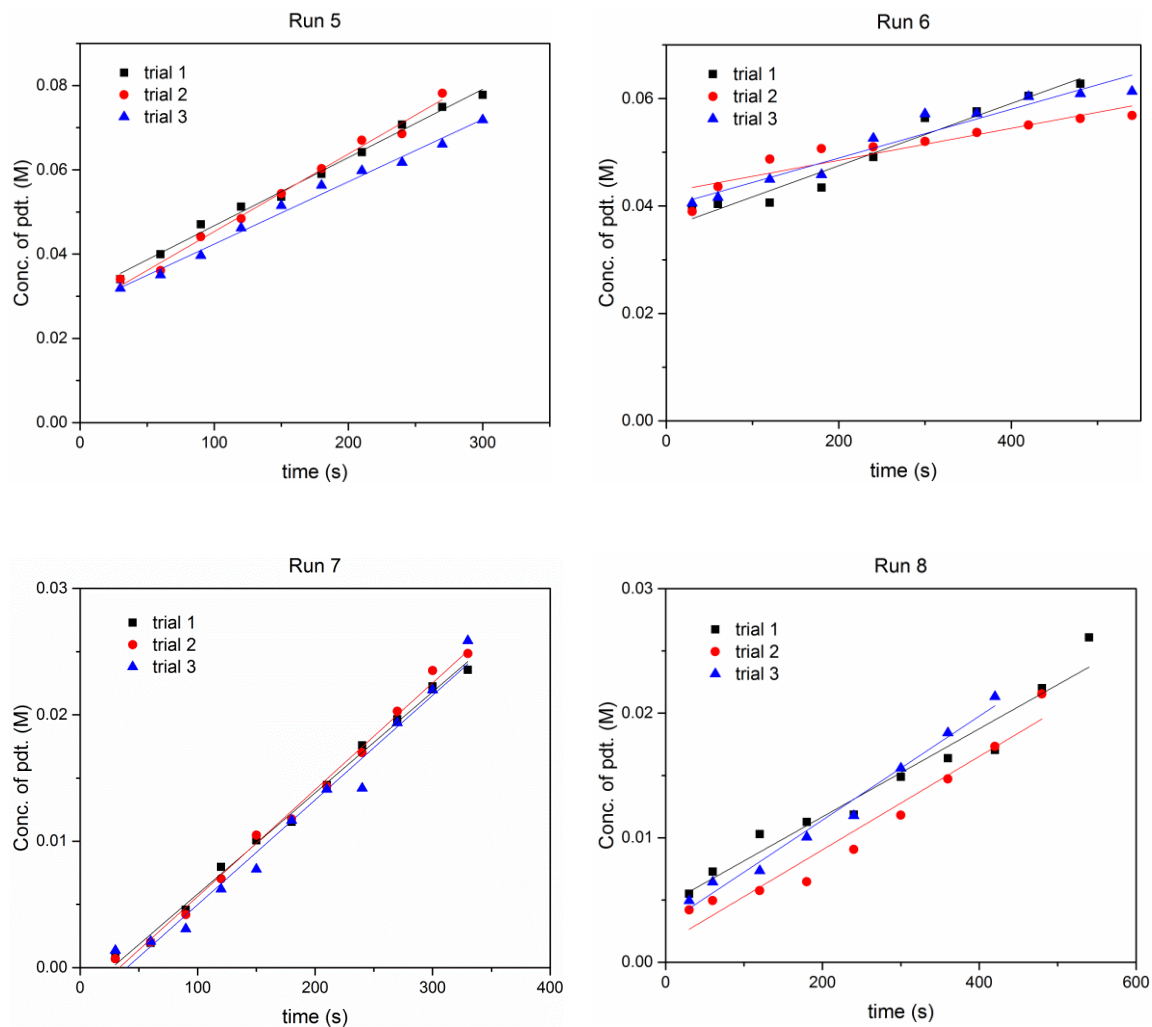


Figure 3.6: Plots of concentration of 2-styryl-BPin (M) vs. time (s) for Runs 5-8.

3.2.3 Kinetic Isotope Effect Determination for the Hydroboration of Phenylacetylene and Phenylacetylene-*d* using poly(vba) (2 separate vessels).

In a nitrogen-filled glove box, 2 separate 3.5 mL vial were charged with stir bars and poly(vba) (0.006 mg, weighed in air). Next phenylacetylene, and phenylacetylene-*d* (0.044 mL, 0.4 mmol), mesitylene (0.055 mL, 0.4 mmol), and octane (1 mL) were loaded into the respective vials and time point 0 was taken. Next, HBPin (0.058 mL, 0.4 mmol)

was added. The reactions were sealed with rubber septum and stirred at 30 °C. The reactions were monitored by gas chromatography using small aliquots of the reaction mixtures, and passing the mixture through a pad of silica gel rinsing with hexane. The rates of reaction, Rate_H and Rate_D , correspond to the rates of formation of 2-styryl-BPin using phenylacetylene and phenylacetylene-d. The overall KIE was calculated taking the average of the ratios of rate_H and rate_D for all the three runs (Figure 3.7 and Table 3.6).

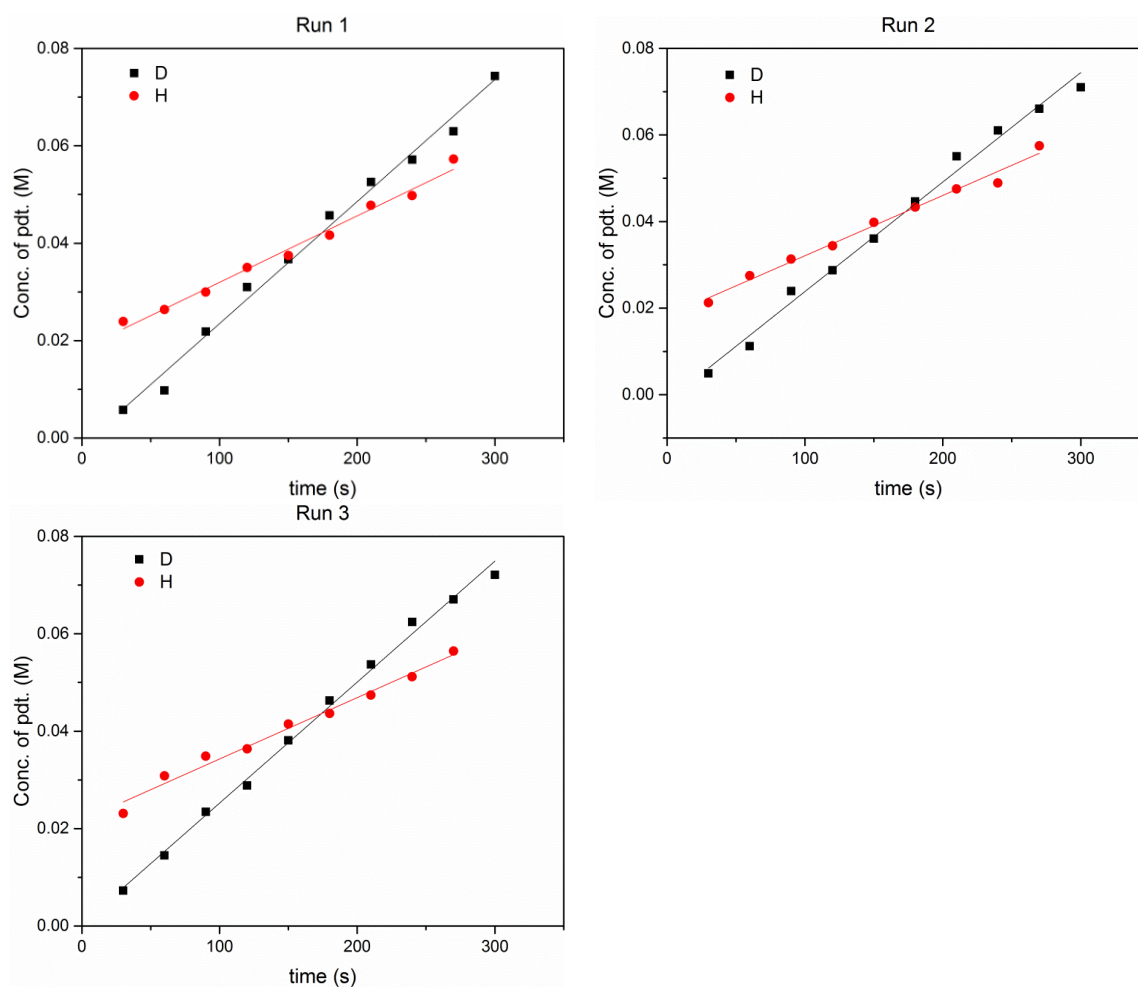


Figure 3.7: Plots of Concentration of 2-styryl-BPin (M) vs. time (s) for Runs 1-3.

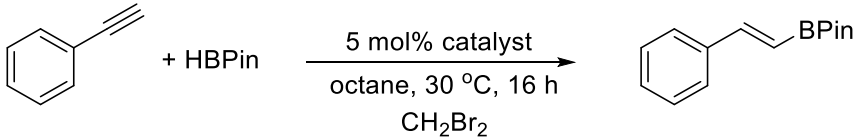
3.2.4 Determination of initial rate of the Hydroboration of 1-ethynylcyclohexene with HBPIn in octane at 30 °C (up to 15% yield).

In a nitrogen-filled glove box, a 3.5 mL vial was charged with a stir bar and 1-ethynylcyclohexene (0.4 mmol), HBPIn (1.2 mmol), octane (1 mL) and poly(vba) (weighed in air, 0.003 g) using mesitylene (0.4 mmol) as the internal standard. The vial was sealed with a rubber septum and stirred at 30 °C. The reaction was monitored by gas chromatography using small aliquots of the reaction mixture, and passing the aliquot through a pad of silica gel rinsing with hexane. The rate law was determined using the initial rates method (up to 15 % yield). The rates of the reaction correspond to the rate of formation of 2-styryl-BPin (Table 3.6).

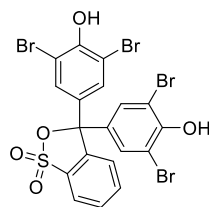
3.2.5 Testing of alternative catalysts for the hydroboration of phenylacetylene with pinacolborane.

In a nitrogen-filled glove box, a 3.5 mL vial was charged with a stir bar and appropriate amounts of phenylacetylene (0.4 mmol), HBPIn (1.2 mmol), octane (1 mL) and catalyst (0.02 mmol) using dibromomethane (0.4 mmol) as the internal standard. The vial was sealed with a plastic cap and stirred at 30 °C for 16 h. The reaction was passed through a pad of silica gel and crude yield determined by ¹H NMR.

Table 3.1: Hydroboration of phenylacetylene with pinacolborane using alternative catalysts^{a,b}

		
Catalyst	pKa	Yield (%) ^b
Bromophenol Blue	3.85	47

^{a)}Reaction conditions: Under an inert atmosphere of N₂, phenylacetylene (0.4 mmol), HBPIn (1.2 mmol, 3 eq.), and 5 mol% catalyst were added to a 3.5 mL vial with octane (1 mL) and CH₂Br₂ as the internal standard at 30 °C stirring vigorously for 16 h. ^{b)}All yields were determined by crude ¹H NMR analysis.



Bromophenol blue

Figure 3.8: Bromophenol blue catalyst structure.

3.2.6 General hydroboration procedure for alkyne substituent effects

In a nitrogen-filled glove box, a 3.5 mL vial was charged with a stir bar and appropriate amounts of alkyne (0.4 mmol), HBPIn (1.2 mmol), octane (1 mL) and poly(vba) (weighed in air, 0.003 g) using dibromomethane as the internal standard. The vial was sealed with a plastic cap and stirred at 30 °C for 16 h. The reaction was passed through a pad of silica gel and crude yield determined by ¹H NMR.

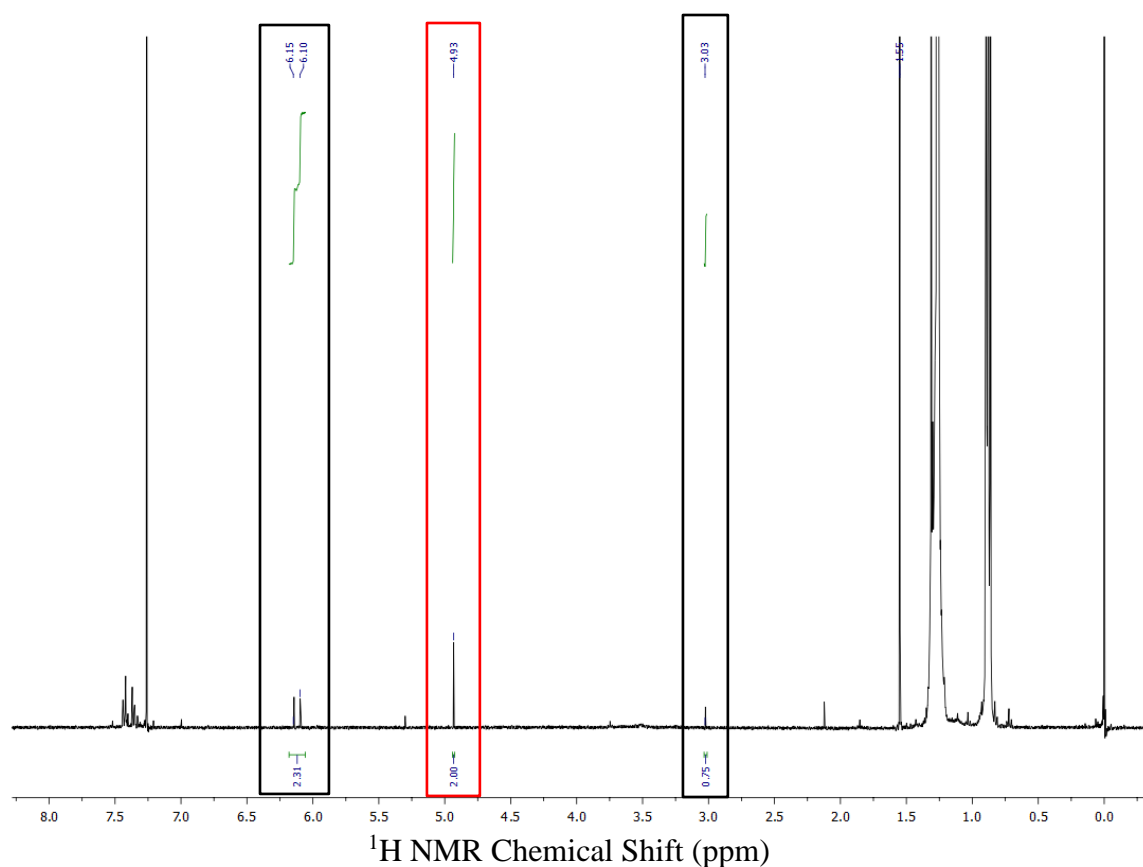
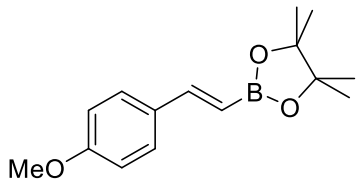


Figure 3.9: Representative ^1H NMR crude product analysis for (E)-2-(4-(*tert*-butyl)styryl)-4,4,5,5-tetramethyl-1,3,2-dioxaborolane in CDCl_3 . CH_2Br_2 used as internal standard at 4.93 ppm (s, 2H). Unreacted product appears at 3.03 ppm (s, 1H) and vinyl product peaks 6.12 ppm (d, 1H).

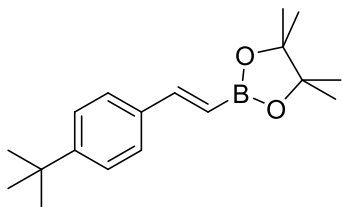
3.2.6.1 Crude product NMR Shifts of substituted alkyne hydroboration

(E)-2-(4-methoxystyryl)-4,4,5,5-tetramethyl-1,3,2-dioxaborolane (2a)¹⁹³



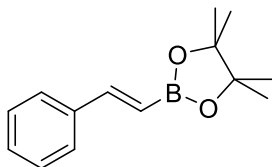
¹H NMR (400 MHz, CDCl₃) δ 7.43 (d, J = 8.8 Hz, 1H), 7.35 (d, J = 18.4 Hz, 1H), 6.85 (d, J = 8.4 Hz, 1H), 6.01 (d, J = 18.4 Hz, 1H), 3.79 (s, 3H), 1.30 (s, 12H); ¹³C NMR (100 MHz, CDCl₃) δ 160.1, 148.9, 130.2, 128.3, 113.8, 83.1, 55.2, 24.8. The carbon signal attached to B was not observed due to low intensity

(E)-2-(4-tert-butylstyryl)-4,4,5,5-tetramethyl-1,3,2-dioxaborolane (2b)¹⁹⁴



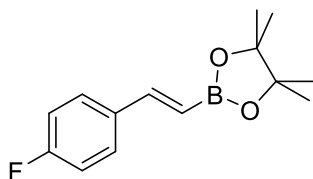
¹H NMR (400 MHz, CDCl₃) δ 7.43 (d, J = 8.3 Hz, 2H), 7.41 – 7.33 (m, 3H), 6.12 (d, J = 18.4 Hz, 1H), 1.31 (s, 21H); ¹³C NMR (100 MHz, CDCl₃) δ 152.3, 149.5, 134.9, 127.0, 125.7, 83.4, 34.9, 31.4, 25.0. The carbon signal attached to B was not observed due to low intensity.

(E)-4,4,5,5-tetramethyl-2-styryl-1,3,2-dioxaborolane (2c)¹⁹³



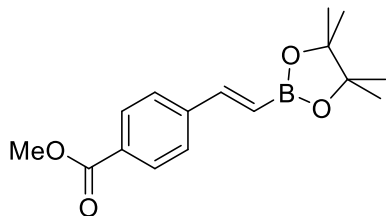
¹H NMR (400 MHz, CDCl₃) δ 7.50-7.48 (m, 2H), 7.40 (d, 1H, J = 18.3 Hz), 7.35-7.25 (m, 3H), 6.17 (d, 1H, J = 18.3 Hz), 1.31 (s, 12H). ¹³C NMR (100 MHz, CDCl₃) δ 149.5, 137.4, 128.8, 128.5, 127.0, 116.4 (br s), 83.3, 24.8. The carbon signal attached to B was not observed due to low intensity.

(E)-2-(4-fluorostyryl)-4,4,5,5-tetramethyl-1,3,2-dioxaborolane (2d)¹⁹¹



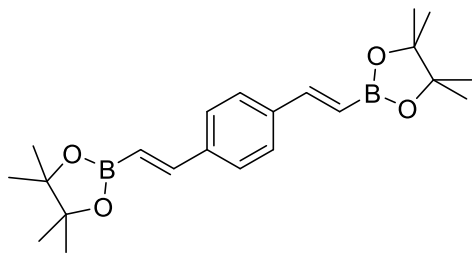
¹H NMR (400 MHz, CDCl₃) δ 7.47-7.42 (m, 2H), 7.35 (d, J = 18.4 Hz, 1H), 7.04- 6.98 (m, 2H), 6.07 (d, J = 18.4 Hz, 1H), 1.30 (s, 12H); ¹³C NMR (100 MHz, CDCl₃) δ 162.9 (d, J = 247.0 Hz), 148.2, 133.5 (d, J = 2.5 Hz), 128.5 (d, J = 8.2 Hz), 115.4 (d, J = 21.4 Hz), 83.1, 24.8. The carbon signal attached to B was not observed due to low intensity.

(E)-Methyl 4-(2-(4,4,5,5-tetramethyl-1,3,2-dioxaborolan-2-yl)vinyl)benzoate (2e)¹⁹¹



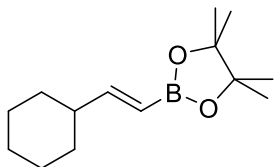
¹H NMR (400 MHz, CDCl₃) δ 8.01-7.98 (m, 2H), 7.52 (d, J = 8.4 Hz, 2H), 7.40 (d, J = 18.4 Hz, 1H), 6.27 (s, J = 18.4, 1H), 3.90 (s, 3H), 1.31 (s, 12H); ¹³C NMR (100 MHz, CDCl₃) δ 166.2, 147.9, 141.5, 130.0, 129.8, 126.8, 83.5, 52.1, 24.8. The carbon signal attached to B was not observed due to low intensity.

1,4-Bis((E)-2-(4,4,5,5-tetramethyl-1,3,2-dioxaborolan-2-yl)vinyl)benzene (2f)¹⁹¹



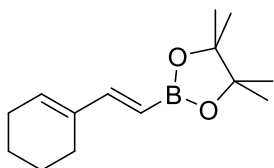
¹H NMR (400 MHz, CDCl₃) δ 7.45 (s, 4H), 7.36 (d, J = 18.4 Hz, 2H), 6.16 (d, J = 18.4 Hz, 2H), 1.31 (s, 24H); ¹³C NMR (100 MHz, CDCl₃) δ 148.7, 137.8, 127.2, 119.6, 83.8, 24.8. The carbon signal attached to B was not observed due to low intensity.

(E)-2-(2-Cyclohexylvinyl)-4,4,5,5-tetramethyl-1,3,2-dioxaborolane (2g)¹⁹¹



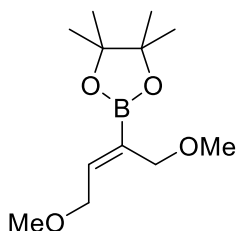
¹H NMR (400 MHz, CDCl₃) δ 6.55 (dd, J = 18.4, 6.0 Hz, 1H), 5.37 (d, J = 18.4 Hz, 1H), 2.06-1.99 (m, 1H), 1.75-1.62 (m, 6H), 1.27 (s, 12H), 1.19-1.05 (m, 4H); ¹³C NMR (100 MHz, CDCl₃) δ 159.7, 82.9, 43.2, 31.9, 26.1, 25.9, 24.8. The carbon signal attached to B was not observed due to low intensity.

(E)-2-(2-Cyclohexenylvinyl)-4,4,5,5-tetramethyl-1,3,2-dioxaborolane (2h)¹⁹¹



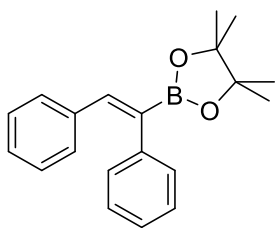
¹H NMR (400 MHz, CDCl₃) δ 7.01 (d, J = 18.4 Hz, 1H), 5.97-5.95 (m, 1H), 5.42 (d, J = 18.4 Hz, 1H), 2.14 (br, 4H), 1.69-1.55 (m, 4H), 1.27 (s, 12H); ¹³C NMR (100 MHz, CDCl₃) δ 153.1, 137.0, 134.1, 82.9, 26.2, 24.8, 23.7, 22.4, 22.3. The carbon signal attached to B was not observed due to low intensity.

(Z)-2-(1,4-Dimethoxybut-2-en-2-yl)-4,4,5,5-tetramethyl-1,3,2-dioxaborolane (2i)¹⁹¹



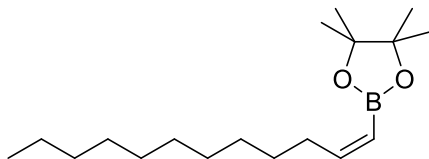
¹H NMR (400 MHz, CDCl₃) δ 6.58 (t, J = 5.6 Hz, 1H), 4.14 (d, J = 5.6 Hz, 2H), 4.02 (s, 2H), 3.34 (s, 3H), 3.28 (s, 3H), 1.24 (s, 12H); ¹³C NMR (100 MHz, CDCl₃) δ 146.5, 83.4, 69.6, 68.9, 58.3, 57.8, 24.7. The carbon signal attached to B was not observed due to low intensity.

(Z)-2-(1,2-Diphenylvinyl)-4,4,5,5-tetramethyl-1,3,2-dioxaborolane (2j)¹⁹¹



¹H NMR (400 MHz, CDCl₃) δ 7.36 (s, 1H), 7.28-7.03 (m, 10H), 1.31 (s, 12H); ¹³C NMR (100 MHz, CDCl₃) δ 143.0, 140.2, 136.8, 129.8, 128.7, 128.1, 127.7, 127.4, 126.1, 83.7, 24.8. The carbon signal attached to B was not observed due to low intensity.

(Z)-2-(dodec-1-en-1-yl)-4,4,5,5-tetramethyl-1,3,2-dioxaborolane (2k)¹⁹⁵



¹H NMR: δ 6.62 (dt, J = 18.0, 6.0 Hz, 1H), 5.41 (dt, J = 18.0, 1.6 Hz, 1H), 2.16–2.10 (m, 2H), 1.25 (s, 12H), 1.42–1.20 (m, 16H), 0.86 (t, J = 7.2 Hz, 3H); ¹³C NMR: δ = 154.9, 118.4, 82.9, 35.8, 31.9, 29.60, 29.56, 29.5, 29.3, 29.2, 28.2, 24.7, 22.7, 14.1. The carbon signal attached to B was not observed due to low intensity.

3.3 Materials Synthesis

3.3.1 Carboxylic acid polymer synthesis

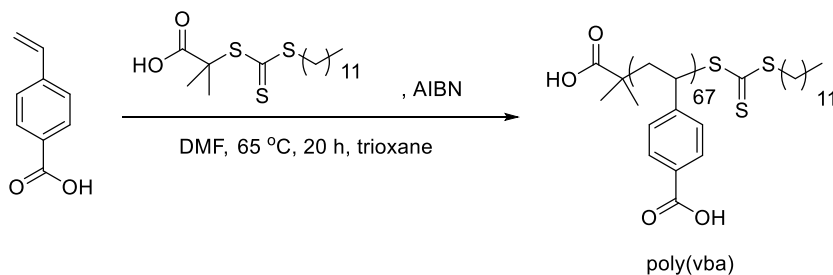


Figure 3.10: Polymer catalyst synthesis via RAFT polymerization.

In a 10 mL schlenk flask, 4.05 mmol (0.600 g, 100 eq.) of 4-vinyl benzoic acid, 0.0405 mmol (0.0148 g, 1 eq.) of 2-(dodecylthiocarbonothioylthio)-2-methylpropionic acid, and 0.00405 mmol (0.001 g, 0.1 eq.) AIBN, 4 mL of DMF and 1,3,5-trioxane (internal standard) underwent 4 cycles of freeze, pump, thawing. The reaction was backfilled with argon, and placed in a 65 °C oil bath for 20 h. The reaction was then

monitored by ^1H NMR to 65% conversion. The resulting solution was purified by 3 reprecipitations in cold DI H_2O to remove unreacted monomer. The polymer was also purified through dialysis in THF, but the catalyst activity as drastically decreased. This is hypothesized to be due to collapsed chains, and lack of redispersion in octane. Purified polymer was characterized below in Table 3.2 and Figure 3.11.

3.4 Materials Characterization

Table 3.2: Characterization of poly(vba)

polymer	M_n^{NMR} (g/mol)	M_n^{GPC} (g/mol)	\bar{D}	Units
poly(vbs)	9,620	10,000	1.18	67

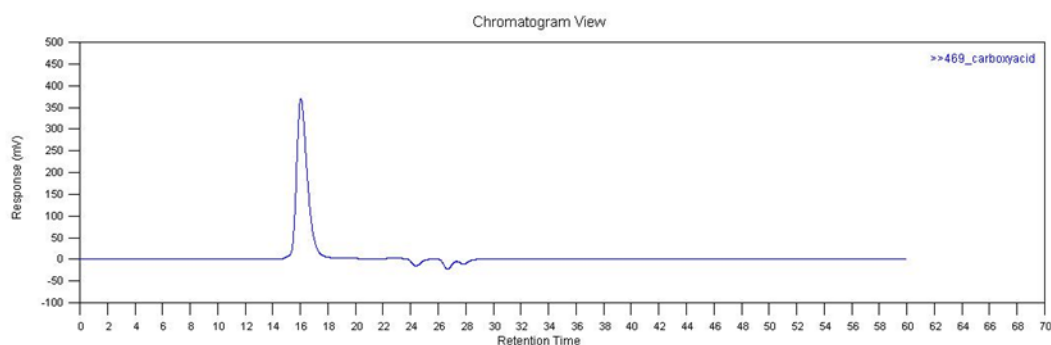


Figure 3.11: GPC chromatogram of poly(vinylbenzoic acid) using THF as the eluent, with polystyrene calibrations.

3.4.1 Recycle Poly(vba) catalyst

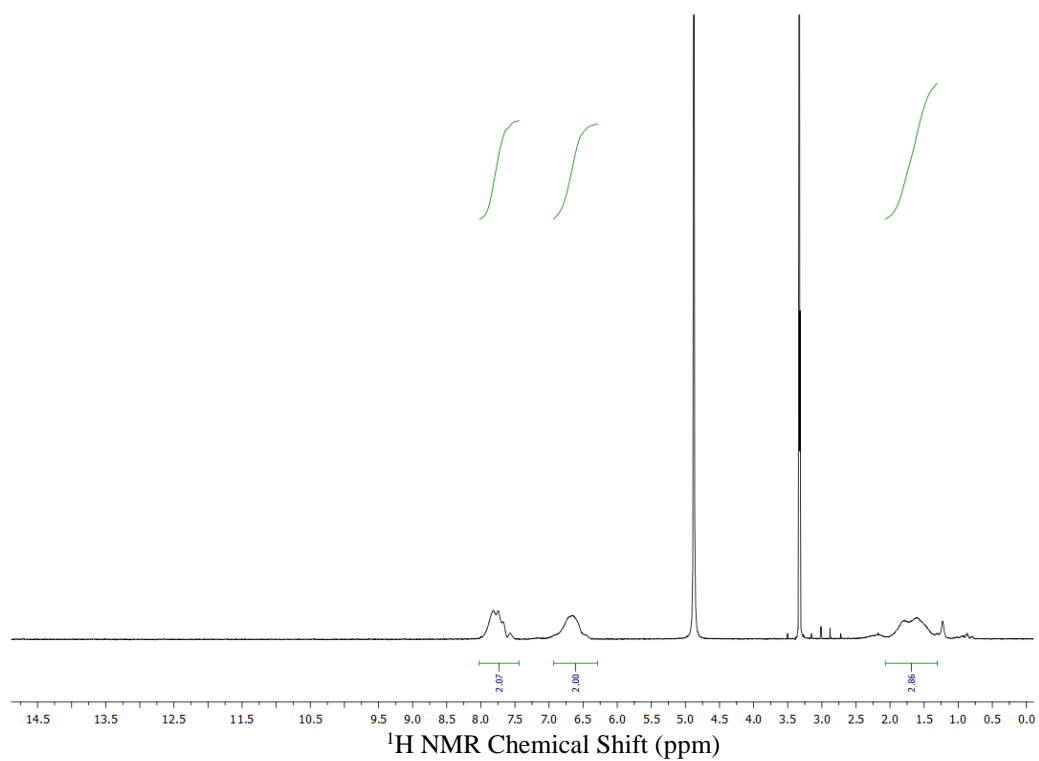


Figure 3.12: ^1H NMR recycled poly(vba) in MeOD.

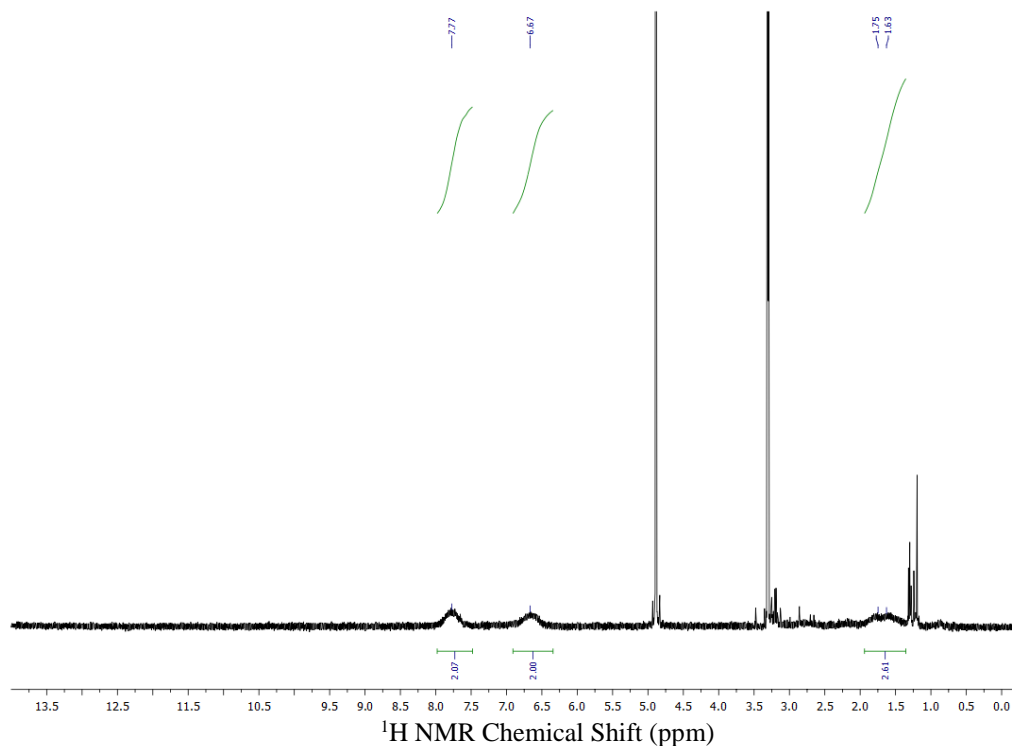


Figure 3.13: ^1H NMR 2nd recycle poly(vba) in MeOD.

3.5 Polymer catalyst optimization

Supporting an organocatalyst provides a reusable handle that homogeneous catalysts lack. In this study, a linear polymer support with carboxylic acid functionality was synthesized using reverse addition-fragmentation chain transfer (RAFT) as a controlled polymerization technique. The controlled synthesis of the homopolymer catalyst ensures the length of polymer chain is controlled through a radical equilibrium which occurs between the chain transfer agent fragment and initiated chain ends. The equilibrium mediates the rate of the polymerization and shares the equilibrium between all the initiated chain ends of the propagating chain ends. Utilizing 4-vinyl benzoic acid as the monomer, polymer chains were polymerized to a molecular weight of 10,000

g/mol and \bar{M}_n 1.12. The narrow polydispersity ensured that various chain lengths did not play a role in the catalysis by inhibiting batch to batch reproducibility that may be associated with a broad \bar{M}_n . Heterogenizing a homogeneous catalyst removes some of the mobility of the catalyst in solution, thus the polymers were polymerized to relatively short chain lengths, as a longer polymer chain was hypothesized to encumber the active sites more compared to shorter lengths.

Once the initial poly(vinylbenzoic acid) catalyst [poly(vba)] was synthesized, we began by exploring the hydroboration of phenylacetylene with HBPIn by optimizing the reaction conditions. A variety of solvents have been reported in the literature to carry out hydroboration reactions, and employing a new acid-polymer catalyst to this reaction required optimizing the solvent as polymer-solvent interactions would potentially affect the folding of the polymer. Once the optimal solvent was identified, kinetic isotope effects and rate law determination was performed to assist in proposing a mechanistic pathway for this reaction with the polymer-supported acid catalyst.

Table 3.3: Solvent effects on hydroboration of phenylacetylene with poly(vba)^a

Entry	Solvent	Solubility	Yield (%) ^b
1	Methanol	Yes	0
2	Acetonitrile	Yes	25
3	Tetrahydrofuran	Yes	60
4	Dichloromethane	Yes	47
5	Octane	No	100

^a) Reaction conditions: In a N₂ filled glove box phenylacetylene (0.4 mmol), HBPIn (1.2 mmol), and 5 mol % poly(vba) are stirred vigorously at 30 °C for 16h in 1 mL solvent. ^b) Crude ¹H NMR analyzed for product yield using CH₂Br₂ as the internal standard.

As seen in Table 3.3, more polar solvents such as methanol and acetonitrile solubilized the polymer, however decreased conversion.¹⁹¹ In less polar solvents such as tetrahydrofuran and octane, the polymer catalyst performed well for the hydroboration. The polymer was dispersed in octane to make a heterogeneous mixture, however was not soluble. The polymer insolubility lead to the titration of the polymer to assess the number of active accessible sites for future studies, which was estimated at roughly 80 mol%. Due to the amount of site accessibility despite the heterogeneity of the polymer in reaction, octane was chosen as the solvent to continue mechanistic studies. As mentioned previously, the ease of recoverability and recycle tests will be discussed later.

3.6 Mechanistic studies of the hydroboration of phenylacetylene with pinacolborane

Previous literature has suggested the uncatalyzed hydroboration mechanism proceeds through a 4-membered transition state, with anti-Markovnikov placement of the boron species.^{71,196,197,76,198} Recent Lewis acid catalysts have been proposed to proceed via a 4-membered concerted mechanism as well.^{199,200,201} The majority of transition-metal catalyzed hydroboration mechanisms proceed via oxidative addition of the boron source, or in the Lewis acid catalyzed mechanism, alkyne coordination to the catalyst.¹⁹⁹ To begin probing the mechanism, the first step began with individually introducing the small molecule catalyst surrogate, benzoic acid, with phenylacetylene and pinacolborane, as shown in Figure 3.14.

3.6.1 NMR studies of intermediate species

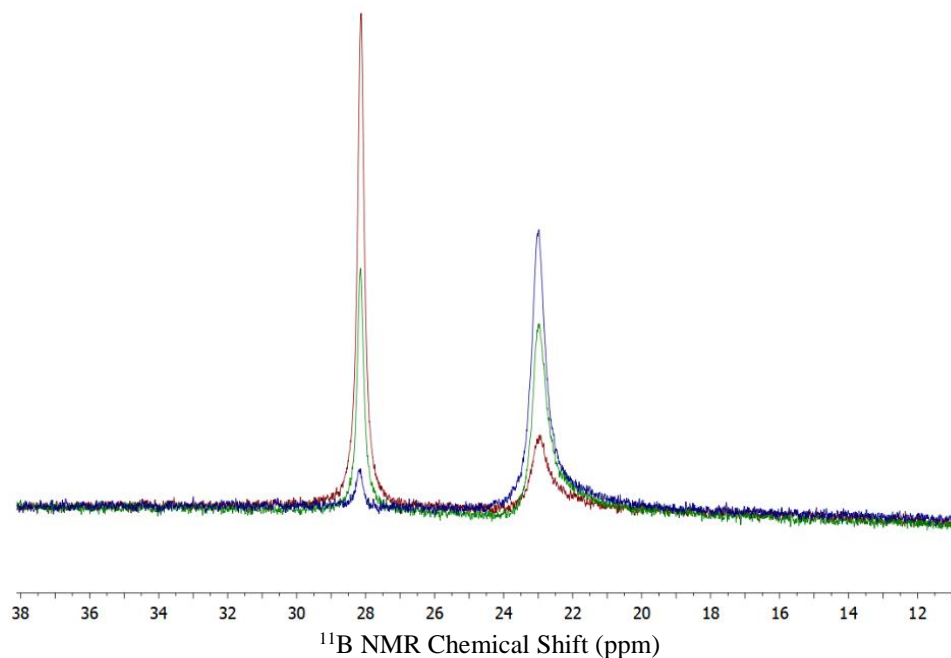


Figure 3.15: ^{11}B NMR analysis of 1:1 ratio of benzoic acid with HBPIn over 24 h in *d*-octane at 30 °C (20 min red, 5 h in green, 24 h in blue). The peak at 28.13 ppm corresponds to HBPIn.

Above in Figure 3.15, the spectrum yielded peaks at 22.98 and 28.14 ppm in (^1H -decoupled) ^{11}B NMR in *d*-octane at 30 °C over time when prepared in an inert atmosphere to minimize observation of structure **3**. The peak at 28.14 ppm is associated with unreacted HBPIn, while the new peak at 22.98 ppm has been hypothesized to be structure **2** in Figure 3.14. The proposed structure **2** is shown above, based on a similar proposed structure using a phosphoric acid catalyst and the detection of H_2 .²⁰² The P-O-B bond shift is reported at 22.13 ppm, supporting the C-O-B bond formation at 22.98 ppm, as well as an evolution of H_2 gas seen in ^1H NMR as a singlet at 4.7 ppm (Figure 3.2).²⁰³ A similar experiment was carried out using benzoic anhydride and the ^{11}B NMR

spectrum, which displayed only unreacted HBPin (Figure 3.4), indicated that a proton is necessary for the proposed structure **2** to form in solution. After 24 h, there was near full consumption of the HBPin peak at 28.14 ppm to 22.98 ppm.

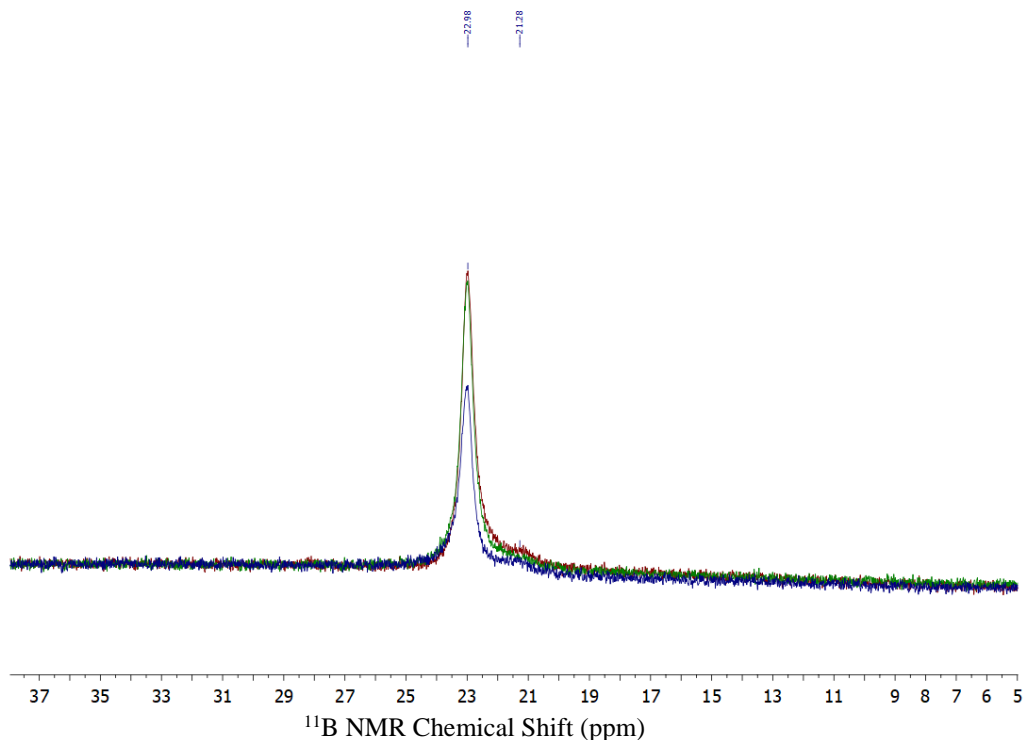


Figure 3.16: ^{11}B NMR analysis of 1:1: ratio of benzoic acid:HBPin:phenylacetylene over 24 h in *d*-octane at 30 °C (20 min blue, 5 h in green, 24 h in red).

After complete consumption of HBPin, 1 eq. of phenylacetylene was added to the NMR tube under nitrogen, and analysis by ^{11}B NMR did not show a shift change in boron species present; rather, the appearance of a slight shoulder that has been associated with small amounts of structure **3** (Figure 3.14) was noted. Structure **2** is not disrupted by the addition of phenylacetylene, but potential hydrolysis with additional HBPin is hypothesized to cleave the adduct upon introduction of water, which is produced from the

dimerization of two benzoic acid molecules.²⁰⁴ Analyzing the poly(vba) under these same 1:1 conditions, the spectra displayed unreacted HBPin peak at 28.14 ppm, as well as the appearance of **3**, likely due to the small amount of water adsorbed on the polymer (Figure 3.3). Analyzing the reaction over time did not display a peak at 22.98 ppm, attributed to the non-productive site-occupation analogous to structure **2** in Figure 3.14, however this is likely due to the insolubility of the polymer in octane.

3.6.2 Determination of Kinetic Isotope Effects

The kinetic isotope effect can be useful in identifying a reaction mechanism through determination of a bond-breaking or rehybridization step. From ¹¹B NMR studies, an intermediate structure produced H₂ when the soluble catalyst and HBPin were introduced, while there was no reaction detected spectroscopically with introduction of phenylacetylene to benzoic acid. A potential alternative pathway for the hydroboration of phenylacetylene to occur would be through deprotonation of the alkyne by the catalyst, similar to a Lewis acid catalyzed hydroboration.¹⁹⁹ The formed species would be trappable, and detected by NMR. The lack of detectable interaction of the alkyne and acid catalyst lead the KIE studies to confirm a rehybridization of the C(sp)–H bond as the key step in the cycle. The kinetic isotope effect was measured by comparison of initial rates (up to 15% conversion) for the hydroboration of both phenylacetylene and phenylacetylene-*d*, measured in 2 separate vessels. KIE determination using labelled phenylacetylene would facilitate a pathway to product formation through a bond-breaking step or a rehybridization step.²⁰⁵ In two separate vessels, under typical reaction conditions with 5 mol% of poly(vba) and HBPin at 30 °C, comparison of the relative initial rates of

the two reactions yielded an inverse secondary deuterium kinetic isotope effect of 0.50(3).

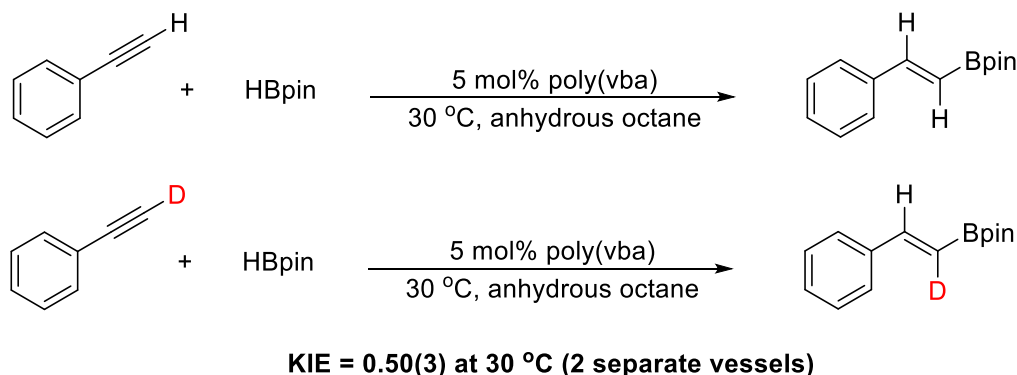


Figure 3.17: Determination of the deuterium kinetic isotope effect for the hydroboration of phenylacetylene and phenylacetylene-d with HBPin as the boron source and poly(vba) as the catalyst.

Table 3.4: KIE determination for the hydroboration of phenylacetylene using HBpin in the presence of poly(vba) at 30 °C using octane as the solvent

Run	Rate _H , Ms ⁻¹	Rate _D , Ms ⁻¹	k _H /k _D (KIE)
1	7.06 x 10 ⁻⁵	1.34 x 10 ⁻⁴	0.53
2	7.16 x 10 ⁻⁵	1.41 x 10 ⁻⁴	0.51
3	6.47 x 10 ⁻⁵	1.36 x 10 ⁻⁴	0.48
Overall KIE = 0.50(3)			

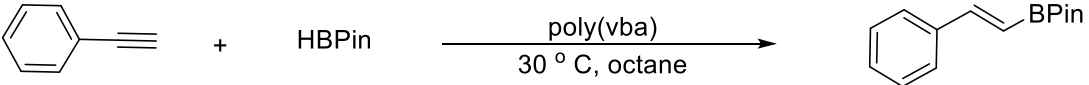
This value typically implies the bond breaking is remote from the reactant substitution site; commonly this arises from the rehybridization of the labelled site in the reaction, supporting the hypothesized mechanistic pathway with the 4-membered concerted hydroboration reaction, over addition to the catalyst via bond breaking.²⁰⁵ Because the 2-styryl-BPin-*d* did not have any deuterium scrambling, the source of H₂

evolution points to the adduct formation of the HBPIn-acid interaction (structure **2**), not deprotonation of the alkyne. Observed in ^1H NMR is the appearance of a broad singlet around 7.40 ppm, associated with a proton split by a deuterium, as well a complete disappearance of vinyl peaks at 6.21 ppm with proton-proton splitting. This confirms there is no scrambling of the deuterium atom, and confirms the KIE is a rehybridization of the $\text{C}(\text{sp})\text{--H}$ to $\text{aC}(\text{sp}^2)\text{--H}$.

3.6.3 Determination of Reaction Orders through Methods of Initial Rates

Next, finding the reaction orders with regard to the reactants and catalyst for the hydroboration of phenylacetylene with HBPIn using poly(vba) were determined using the method of initial rates, as shown below in Table 3.5, with the goal of understanding pathways alluded to in Figure 3.14, whether the addition of the boron source to the catalyst, alkyne coordination, or a concerted mechanism is the turnover-limiting step of the catalytic reaction.

Table 3.5: Determination of the Rate Law of the Hydroboration of Phenylacetylene with HBPIn

			
[phenylacetylene]	[HBPIn]	[cat]	Initial rate (M/s)
0.40 M	0.40 M	0.025 M	$1.9(6) \times 10^{-5}$
0.40 M	0.40 M	0.05 M	$6.5(8) \times 10^{-5}$
0.40 M	0.40 M	0.075 M	$8.3(6) \times 10^{-5}$
0.40 M	0.40 M	0.10 M	$1.3(0) \times 10^{-4}$
0.40 M	0.80 M	0.10 M	$9.1(5) \times 10^{-5}$
0.40 M	1.20 M	0.10 M	$4.1(7) \times 10^{-5}$
0.80 M	0.40 M	0.10 M	$4.2(2) \times 10^{-5}$
1.20 M	0.40 M	0.10 M	$1.2(7) \times 10^{-5}$

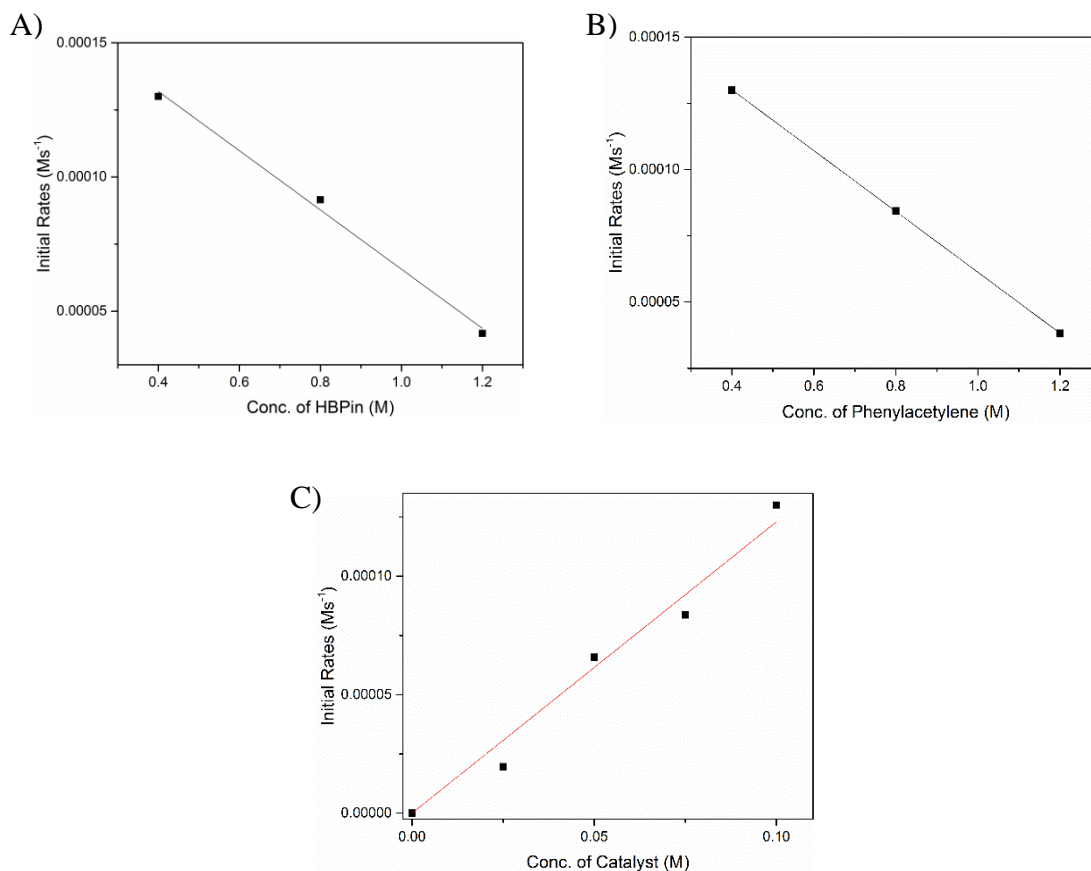


Figure 3.18: Inverse first-order dependence on the initial rates for the formation of 2-styryl-BPin on the concentration of HBPIn (A) and phenylacetylene (B). First-order dependence on the initial rate for the formation of 2-styryl-BPin on the concentration of the acid catalyst (C).

The observed reaction orders found were first-order with respect to the poly(vba) catalyst (Figure 3.18, C) and inverse first-order dependence on HBPIn as well as phenylacetylene. Both reactants have a -1 integer, indicating there is equal inhibition by both reagents in the reaction. Potential over addition to active sites or site blocking can lead to inverse first-order dependence for reactants. To explore the possibility of site blocking with phenylacetylene, initial rates were tested with an aliphatic cyclic alkyne, 1-ethynylcyclohexene.

Table 3.6: Determination of initial rate of the Hydroboration of 1-ethynylcyclohexene with HBPIn in octane at 30 °C (up to 15% yield)

[alkyne]	[HBPIn]	[cat]	Initial Rate, Ms ⁻¹			
			Trial 1	Trial 2	Trial 3	Average
0.4 M	0.4 M	0.05 M	1.99 x 10 ⁻⁴	1.96 x 10 ⁻⁴	1.69 x 10 ⁻⁴	1.88 x 10 ⁻⁴

The alkyne retains similar electronics to the aromatic ring, but is not a planar molecule and faster initial rates were seen (Table 3.6). We hypothesize phenylacetylene, as a planar molecule, lays flat on the catalyst surface and has the ability to sterically hinder available sites. This may be facilitated by pi-pi stacking between the aromatic ring in phenylacetylene and the poly(vba). The inverse behavior of HBPIn may allude to the nonproductive structure **2** depicted in Figure 3.14, or active-site occupation due to adduct formation. KIE studies demonstrate a rehybridization of the alkyne with the HBPIn as a key step, which could be impeded by the increased concentration of either substrate interacting with the catalyst and blocking active sites. If there is an over addition or site blocking of one reactant, the rate of product formation would decrease.

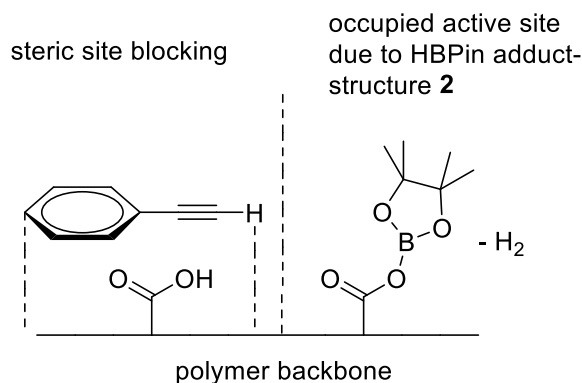


Figure 3.19: Illustrative site inhibition due to over adsorption of species to active sites and steric site blocking, leading to inverse reaction order dependence of the hydroboration of phenylacetylene with HBPIn.

Illustrated in Figure 3.19 are the possible site inhibition structures from each reactant on the acid polymer. The insolubility of poly(vba) in octane likely depresses formation of structure **2**, which forms over extended reaction times, as seen in Figure 3.15. Due to the extended times necessary for complete consumption of HBPIn, the product release and catalyst turnover is not completed inhibited by the minimal formation of structure **2**. The polymer, as seen in ^{11}B NMR in Figure 3.3, introduces a small amount of water to the system due to the hydrophilicity of the polymer. The water introduces hydrolysis of HBPIn, thus for extended reaction times, 3 equivalents of HBPIn is necessary for quantitative yields.

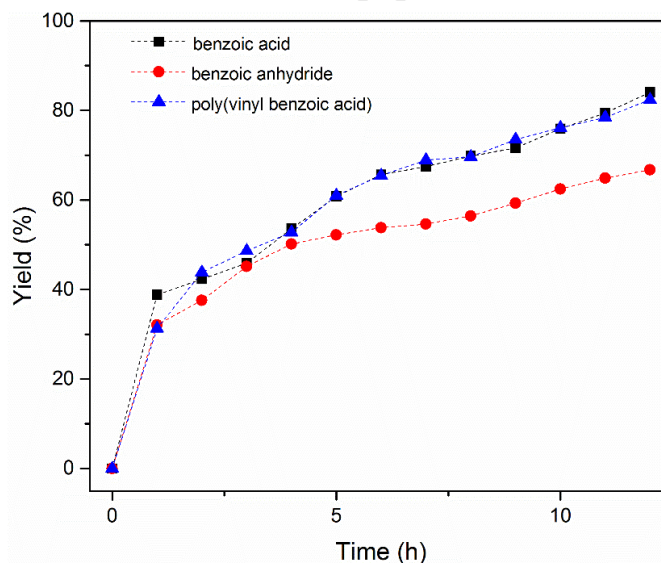
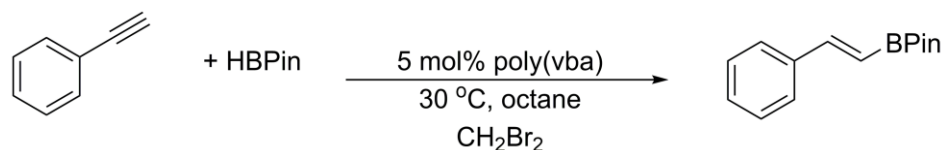


Figure 3.20: Reaction profiles for the hydroboration of phenylacetylene with HBPi using benzoic acid (black), benzoic anhydride (red), and poly(vba) (blue) as catalysts.

In Figure 3.20, the overall reaction profile displays similar activity with both the homogeneous benzoic acid and the heterogeneous poly(vba). Benzoic anhydride was used to test the role of hydrogen-bonding as part of the mechanism. This initial catalyst has the potential to be cleaved into active benzoic acid in the presence of trace water, which explains the activity seen, albeit with slower rates than benzoic acid. A previous study investigated a similar principle with methyl benzoate under similar reaction conditions, and no activity was detected.¹⁹¹ An alternative small molecule catalyst with similar acidity were tested to understand the role of the acidic proton; however, the slight depression of catalytic activity was observed (Table 3.1). Bromophenol blue performed the hydroboration with limited product yield. The acidity of the proton is similar to benzoic acid, flanked by two electron-withdrawing bromines. The structure of

bromophenol blue is a sterically demanding system, with the polymer catalyst having perhaps similar steric encumbrment. The acidity of the catalyst does play a role in the hydroboration of alkynes with HBPIn, based on the results obtained here and a prior study that motivated this work, as shown in the hypothesized cycle below in Figure 3.21. The proton likely polarizes the alkyne, which is then poised for coordination with HBPIn in solution. If the proton were tightly associated with the catalyst, polarization of the alkyne would not occur and the catalytic cycle would not take place.

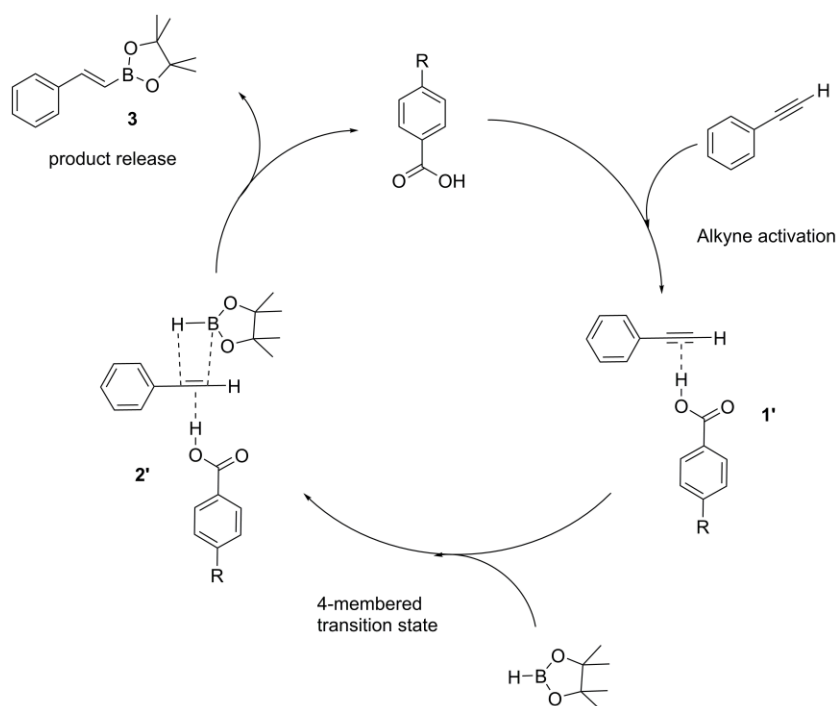


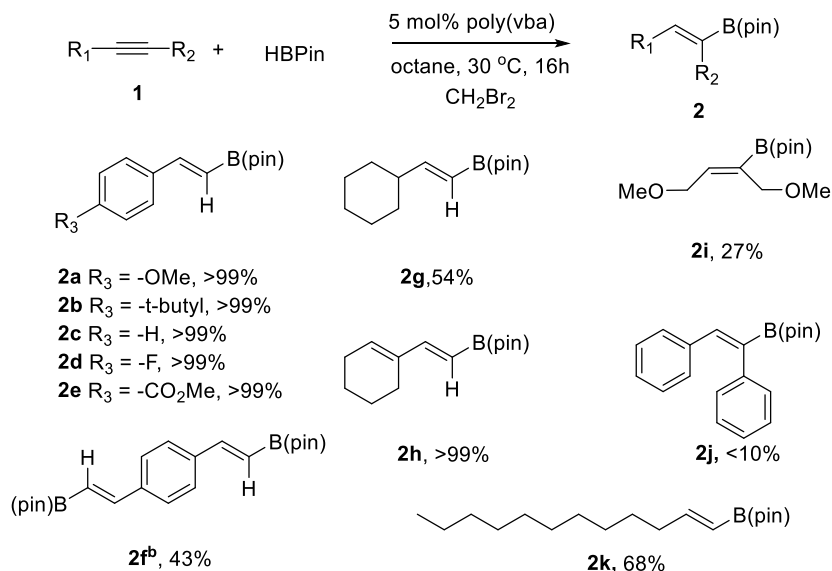
Figure 3.21: Proposed catalytic pathway for the hydroboration of phenylacetylene with HBPIn using poly(vba).

Applying the acid strength, KIE studies, and rate orders of reactants and catalyst, a proposed catalytic pathway is depicted above in Figure 3.21. The cycle begins through polarization of the alkyne by the proton, to promote a 4-membered transition state upon

coordination with HBPIn (Figure 3.21, **2'**). This concerted step is supported by the inverse KIE which dictates a rehybridization as the rate determining step. Once the product has been formed, the alkene is less polarized by the acid and released to generate product and regenerate the catalyst. The proton is most likely associated with the catalyst because of the nonpolar reaction solvent, which is not likely to stabilize charge formation. The acidity of the proton impacts how available the proton is for polarization of the alkyne. If the acid is too weak, the proton will not interact strongly with the alkyne.¹⁹¹ The data suggest productive catalysis comes from acid-alkyne interaction **1'**, with acid-acid interaction likely inhibiting the reaction. This anhydride formation can be limited using the poly(vba) catalyst under conditions where it is sparingly soluble, relative to use of homogeneous benzoic acid. Acid-HBPIn interactions also likely do not lead to productive catalysis, forming side product **2** and liberating H₂, removing catalyst from the cycle. Despite its inhibiting kinetic effect, excess HBPIn is need to achieve a high yield of the desired product due to the side reactions that can occur, consuming this reagent to form products **2'** and **3**.

3.7 Substituent scope of hydroboration of substituted alkynes with pinacolborane

Table 3.7: Substituent effect of alkyne in hydroboration with pinacolborane^{a,b}

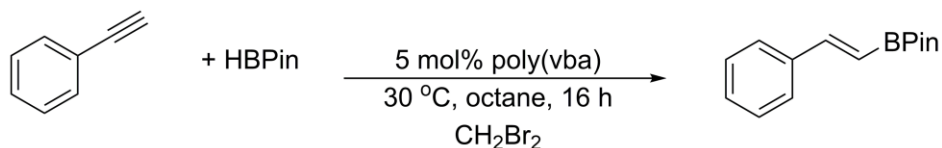


^a) Reaction conditions: Under an inert atmosphere of N_2 , phenylacetylene (0.4 mmol), HBPin (1.2 mmol, 3 eq.), and 5 mol% poly(v) were added to a 3 mL vial with octane (1 mL) and CH_2Br_2 as the internal standard at 30 °C stirring vigorously for 16 h. All yields were determined by crude ^1H NMR analysis. ^b) 5 eq. HBPin used.

The robustness of the catalyst was tested with a variety of substituted alkynes. Both electron-donating and withdrawing substituted alkynes were very active under these conditions. Donation into the aryl ring facilitated the reaction by pushing electron density into the alpha carbon to the aryl ring and promoting anti-markovnikov addition.¹⁹⁷ Aliphatic alkynes were less active under reaction conditions compared to aromatic likely due to lack of donation from the ring and further substitutions as seen with **2g** and **2k**. Turning to internal alkynes, this catalyst was not as active, as seen by **2i** and **2j**. It is not uncommon for internal alkynes to have a higher activation energy barrier compared to terminal, as well as sterically encumbered. Poly(vba) demonstrated high activity for the hydroboration of various alkynes under mild reaction conditions.

3.8 Recycle studies of poly(vba)

Table 3.8: Recycle studies of poly(vba) for the hydroboration of phenylacetylene^{a,b}



Entry	Catalyst	Yield % ^b
1	5 mol % poly(vba)	>99
2	5 mol % recycled poly(vba)	>99
3	5 mol % recycled poly(vba) [from entry 2]	97

^a) Reaction conditions: Under an inert atmosphere of N₂, phenylacetylene (0.4 mmol), HBPiN (1.2 mmol, 3 eq.), and 5 mol% poly(vba) were added to a 3 mL vial with octane (1 mL) and CH₂Br₂ as the internal standard at 30 °C stirring vigorously for 16 h. ^b) All yields were determined by crude ¹H NMR analysis.

Lastly, the catalyst is insoluble under reaction conditions with octane, and ease of recoverability was explored. The polymer catalyst was recycled at least 3 times with no reduction of reactivity. Entry 1 in Table 3.8 began with 100 mg of poly(vba) and 80 mg were recovered for Entry 2, which was run at 4/5 scale. The recycled polymer was easily filtered with copious washes of hexane and dried to be reused. The polymer catalyst appears to have no structural changes from ¹H NMR (Figure 3.12 and Figure 3.13). Once reused for a second time, the yield of 2-styryl-BPiN has decreased slightly to 97%, with 60 mg of catalyst recovered. The catalyst possessed robust activity through three recycles, and negligible loss of reactivity.

3.9 Conclusions

The solid polymeric acid catalyst demonstrated robust activity with a variety of substituted alkynes, as well as multiple successful recycles. The catalyst has demonstrated performance comparable to the homogeneous catalyst, with improved understanding of the mechanistic pathway and catalyst design. The identification of a benzoic acid-Bpin adduct to occupy active sites, along with thorough kinetic studies have identified the site adsorption of phenylacetylene as key in product formation and release, thus regenerating the active sites for further reactivity. The KIE studies support a concerted hydroboration mechanism through the rehybridization of the labelled C(sp)–D bond of phenylacetylene. Through a combination of both KIE, reaction orders of reactants and catalyst, and ^{11}B NMR studies, a proposed catalytic cycle for the acid-catalyzed hydroboration was formed. This study provides a platform for further catalyst development utilizing polymer structures as the basis for heterogeneous catalysts.

CHAPTER 4.

HYBRID PYRROLIDINE POLYMER BRUSH ON SILICA-SUPPORTED SULFONIC ACID MATERIAL AND ITS APPLICATION IN CASCADE CATALYSIS

4.1 Introduction

Many investigations over the past decade have focused on more efficient chemical processes in attempts to streamline synthetic methods.²⁰⁶ As one example, many researchers have sought to carry out multiple reactions in one pot, eliminating the need for some work up steps and chemical separations. To facilitate this, researchers have sought to develop multicompartment catalysts, or materials that contain different catalysts in distinct zones within a solid material. These can be thought of as a distinct class of bifunctional catalysts. Invoking inspiration from biological systems, whereby large numbers of catalytic transformations occur simultaneously in distinct locations within a cell, catalyst compartmentalization in specific active pockets or zones is an important step in facilitating one-pot, multi-step reactions using opposing or incompatible catalysts. There have been many examples of site-isolated catalytic materials containing multiple distinct types of active sites, including examples based on solid supports^{207,208,209,210} and sol-gels,^{211,212} and most recently polymers.^{116,213,214,113,215,216,217}

Polymeric structures such as soluble hyperbranched polymers or dendrimers,^{13,213} as well as micelles,²¹³ all provide attractive supports for nanoscale reactors with encapsulation of various catalytic species. A solid support previously employed for many acid-base reactions has been mesoporous silica. Though silica supported catalysts have performed well in allowing for site-isolation,^{208,218,219,220,221,222} there are drawbacks to known methods of creating multifunctional catalysts based on mesoporous silica materials. For example, typical methods do not allow for precise control of the placement of key functionalities on the silica surface. Grafting of organosilanes to the silica surface and co-condensation of the organosilane with a silica precursor, such as tetraethyl orthosilicate (TEOS) are the two main methods widely used for functionalizing these supports with specific, catalytically active sites.⁶⁹ Both typically result in a random distribution of active species on the silica surface.

In contrast to traditional mesoporous silica materials, a hybrid structure that could offer an enhanced degree of tunability and alternate routes to achieve site isolation is a polymer brush. These materials are made of individual polymer chains tethered by one chain end to a solid interface.^{223,224,225} A SiO_x surface is the most common substrate from which controlled polymerizations have been employed to create well-defined polymer brushes.^{226,227,228,229,230} Such polymer brushes can be synthesized through a variety of methods. A widely used technique for brush synthesis has been surface-initiated reversible addition-fragmentation chain-transfer polymerization or SI-RAFT.^{231,232,233,39,234,40} In this work, this technique was chosen to build a catalyst designed to have the acid in the pores of the mesoporous silica support, with a basic moiety polymerized on the exterior of the mesoporous silica particles to create a

bifunctional catalyst. The two incompatible species are site isolated such that a two-step reaction cascade is readily achievable, with the ultimate goal being the synthesis of complex chromenes with the addition of a third, base catalyzed step. Many cascades demonstrate site isolation with two separately catalyzed steps, and the necessity to extend cascades to three steps begins to address the synthesis of more complex molecules in one pot with less separation cost and time. The use of a polymer brush catalyst for site isolation can incorporate multiple catalysts in two or even three domains if designed with an added level complexity based on use of block copolymer brushes. To date, this first generation of polymer brush catalyst has been used for the two-step cascade, and activity has been demonstrated for the addition of the third base catalyzed step, working towards toward synthesizing complex molecules in one pot.

4.2 Experiments

4.2.1 *Synthesis of co-condensed MCM-SH-CTAB support*

The procedure was adapted from a previously reported literature.²¹⁹ To a 1 L round bottom flask, 2.0 g of CTAB and 7.0 mL of aqueous sodium hydroxide (2.0 mol/L) were dissolved into 480 mL of water at 80 °C with stirring; 10.0 mL of TEOS (44.0 mmol) and 190.6 μ L (1.0 mmol) of 3-mercaptopropyltrimethoxysilane were then injected into the solution with vigorous stirring. After 1 h stirring, 1.0 mL of additional TEOS was injected to the solution with continued vigorous stirring. After 2 h, the produced solid was separated by hot filtration, washed with excess water, dried at 75 °C under vacuum overnight. To ensure selective functionalization of the external surface of the mesoporous silica, the as-made solid containing the template, CTAB, was analyzed

by nitrogen physisorption to confirm the template was inside mesoporous channels and blocking the pores. The support is labelled as MCM-SH-CTAB, with a BET surface area of 17 m² /g. Owing to the CTAB-blocked pores, the pore volume is less than 0.1 cm³ /g, as shown in Table 4.3.

4.2.2 Thiol oxidation of MCM-SH-CTAB support

Adapted from previous literature procedures,^{219,235} the co-condensed MCM-SH-CTAB support was dispersed in 30 % H₂O₂ in H₂O (50 mL) at 60 °C for 6h. The resulting oxidized material, known as MCM-SO₃H, was characterized by nitrogen physisorption to confirm the template CTAB remained inside the mesoporous channels, with a BET surface area of 75 m²/g and blocked pores (pore volume is less than 0.1 cm³/g), as shown in Table 4.3.

4.2.3 RAFT chain transfer agent silane synthesis

In a 50 mL round bottom flask, 0.100 g (0.274 mmol, 1eq.) of 2-(dodecylthiocarbonothioylthio)-2-methylpropanoic acid was dissolved in anhydrous CHCl₃. Slowly, 1.2 eq. (0.329 mmol) of oxalyl chloride was then added under Ar. The solution was stirred and monitored by TLC (1:1 EtOAc:Hex) over the course of 2 h until the reaction was complete. The resulting solution was removed by rotary evaporation to yield the acid chloride product **2**. ¹H NMR (δ, ppm): 3.25-3.21 (t, 2H, J = 7.4 Hz, -CH₂-CH₂-S-C=S), 1.77 (s, 6H, -S-C(CH₃)₂-COCl), 1.70-1.66 (t, 2H, J = 7.3 Hz, -CH₂-CH₂-S-C=S), 1.39-1.25 (m, 18H, CH₃-C₉H₁₈-CH₂-CH₂-S-C=S), 0.89-0.86 (t, 3H, J = 6.2 Hz, CH₃-C₉H₁₈-CH₂-CH₂-S-C=S).¹ The solid **2** was then dissolved in anhydrous toluene, and 1.05 eq. (0.288 mmol) of 3-aminopropyltriethoxysilane (APTES) was added. The

reaction was stirred under argon for 24 h at 80 °C with a reflux condenser. The resulting product **3** was first filtered to remove residual salt and yielded a yellow oil (0.153 g, 98%).

4.2.4 Synthesis of (S)-((1-(Tert-Butoxycarbonyl)Pyrrolidin-2-yl)Methyl) Acrylamide

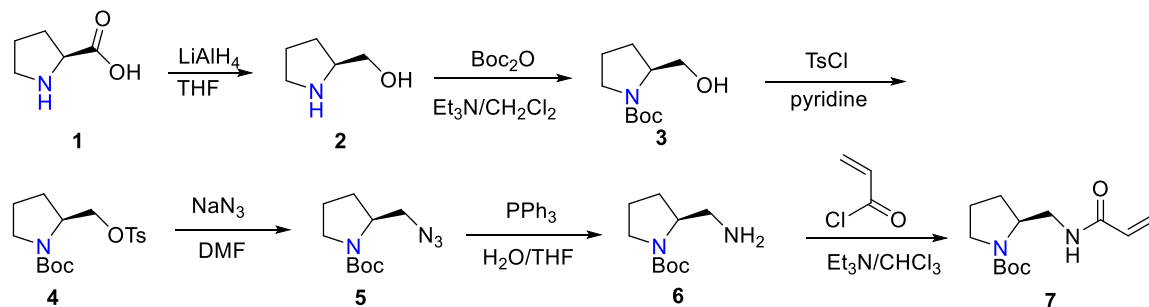


Figure 4.1: General synthesis of boc-pyrrolidine acrylamide monomer.

4.2.4.1 (S)-2-Pyrrolidinemethanol (**2**)

(S)-Prolinol was synthesized according to an adapted literature procedure. At 0 °C, a solution of L-proline (5 g, 43.4 mmol) was stirred with anhydrous THF (100 mL) under Ar. LiAlH_4 (3 eq.) was weighed out in air, and slowly added to the solution. The solution was stirred vigorously and allowed to warm to room temperature. Next the solution was refluxed for 24 h. The solution was then cooled in an ice bath, and slowly neutralized with cold MeOH and DI H_2O . The solid was filtered from solution, and the filtrate was condensed by rotary evaporation to yield a light yellow thick oil (4.0 g, 91 %). ^1H NMR (300 MHz, CDCl_3) δ 3.50 (m, 1H), 3.29 (m, 2H), 2.92 (m, 1H), 2.85 (m, 1H), 1.85–1.65 (m, 3H), 1.41 (m, 1H).

4.2.4.2 (S)-1-(*Tert*-butoxycarbonyl)-2-pyrrolidinemethanol (3)

Product **3** was synthesized according to previously reported literature.²³⁶ Di-*tert*-butyl decarbonate (8.64 g, 39.6 mmol) was added to a solution of L-prolinol (4.0 g, 19.8 mmol) and triethylamine (8.28 mL, 59.4 mmol) in dichloromethane at 0 °C. The reaction was stirred vigorously overnight at room temperature. The resulting solution was washed with saturated NaHCO₃ and brine. The organic layer was dried over MgSO₄ and the solvent removed by rotary evaporation to give (S)-1-(*tert*-butoxycarbonyl)-2-pyrrolidinemethanol (95 %) as a white solid. ¹H NMR (300 MHz, CDCl₃) δ 4.84-4.64 (m, 1H), 4.06-3.72 (m, 1H), 2.08-1.94 (m, 2H), 1.89-1.70 (m, 2H), 3.72-3.30 (m, 4H), 1.60-1.50 (m, 1H), 1.47 (s, 9H, *tert*-butyl).

4.2.4.3 (S)-2-[(4-Toluenesulfonyloxy)methyl]pyrrolidine-1-carboxylic acid *tert*-butyl ester (4)

The preparation of product **4** was adapted from previous literature.²³⁶ (S)-1-(*Tert*-butoxycarbonyl)-2-pyrrolidinemethanol (7.56 g, 37.6 mmol) was dissolved in excess pyridine (40 mL) and cooled to 0 °C. *p*-Toluenesulfonyl chloride (8.6 g, 45.1 mmol) was added and the mixture slowly turned dark pink, and stirred at 0 °C overnight. The reaction was diluted with ethyl acetate (200 mL). The mixture was washed with 1 M HCl (3 x 100 mL), saturated NaHCO₃ (3 x 100 mL), and brine (2 x 100 mL). The organic layer was dried over Na₂SO₄ and the solvent removed by rotary evaporation to yield (S)-2-[(4-toluenesulfonyloxy)methyl]pyrrolidine-1-carboxylic acid *tert*-butyl ester (75 %) as a light pink oil. ¹H NMR (300 MHz, CDCl₃) δ 7.78 (d, 2H, *J* = 4.05 Hz), 7.42-7.28 (m,

2H), 4.22-3.76 (m, 2H), 3.46-3.22 (m, 2H), 2.02-1.70 (br-m, 4H), 1.50-1.14 (s, 9H, *tert*-butyl).

4.2.4.4 (S)-2-(Azidomethyl)pyrrolidine-1-carboxylic acid *tert*-butyl ester (5)

The synthesis of product **5** was adapted from previously reported literature.²³⁶ (S)-2-[(4-Toluenesulfonyloxy)methyl]pyrrolidine-1-carboxylic acid *tert*-butyl ester (10 g, 28.2 mmol) was dissolved in DMF (100 mL). Sodium azide (5.5 g, 84.6 mmol) was added to the mixture and the reaction was heated to 65 °C for 24 h. The reaction was cooled to room temperature and diluted with diethyl ether (50 mL). The organic phase was washed with water (4 x 100 mL) and brine (100 mL). The organic phase was dried over Na₂SO₄ and concentrated down by rotary evaporation to give (S)-2-(azidomethyl)pyrrolidine-1-carboxylic acid *tert*-butyl ester (70 %) as a colorless oil. ¹H NMR (300 MHz, CDCl₃) δ 4.10-3.80 (m, 1H), 3.65-3.40 (m, 3H), 2.10-1.76 (m, 4H), 1.47 (m, 9H, *tert*-butyl).

4.2.4.5 (S)-1-(*Tert*-butoxycarbonyl)-2-aminomethylpyrrolidine (6)

Product **6** was adapted from previously reported literature.²³⁶ (S)-2-(Azidomethyl)pyrrolidine-1-carboxylic acid *tert*-butyl ester (4.46 g, 19.7 mmol) was dissolved in THF (100 mL) and water (10 mL). Triphenylphosphine (10.3 g, 39.4 mmol) was added and the mixture refluxed for 24 hours. The organic solvent was removed under reduced pressure and the resulting solid was dissolved in diethyl ether (100 mL). The solution was extracted, and using 1 M HCl the aqueous layer was acidified to a pH of 1. The aqueous layer was washed with diethyl ether (4 x 100 mL) and the pH was then raised to 13 using 1 M NaOH solution. The product was extracted into dichloromethane

(2 x 100 mL) and the organic layers combined and dried using Na₂SO₄ and concentrated to give (S)-1-(*tert*-butoxycarbonyl)-2-aminomethylpyrrolidine (85 %) as a light yellow oil. ¹H NMR (300 MHz, CDCl₃) δ 3.90-3.65 (m, 2H), 3.60-3.25 (m, 2H), 2.95-2.60 (m, 2H), 2.05-1.75 (m, 4H), 1.47 (m, 9H, *tert*-butyl).

4.2.4.6 (S)-((1-(*Tert*-butoxycarbonxyl)pyrrolidin-2-yl)methyl) Acrylamide (7)

The final monomer **7** was synthesized according to a previously reported literature.²³⁶ (S)-1-(*tert*-butoxycarbonyl)-2-aminomethylpyrrolidine (3.36 g, 16.7 mmol) and triethylamine (3.49 mL, 25.1 mmol) were dissolved in anhydrous dichloromethane (50 mL), and the solution was stirred at 0 °C under Ar atmosphere. Acryloyl chloride (1.61 mL, 20.0 mmol) was slowly added dropwise to the solution, and the solution stirred at 0 °C for 7h. The reaction was monitored by TLC until completion. The resulting solution was concentrated down, and re-dissolved in ethyl acetate. The solution was kept overnight at 0 °C to precipitate triethylamine hydrochloride, and filtration was then carried out to remove the salts. The filtrate was concentrated and the residue purified by column chromatography (silica gel/ethyl acetate) to give the boc-pyrrolidine acrylamide monomer (70 %) as a colorless solid. ¹H NMR (300 MHz, CDCl₃) δ 6.38-5.80 (m, 2H), 5.60 (d, 2H, J = 5.10 Hz), 4.20-3.85 (m, 2H), 3.55-3.00 (m, 4H), 2.14-1.60 (m, 4H), 1.47 (m, 9H, *tert*-butyl).

4.2.5 *Poly(Boc-pyrrolidine acrylamide) polymer silane synthesis*

The poly(boc-pyrrolidine acrylamide) silane was synthesized through a typical RAFT procedure and used in the “grafting to” approach. 0.688 g of monomer (2.7 mmol, 50 eq.), 0.030 g modified-CTA (0.54 mmol, 1 eq.), 0.001 g AIBN (0.0054 mmol, 0.1

eq.), 4 mL of DMF, and trioxane as the internal standard was dissolved and sonicated in a 10 mL Schlenk flask. Five freeze, pump, thaw cycles were performed on the reaction solution. The reaction was purged with argon and vigorously stirred for 8 h at 80 °C. The polymerization was monitored by ^1H NMR until 60% conversion. The resulting solution was dialyzed in a 2 KDa bag, in THF. The dialyzed solution was removed by rotary evaporation yielding a light yellow oil (0.480 g, 70%). The resulting polymer was analyzed by chloroform GPC to give $M_n = 2800$ g/mol with a $\bar{D} 1.24$.

4.2.6 General grafting procedure

The grafting procedure was adapted from previous literature.⁷⁰ To start, 0.500g of MCM-SO₃H-CTAB was dried overnight at 100 °C. under reduced pressure. The silica was then stirred vigorously in anhydrous toluene under a flow of argon and taken into the glove box. The poly(boc-pyrrolidine acrylamide) silane (0.200 mL) was added to the solution via micropipette. The reaction was stirred at room temperature for 8 h, then heated to 80 °C for an additional 24 h. The reaction mixture was allowed to cool, and filtered and washed with 100 mL of toluene, 100 mL hexanes and 100 mL of ethanol. The functionalized MCM-SO₃H-CTAB was dried overnight at 100 °C to yield MCM-SO₃H-bocpyrrol-gt functionalized at a loading of 0.57 mmol N/g silica support.

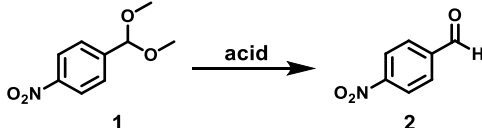
4.2.7 General 2-step cascade reaction procedure

In a pressure tube, 0.25 mmol (1 eq.) of 4-nitrobenzaldehyde dimethylacetal, 0.30 mmol (1.2 eq.) of malononitrile, and 40 mg of MCM-catalyst were combined with 1 mL of anhydrous CH₃CN and 2 eq. H₂O. The reaction was heated to 90 °C for 48 h. The resulting solution was then allowed to cool to room temperature, and the CH₃CN and

H₂O were removed by vacuum. The solution was dissolved in DMSO-*d*₆, filtered through a plug of silica gel and 0.25 mmol DMF added. Finally, ¹H NMR was used to determine the yield (%).

4.2.8 Optimization of acid-catalyzed deacetalization

Table 4.1: Control reactions of sulfonic-acid catalyzed deprotection of 4-nitrobenzaldehyde dimethylacetal^{a,b}

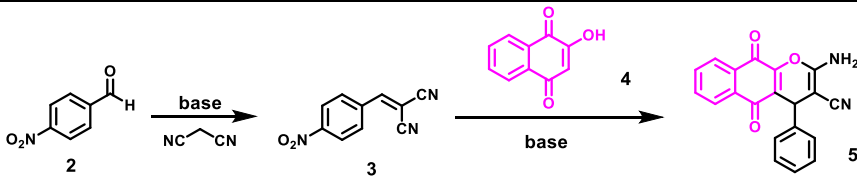
		
Entry	Catalyst	Yield 2 ^b
1	--	0
2	MCM-41 (40 mg)	0
3	MCM-SH	0

^{a)} Reaction conditions: 0.25 mmol of compound **1** in 1.0 mL anhydrous CH₃CN at 90 °C for 48 h.

^{b)} Yield % was determined by ¹H NMR.

4.2.9 Optimization of base-catalyzed Knoevenagel and Michael addition

Table 4.2: Control reactions of base-catalyzed Knoevenagel and Michael addition^{a,b}

		
Entry	Catalyst	Yield
1	--	0
2	MCM-41 (40 mg)	0
3	Proline	32
4*	MCM-Pyrrolidine	88
5	MCM-pyrrolidine-gt	88

^{a)} Reaction conditions: 4-nitrobenzaldehyde (0.25 mmol), catalyst (5 mol%) in anhydrous CH₃CN (1 mL) at rt for 24h. ^{b)} The yield % was determined by ¹H NMR; 0.25 mmol DMF was used for internal standard. *10 mol% catalyst

4.3 Materials Characterization

Table 4.3: Nitrogen physisorption of mesoporous silica catalysts

Catalyst	BET surface area (m²/g_{SiO₂})	Pore volume (cm³/g)
MCM-SH-CTAB	17	-
MCM-SH	686	0.21
MCM-SO ₃ H-CTAB	75	0.08
MCM-SO ₃ H	820	0.50
MCM-SO ₃ H-CTA-CTAB	320	0.16
MCM-SO ₃ H-t-butyl	780	0.33
MCM-SO ₃ H-bocpyrrol-m-CTAB	300	0.07
MCM-SO ₃ H-pyrrol-m	765	0.35
MCM-SO ₃ H-bocpyrrol-gt CTAB	320	0.09
MCM-SO ₃ H-pyrrol-gt	740	0.30

Table 4.4: Elemental analysis of mesoporous silica catalysts

Catalyst	EA C wt %	EA N wt %	EA S wt %
MCM-SH	2.57	--	1.2
MCM-SO ₃ H	1.55	--	0.43
MCM-SO ₃ H-t-butyl	4.77	--	0.38
MCM-SO ₃ H-COOH	4.27	--	0.37
MCM-SO ₃ H-COCl	6.96	0.72	0.35
MCM-SO ₃ H-bocpyrrol-m	6.76	1.17	0.36
MCM-SO ₃ H-pyrrol-m	4.5	0.97	0.31
MCM-SO ₃ H-CTA	3.94	0.46	0.92
MCM-SO ₃ H-pyrrol-gt	3.66	1.32	0.31
MCM-SO ₃ H-pyrrol-gf	5.37	0.80	0.87

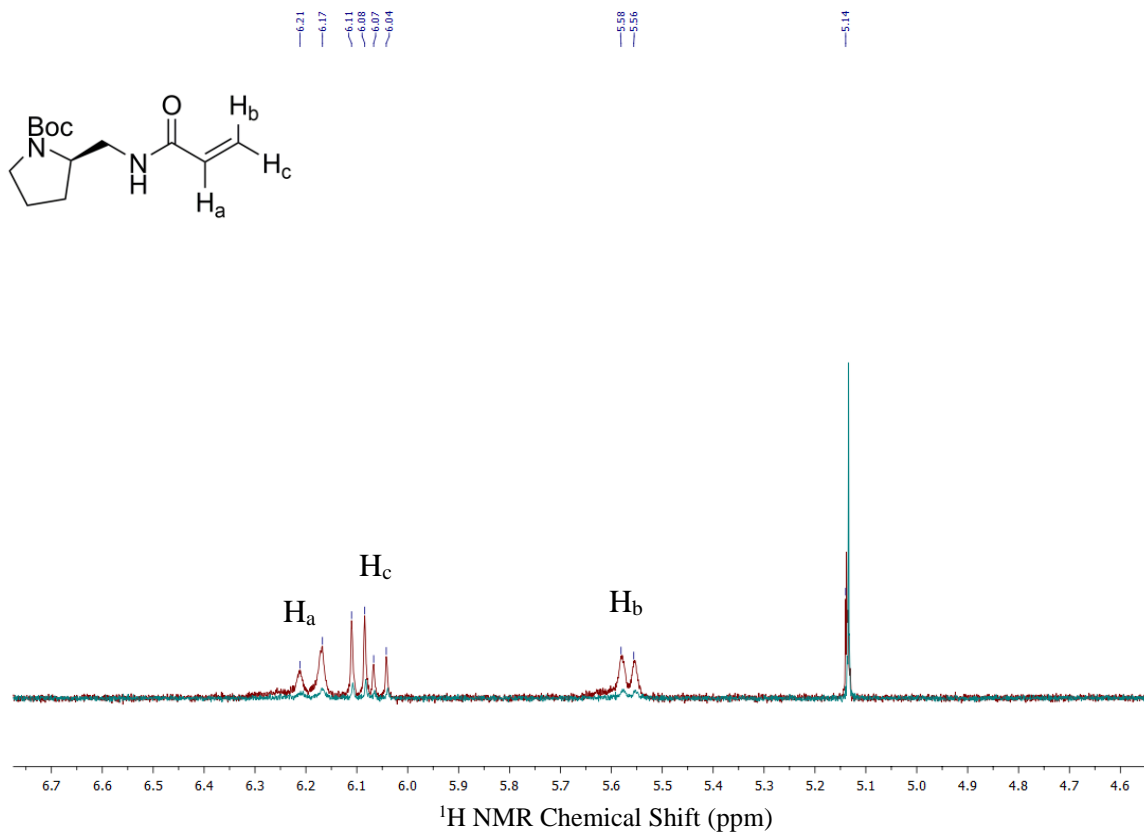


Figure 4.2: ^1H NMR spectra of vinyl protons in RAFT polymerization of poly(boc-pyrrolidine acrylamide) silane (t = 0, red; t = 18 h, blue).

Table 4.5: ^1H NMR vinyl proton integration values derived from Figure 4.2 spectra

Spectra	Integration*		
	H _a	H _b	H _c
t = 0	1.00	1.05	1.02
t = 18 h	0.26	0.28	0.25

*Integration of proton peaks with respect to 1,3,5-trioxane (5.14 ppm)

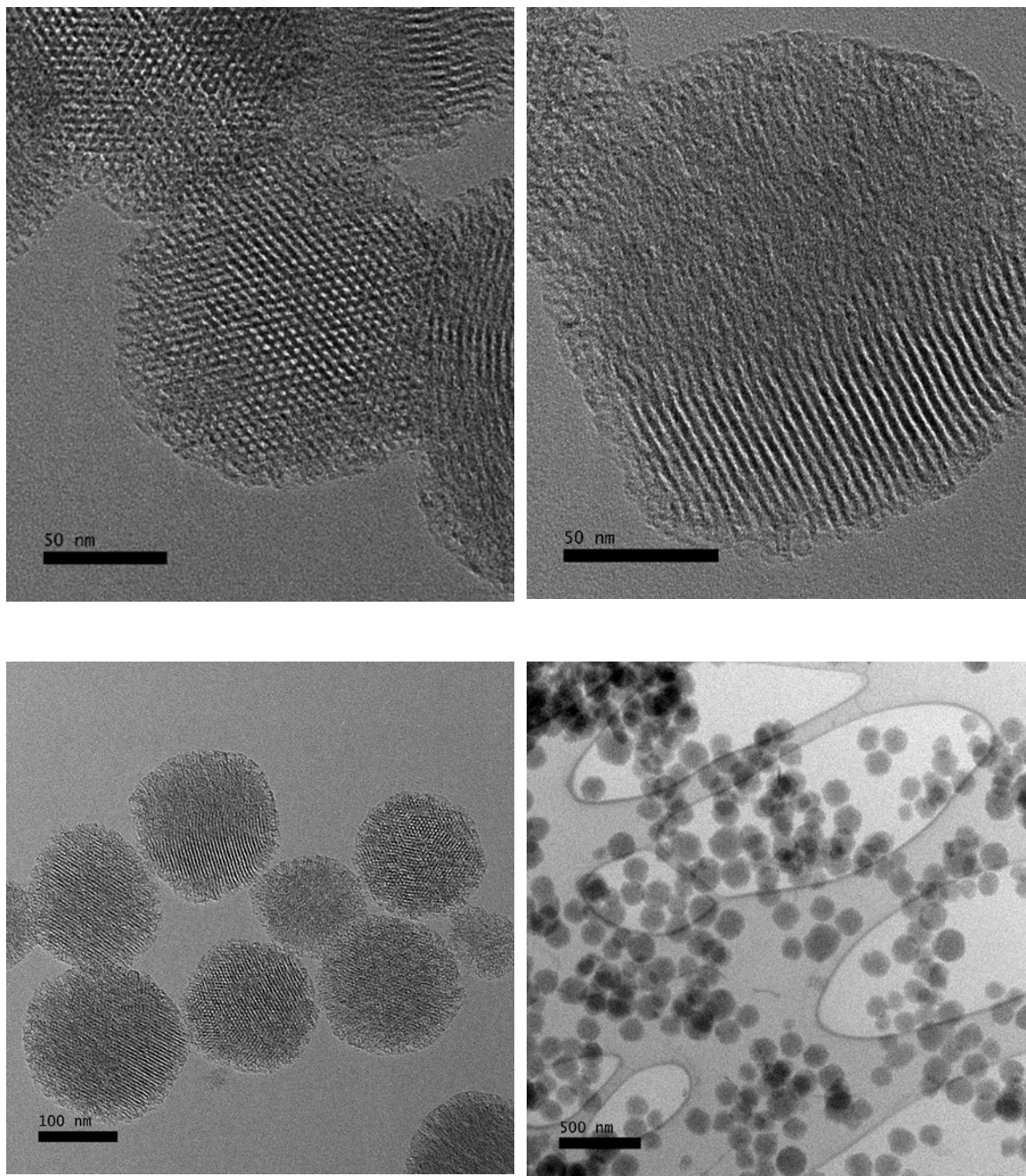


Figure 4.3: TEM images of core-shell mesoporous silica catalyst support, referred to as MCM-SO₃H-CTAB is removed from the pores for imaging.

4.4 Results and Discussion

4.4.1 Design of acid-base polymer brush catalyst

The design of the hybrid polymer brush material began with identifying key catalytic species for each step and incorporation of the catalytic sites in different zones on the support. In many cascade reactions, proof of site isolation is demonstrated through an acid-base cascade due to the inherent site annihilation that would occur otherwise. The acidic and basic moieties were separated by utilizing a rigid support for the encapsulation of the acidic catalyst, while a flexible polymer brush provided a tunable platform for incorporation of the base on the external surface of the silica particles. Together these two species could participate in distinct steps of the proposed reaction cascade without fear of quenching

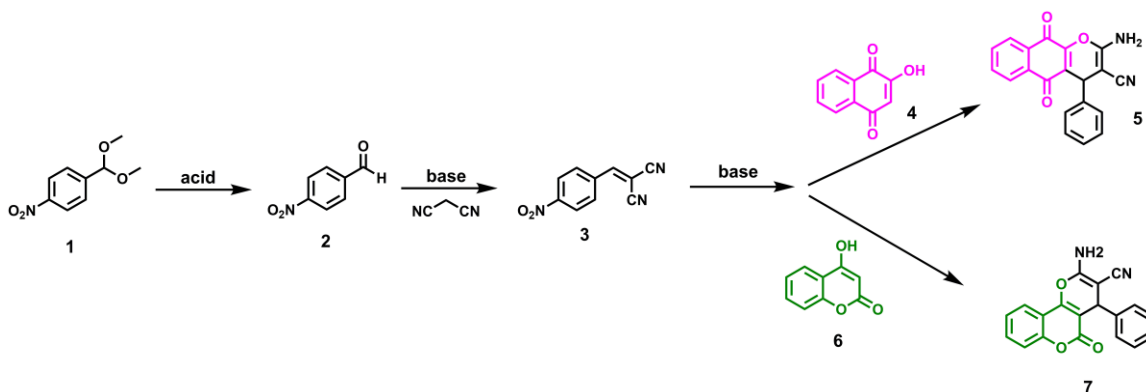


Figure 4.4: 3-Step cascade reaction catalyzed by a site-isolated acid-base polymer brush.

The cascade chosen incorporates both a strong acid and base, with the basic moiety performing two separate steps in the cascade (Figure 4.4), while requiring a

catalyst structure that accommodates a large final molecule. The catalyst designed accounted for the size of both the starting material and final product, through performing the acetal-deprotection step in the pores of the silica, with the resulting 4-nitrobenzaldehyde material condensing with malononitrile in a Knoevenagel condensation. The product of this reaction can then react via a Michael addition to yield a large chromene in the polymer brush domain, outside the silica pores, where it might otherwise be sterically hindered within the mesopores of the silica. The size of the resulting product required the design of a bifunctional material with an acidic moiety in the interior pores and basic moiety, which is provided in excess, on the exterior of the catalyst.

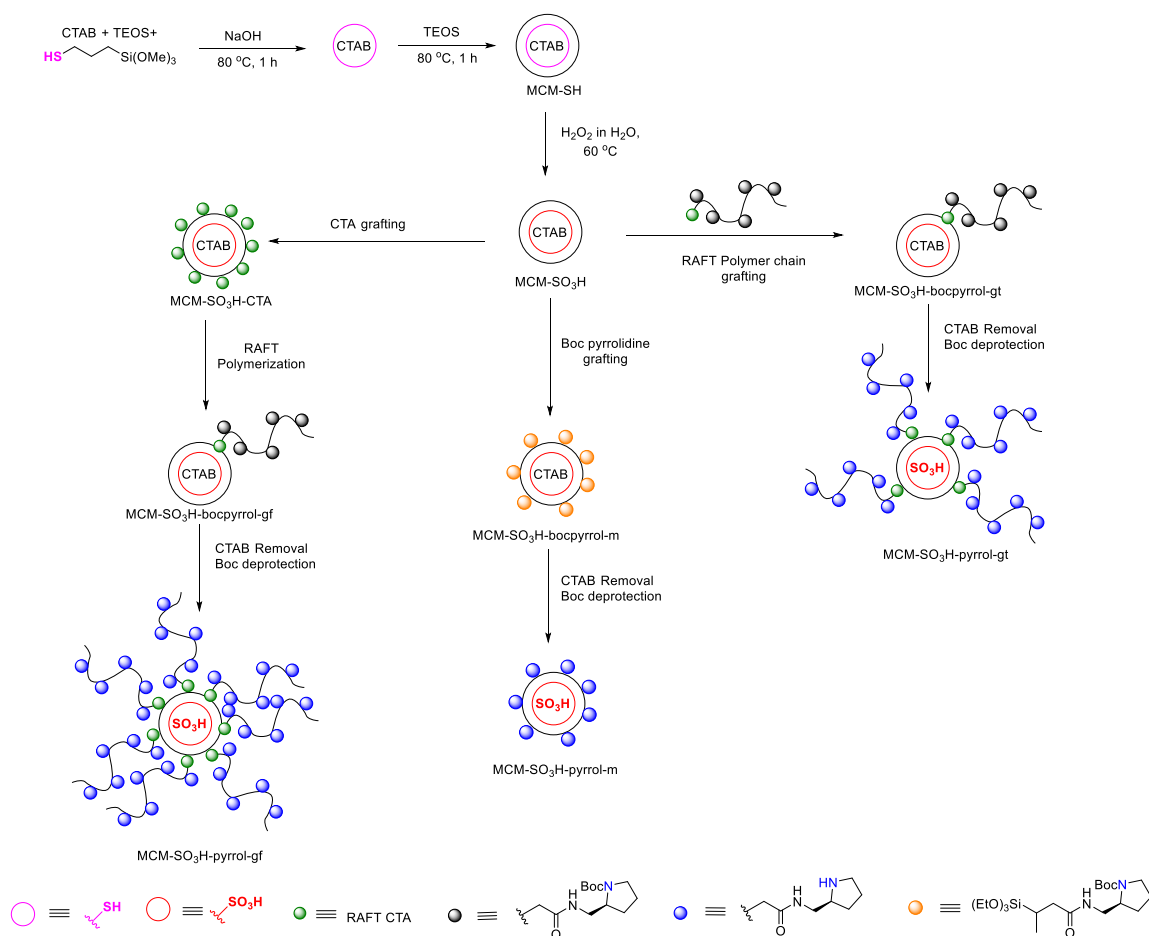


Figure 4.5: General syntheses of three hybrid sulfonic-acid pyrrolidine supported catalysts.

Above in Figure 4.5, the general synthetic paths to three different site isolated catalysts is shown. The final catalysts are labelled as the “support-acid-base-synthesis method” to differentiate the brush structures from a molecularly functionalized catalyst. To begin the synthesis of the acidic support, the co-condensation method was employed, which incorporates a functional organosilane throughout the entire structure in the initial stages of the synthesis.⁶⁴ In this study, (3-mercaptopropyl)triethoxysilane was chosen, which was further oxidized to create a strong sulfonic acid in mesoporous MCM-41 as the silica support. Exposed thiol groups on the exterior of the support would likely inhibit

the polymerization of the polymer brush on the outer surface in further steps, so a thin, porous silica shell layer was added to prevent thiol exposure and potential quenching of the polymerization process. In previous literature, a mesoporous silica support combined both acids and bases for a cascade reaction, and a core-shell structure was synthesized to avoid quenching of the two functionalities.²²⁰ Applying a thin shell layer of silica onto the acid functionalized support successfully prevented quenching of the RAFT polymerization, as well as provided a bare exterior silica surface to further functionalize.

Once the core-shell structure was synthesized, the strong acid was exposed through oxidation of the thiol to a sulfonic acid using hydrogen peroxide.²³⁵ Nitrogen physisorption was conducted on each material after modification to analyze for residual surfactant in the pores, which is important for preventing the interior of the silica from modification in subsequent polymerization or grafting steps that are designed to target only the external surface of the silica particles. The low concentration of thiol incorporation into the silica material proved challenging to assess its presence through IR or solid state NMR. Therefore, the thiol oxidation was quantified through titrating the material with sodium hydroxide. The resulting number of acid groups titrated was compared with the mole percent sulfur incorporated into the structure from elemental analysis, which gave 0.10 mmol SO₃H/g silica support by titration vs. 0.125 mmol S/g silica support by elemental analysis. The material referred to as MCM-SO₃H was carried through as the catalyst support for the three catalysts with the added thin layer of silica, as observed in TEM (Figure 4.3). Prior to oxidation, MCM-SH exhibited a surface area of < 20 m²/g and post-oxidation, the MCM-SO₃H material displayed a surface area of 75

surface of the support and the polymerization occurs from the initiator or chain transfer agent on the surface. The “grafting from” approach often yields a higher density of polymer brushes on the surface of the substrate, as the steric hindrance of grafting a polymer chain to a surface becomes a challenge. The choice of RAFT chain transfer agent (CTA) is critical for the polymerization process and dependent on the monomer structure.²³⁷

For the “grafting from” approach, the SI-RAFT process proceeds by anchoring the CTA to the surface via the R group or the Z group.²³⁸ Most commonly the R group is anchored, likely because the carboxylic acid end group provides a functional handle for further modification. As shown in Figure 4.6, the R group of the CTA was modified to an acyl chloride which coupled to 3-aminopropyltriethoxysilane that was grafted to the surface of the silica-acid support to a 0.3 mmol CTA/g silica support (Table 4.4). Once the modified CTA-silane was grafted to the exterior of MCM-SO₃H-CTAB, the next step was polymerization with the acrylamide monomer (Figure 4.1).²³⁶ In a previous report, a proline-functionalized magnetic nanoparticle was an efficient base catalyst for the Knoevenagel and Michael addition steps of the planned cascade, thus we synthesized an analogous monomer for the basic brushes.²³⁹

The two methods of polymerization shown in Figure 4.6 were optimized for each method. For the “grafting from” method, polymerization conditions were found to be 24 h, at 70 °C using AIBN as the radical source in DMF. The polymerization demonstrated an induction period of about 12 h, which is not uncommon for SI-RAFT.²⁴⁰ The polymerization was monitored by liquid ¹H NMR for the decrease of vinyl proton peaks, and the polymerization was quenched in liquid nitrogen and exposed to air throughout the

reaction. The material was further washed with copious amounts of water, methanol, and chloroform to remove unreacted monomer or polymer formed in solution.

Using the boc-pyrrolidine acrylamide monomer with the modified CTA and AIBN as the initiator, the polymerization was carried out for 8 h, approaching a similar length polymer chain synthesized with the “grafting from” approach on the MCM-SO₃H-CTAB surface. Grafting the polymer chain required additional heating and extended reaction times on previously dried MCM-SO₃H-CTAB. The grafting chain density was expected to be lower compared to the “grafting from” method, as confirmed by elemental analysis, which showed 0.57 mmol N/g MCM-SO₃H-pyrrol-gt. In a final step, to expose the basic moiety and remove the structure directing agent, CTAB, stirring of the samples in acidic methanol was performed. The resulting materials were then neutralized with sodium bicarbonate and dried overnight on the high vacuum line.

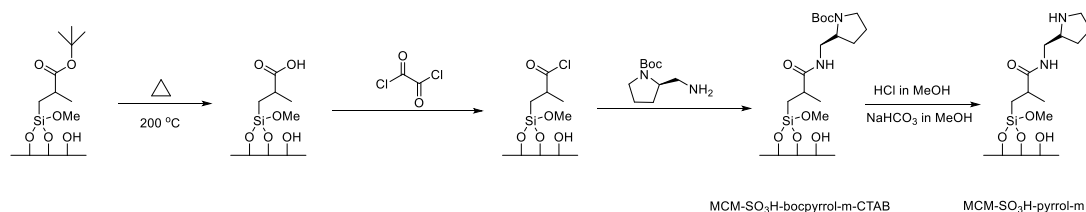


Figure 4.7: General preparation of MCM-SO₃H-pyrrol molecular catalyst.

The third catalyst was a material containing a molecular basic active site grafted on the external surface of the mesoporous silica, as depicted above in Figure 4.7. The molecular pyrrole should have the same basicity as the analogous polymer chain, to evaluate the impact of placing the basic catalyst in a polymer phase in high density, vs. as isolated base sites on the external surface of the mesoporous silica solid. The synthesis

began with a protected carboxylic-acid silane that was synthesized following literature procedures,⁶⁹ and grafted onto the same batch of co-condensed MCM-SO₃H-CTAB with the thin additional layer of silica to ensure continuity of support structure with all three catalysts. Next, the carboxylic acid was exposed via thermal deprotection, and reacted with oxalyl chloride to yield the active acyl chloride. The acyl chloride was then converted to the protected pyrrolidine via substitution using the amine functionalized monomer. The final silane is then deprotected to yield the acrylamide pyrrole that is analogous to the monomer structure of the polymer chains.

4.4.2 *Catalyst structure effects on Acid-Base cascade reaction*

The array of catalytic materials was anticipated to perform with varying catalytic efficiency, depending on the final structure of the materials, as influenced by the synthetic pathways used. The exploration of cascade reactions began with substituted chromenes as the target, due to the complexity of the structure, and demonstration of three steps in one pot from a simple starting material like 4-nitrobenzaldehyde dimethyl acetal. The acid-catalyzed deacetalization reaction conditions have been known to be highly dependent on the amount of water present,^{16,17} and control reactions were carried out to demonstrate no background conversion was observed with the MCM-41 silica support (Table 4.1 and Table 4.2). For the deacetalization, extended reaction times were needed to reach completion with the molecular MCM-SO₃H-pyrrol-m. This is hypothesized to be due to diffusion limitations associated with transport of the reagent into the interior of the mesoporous support, and not necessarily due to steric hindrance associated with the polymer layer because long reaction times were necessary for both the MCM-SO₃H-pyrrol-m and MCM-SO₃H-pyrrol-gt catalysts. In testing the materials

for the Knoevenagel and Michael addition steps, shorter reaction times were needed for the basic steps, where the needed active sites are more exposed to the reagents. There was no background conversion observed with the MCM-41 silica support, and minimal conversion when proline was used as a bifunctional, homogeneous acid/base catalyst (Table 4.2). The notable observation with the control testing of the base-catalyzed steps was the need for an additional 5 mol% MCM-SO₃H-pyrrol-m based on amine content to achieve the same conversion as the brush catalyst, MCM-SO₃H-pyrrol-gt. in the 24 h reaction time. The MCM-SO₃H-pyrrol-gt. catalyst incorporates more amine active sites per gram of silica because of the brush structure synthesized, demonstrating the utility of a polymer brush catalyst structure versus grafting single molecular units. The activity for both steps with the two base-functionalized catalysts was encouraging for further extending the cascade to including a third step in the full three step cascade.

Table 4.6: 2-step cascade reaction of 4-nitrobenzaldehyde dimethyl acetal to 2-benzylidenemalononitrile^{a,b}

Entry	Catalyst	Conv. 1 (%)	Yield 2 (%)	Yield 3 (%) ^b
1	MCM-SH	--	--	--
2	MCM-SO ₃ H	100	--	--
3	MCM-pyrrol	--	--	--
4	MCM-SO ₃ H-pyrrol-m	96	31	65
5	MCM-SO ₃ H-pyrrol g.t.	97	27	70

^{a)} Reaction conditions: 4-nitrobenzaldehyde (0.25 mmol), 2 eq. DI H₂O, catalyst (5 mol% acid) in anhydrous CH₃CN (1 mL) at 90 °C for 72 h. ^{b)} The yield % was determined by ¹H NMR; 0.25 mmol DMF was used as an internal standard.

To begin testing the activity of the bifunctional materials in both the acid and base catalyzed steps together, we began with a two-step cascade reaction of 4-nitrobenzaldehyde dimethyl acetal to 2-benzylidenemalononitrile. The reaction with a control MCM-SH catalyst that was devoid of intentionally added acid or base sites did not show any activity toward the conversion of **1**, as shown in Entry 1, Table 4.6. Next, using MCM-SO₃H with no basic functionality, there was full conversion of **1** to **2**, and no further reactivity in the base catalyzed reaction, as expected. With introduction of the bifunctional materials, both reactions proceeded to full conversion of the starting compound **1** to **2**, and further 70 % yield of **3**. Both catalysts demonstrating similar conversion to **3** is possibly due to the delayed conversion of **1** to **2**. The acid deprotection takes 48 h to reach completion, and the conversion of **3** is dependent on the diffusion of **2** to the exterior of the particle, and then reacting with the basic moieties. Hypothesized longer reaction times could facilitate higher conversion of **2** to **3** using the brush or molecular catalyst. However, additional kinetic data are needed to elucidate the activity of the molecular catalyst versus the brush systems. The MCM-SO₃H-pyrrol-gt has an amine content of 0.57 mmol N/g MCM-SO₃H-pyrrol-gt, and the MCM-SO₃H-pyrrol-m has an estimated 0.69 mmol N/g MCM-SO₃H-pyrrol-m. Though the brush catalyst has a slightly reduced number of amine sites per gram of silica support, it is hypothesized that the brush structure allows the amines more mobility in solution, as opposed to the 2 carbon alkyl chain of the molecular species. Though the MCM-SO₃H-pyrrol-gt likely has sparsely grafted amine chains, compared to the molecular catalyst, the freedom of mobility of those chains in solution could facilitate the similar conversions of **2** to **3** in the base catalyzed Knoevenagel condensation. The demonstration of both catalyst's activity for

the two-step cascade indicate the two catalysts have active sites that are relatively isolated and active for this cascade, with additional cascade reaction optimization necessary for the addition third base-catalyzed Michael addition.

4.5 Conclusions

The rational design of polymer brush material comprised of a strong acid in the mesopores of the support, and polymerization of a basic moiety off the external surface, forming polymer brushes, catalyzed a two-step acetal deprotection-Knoevenagel cascade reaction with the potential for a third step. From reactions using the MCM-SO₃H-pyrrolidine-gt versus MCM-SO₃H-pyrrolidine-m, there was a need for more molecular active sites to reach the same conversion as the catalyst containing the brushes. The acid-catalyzed deacetalization needed longer reaction times to reach completion, hypothesized to be due to steric constraints of the mesopores and diffusion limitations within the support. The basic catalyst efficiently catalyzed both Knoevenagel and Michael additions, needing additional molecular catalyst to enhance the reaction rate. The acid and base moieties demonstrated activity for both steps in the cascade, as well as effective site-isolation of each type of active site. This work demonstrates the utility of the brush structure and the application of the hybrid materials in future catalytic cascades.

CHAPTER 5.

C(SP³)-H MONOARYLATION CATALYZED BY A COVALENTLY CROSS-LINKED REVERSE MICELLE- SUPPORTED PALLADIUM CATALYST

This project was completed with assistance from Dr. Li-Chen Lee on both synthesis and catalytic reactions. The double tail micelle was synthesized by Dr. Li-Chen Lee for reaction optimization and ¹H NMR for crude product analysis. Parts of this chapter are reproduced from ‘Hoyt, C.B.; Chen, L. – C.; He, J.; Yu, J. – Q.; Jones, C. W. Selective C(sp³) – H monoarylation catalyzed by a covalently cross-linked reverse micelle-supported palladium catalyst. *AdvSynthCatal*, **2017**, 359, 3611-3617.’

5.1 Background

Development of methods for direct insertion of C–H bonds has attracted substantial attention over the past two decades due to the abundance of these bonds. Unfortunately, the typical C(sp³)-H bond is highly inert and thermodynamically stable, requiring eloquent catalytic strategies to activate the bond compared to conventional C–H functionalization methods.^{241,242} Transition-metal-catalyzed directed C–H activation has been extensively explored by installing powerful directing groups,^{243,244,245,246,247,248,249,250,251,252} and the scope of the transformations can be further expanded through the incorporation of ligands into the catalysis.^{169,253,254,255,256,257,258,259,260,261} Recent studies of specific ligand design for

coordination with palladium have proved to be critical for C–H activation, and advantageously require less synthetic steps.¹⁶⁹ Tuning the coordination environments of palladium catalysts with various ligands has been used to selectively activate different types of C(sp³)–H bonds.

One of the first examples of Pd(II)-catalyzed C(sp³)–H arylation was reported in 2005, where pyridine acted as a directing group. Considering C(sp³)–H arylation could be directed by a pyridine moiety, it was reasoned that bidentate coordination between the active palladium center and an aminoquinoline species would benefit the reaction specificity.²⁶² Later, the reaction was honed for specific monoarylation employing substituted aryl iodides not requiring steric bulk, such as a tert-butyl group, which allowed for further functionalization strategies. The Yu group employed a non-natural amino acid starting material with excess amounts of aryl iodides, and identified 2-picoline as a ligand for selective monoarylation using homogeneous palladium(II) trifluoroacetate.¹⁶⁹

While homogeneous Pd catalysts have been widely used in C(sp³)–H arylation, relatively high catalyst loadings are often required to obtain good yields in these C(sp³)–H activation/C–C bond-forming reactions, since the catalysts are prone to decomposition under harsh reaction conditions. One way to enhance the turnover numbers (TONs) and better utilize the ligand and metal species is to recover and recycle these components. However, in many cases, reuse of homogeneous transition metal catalysts remains a significant challenge. We have recently demonstrated the feasibility of reuse of Pd(II) combined with Yu’s mono-dentate pyridine ligands and have shown that the catalyst, both ligand and metal, can be recovered and recycled, modestly improving the TON.

Using soluble polymeric supports with tailorable structures, we also demonstrated that the supported Pd species could impart altered (relative to the homogeneous catalyst) selectivity trends using several model substrates.²⁶³ Other types of supported catalysts have also been utilized in C–H activation, with use of metal organic framework (MOF) supported Pd,^{264,265} and Pd-nanoparticles embedded in various supports^{266,267} as examples. A particularly attractive support that has not yet been explored for Pd catalysts in C–H activation reactions is a micelle, which has classically been employed with both homogeneous and heterogeneous catalysts that can exploit this unique microenvironment,^{268,269,270} but also can provide a very tunable and recoverable catalytic platform. Solvated micelles have been used as transition metal catalyst supports, for example coordinating palladium inside the micelle core for C–N bond formation and C–C bond formation; however, the use of a micelle for C–H activation has not been reported to this point.^{271,272} In this work, we demonstrate the use of micelles as a reusable support for Pd-catalyzed C–H monoarylation reactions as an initial example, and subsequently a cross-linked, reverse micellar design with tunable spatial constraints around the supported ligands used to bind palladium that imparts selectivity by restricting the space around the metal-ligand complex. Previous reports have used ligand control for achieving monoarylation versus diarylation selectivity,¹⁶⁹ and the micelle support creates a well-defined catalytic nanoenvironment that can be reused with high selectivity.

5.2 Experiments

5.2.1 General preparation of cross-linked micelle (DM)

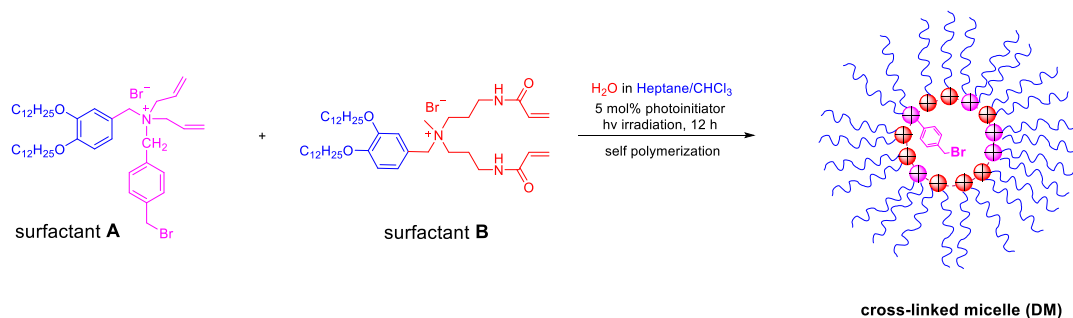


Figure 5.1: Typical preparation of cross-linked micelle.

Water (5.7 μ L, 0.30 mmol) was added to solution of surfactant **A** (10.3 mg, 0.012 mmol) and surfactant **B** (50 mg, 0.06 mmol) in heptane (3.0 mL) and CHCl₃ (0.1 mL). The mixture was hand shaken and sonicated at room temperature to give an optically clear solution. After addition of 2,2-dimethoxy-2-phenylacetophenone (5 mol%), the mixture was irradiated in a Rayonet photoreactor for ca. 12 h until most vinylic protons in surfactants were consumed. The organic solvents were removed by rotary evaporation and the residue was washed by chilled methanol to give a yellowish power (52 mg) in Figure 5.1.

5.2.2 General immobilization of ligand in cross-linked micelle (DML)

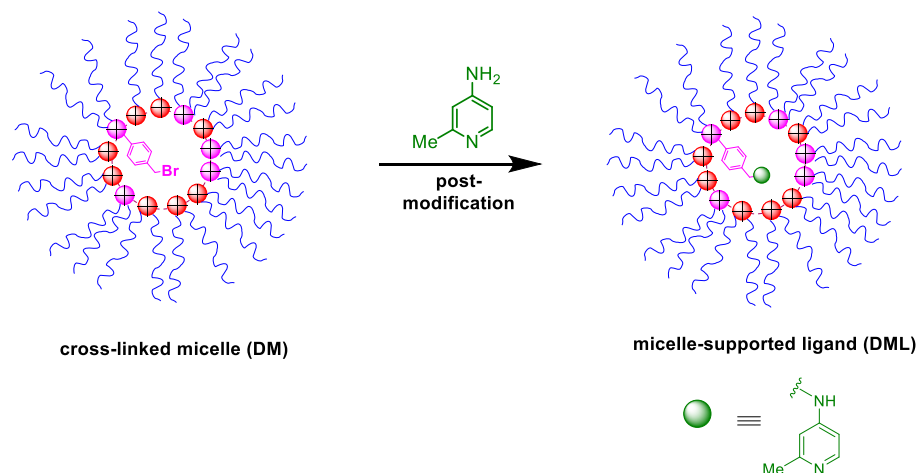


Figure 5.2: Immobilization of ligand in cross-linked micelle.

4-Amino-2-methylpyridine (14 mg) was added into micelle (100 mg) solution in CHCl_3 and stirred at 50°C for 48 h. The organic solvent was removed in *vacuo*, and the residue was washed by cold methanol to remove unreacted 4-amino-2-methylpyridine. The final light brown powder will be obtained by drying under vacuum (Figure 5.2).

5.2.3 General arylation procedure

Substrate (0.05 mmol), $\text{Pd}(\text{TFA})_2$ (0.01 mmol), ligand (0.02 mmol), and Ag_2CO_3 (0.075 mmol) were weighed out open to air and placed in a pressure tube (5 mL) with a magnetic stir bar. The aryl iodide (0.15 mmol), TFA (0.01 mmol), and solvent (0.3 mL) were added. The reaction vessel was sealed and the mixture was first stirred at room temperature for 10 min and then heated to 100°C for 20 h with vigorous stirring. Upon completion, the reaction mixture was cooled to room temperature. All yields were

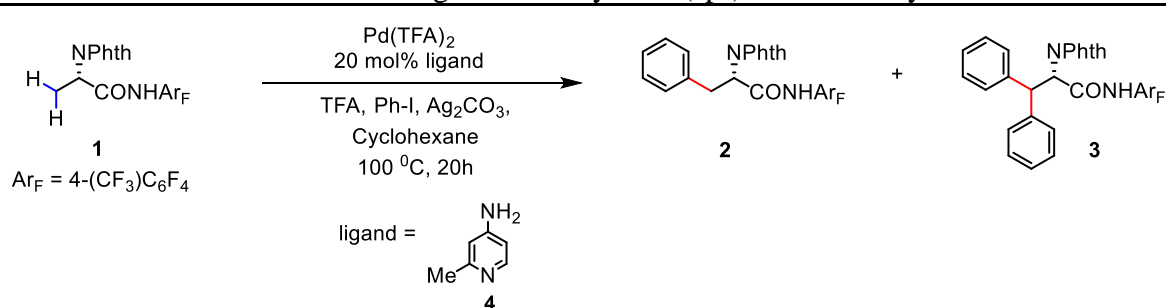
determined by analysis of the crude ^1H NMR (CDCl_3) spectrum using CH_2Br_2 as the internal standard.

5.2.4 *General micelle recycling procedure*

Substrate (0.4 mmol), $\text{Pd}(\text{TFA})_2$ (0.08 mmol), ligand (0.16 mmol), and Ag_2CO_3 (0.6 mmol) were weighed out open to air and placed in a pressure tube (5 mL) with a magnetic stir bar. The aryl iodide (1.2 mmol), TFA (0.08 mmol), and solvent (2.4 mL) were added. The reaction vessel was sealed and the mixture was first stirred at room temperature for 10 min and then heated to 100 °C for 20 h with vigorous stirring. Upon completion, the reaction mixture was cooled to room temperature. Reaction mixture is then filtered through a pad of silica gel with ethyl acetate, and chloroform to filter AgI and Ag_2CO_3 solid species from solution, while the micelle and products passed through. All yields were measure via crude ^1H NMR using CH_2Br_2 as the internal standard. Next, the solvent was evaporated and the remaining solid was washed with cold MeOH, to remove reaction products and reactants and precipitate the recycled micelle. The solid micelle was analyzed by ^1H NMR, and dried overnight for further experiments.

5.2.5 Initial Micelle loading optimization of Pd catalyzed C(sp³)-H Monoarylation^a

Table 5.1: Initial Micelle Loading in Pd catalyzed C(sp³) – H Monoarylation^a



Entry ^a	Ligand	Pd (mol%)	Ph-I (equiv.)	Yield ^b (%)	2 : 3 ^b	Selectivity ^b (%)
1	--			33	33:0	100
2	4			<10	N.D.	N.D.
3	DM-5 (20 mg)			N.R.	N.D.	N.D.
4	DML-5 (20 mg)	10	1.5	25	25:0	100
5	DML-5 (15 mg)			43	41:2	95:5
6	DML-5 (10 mg)			65	58:7	89
7	DML-5 (5 mg)			37	37:0	100

^a Substrate (0.05 mmol), Pd(TFA)₂ (0.005 mmol), ligand (0.01 mmol), and Ag₂CO₃ (0.075 mmol) were weighed out open to air and placed in a pressure tube (5 mL) with a magnetic stir bar. The aryl iodide (0.075 mmol), TFA (0.005 mmol), and solvent (0.3 mL) were added. The reaction vessel was sealed and the mixture was first stirred at room temperature for 10 min and then heated to 100 °C for 20 h with vigorous stirring. Upon completion, the reaction mixture was cooled to room temperature. ^b All yields were determined by analysis of the crude ¹H NMR (CDCl₃) spectrum using CH₂Br₂ as the internal standard.

5.2.6 Pd Catalyzed C(sp³)–H Monoarylation Optimization

Table 5.2: Optimization of Pd catalyzed C(sp³) – H Monoarylation

Pd(TFA)_2
20 mol% ligand
TFA, Ph-I, Ag₂CO₃,
Cyclohexane
100 °C, 20h
ligand =

Entry ^a	Ligand	Pd (mol%)	Ph-I (equiv.)	Yield ^b (%)	2 : 3 ^b	Selectivity ^b (%)
1	--			59	56:3	95
2	4	20	1.5	10	10:0	100
3	DML-5 (10 mg)			52	48:4	92
4	--			41	41:0	100
5	4	10	3.0	<10	N.D.	N.D.
6	DML-5 (10 mg)			23	23:0	100
7	--			63	61:2	97
8	4	20	3.0	17	17:0	100
9	DML-5 (10 mg)			99	83:17	83
10	TML-5 (10 mg)	20	3.0	55	51:4	93
11	TML-5 (13 mg)			48	44:4	92

^a Substrate (0.05 mmol), Pd(TFA)₂ (0.01 mmol), ligand (0.02 mmol), and Ag₂CO₃ (0.075 mmol) were weighed out open to air and placed in a pressure tube (5 mL) with a magnetic stir bar. The aryl iodide (0.15 mmol), TFA (0.01 mmol), and solvent (0.3 mL) were added. The reaction vessel was sealed and the mixture was first stirred at room temperature for 10 min and then heated to 100 °C for 20 h with vigorous stirring. Upon completion, the reaction mixture was cooled to room temperature. ^b All yields were determined by analysis of the crude ¹H NMR (CDCl₃) spectrum using CH₂Br₂ as the internal standard.

5.2.7 Solvent Screen of Pd catalyzed C(sp³)-H Monoarylation

Table 5.3: Solvent Optimization of Pd Catalyzed C(sp³) - H Monoarylation^a

Entry ^a	Solvent	Yield (%)	2:3	Selectivity
1	Cyclohexane	99	83:16	84
2	Cyclohexane/ DMF (8/1)	34	34:0	100
3	Cyclohexane/ EtOH (8/1)	80	73:7	91
4	Cyclohexane/ CH₃CN (8/1)	82	75:7	91
5	Toluene	23	23:0	100
6	DCE	21	21:0	100

^a Substrate (0.05 mmol), Pd(TFA)₂ (0.01 mmol), ligand (0.02 mmol), and Ag₂CO₃ (0.075 mmol) were weighed out open to air and placed in a pressure tube (5 mL) with a magnetic stir bar. The aryl iodide (0.15 mmol), TFA (0.01 mmol), and solvent (0.3 mL) were added. The reaction vessel was sealed and the mixture was first stirred at room temperature for 10 min and then heated to 100 °C for 20 h with vigorous stirring. Upon completion, the reaction mixture was cooled to room temperature. ^b All yields were determined by analysis of the crude ¹H NMR (CDCl₃) spectrum using CH₂Br₂ as the internal standard.

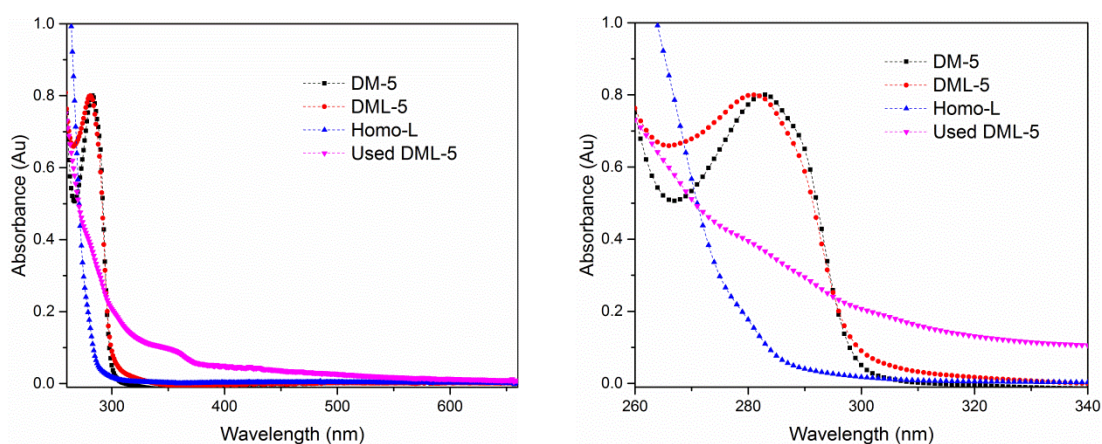


Figure 5.3: Absorption spectra of DM-5, DML-5, recycled DML-5, and homogeneous ligand in chloroform. $W_o = [\text{H}_2\text{O}]/[\text{surfactant}] = 5$.

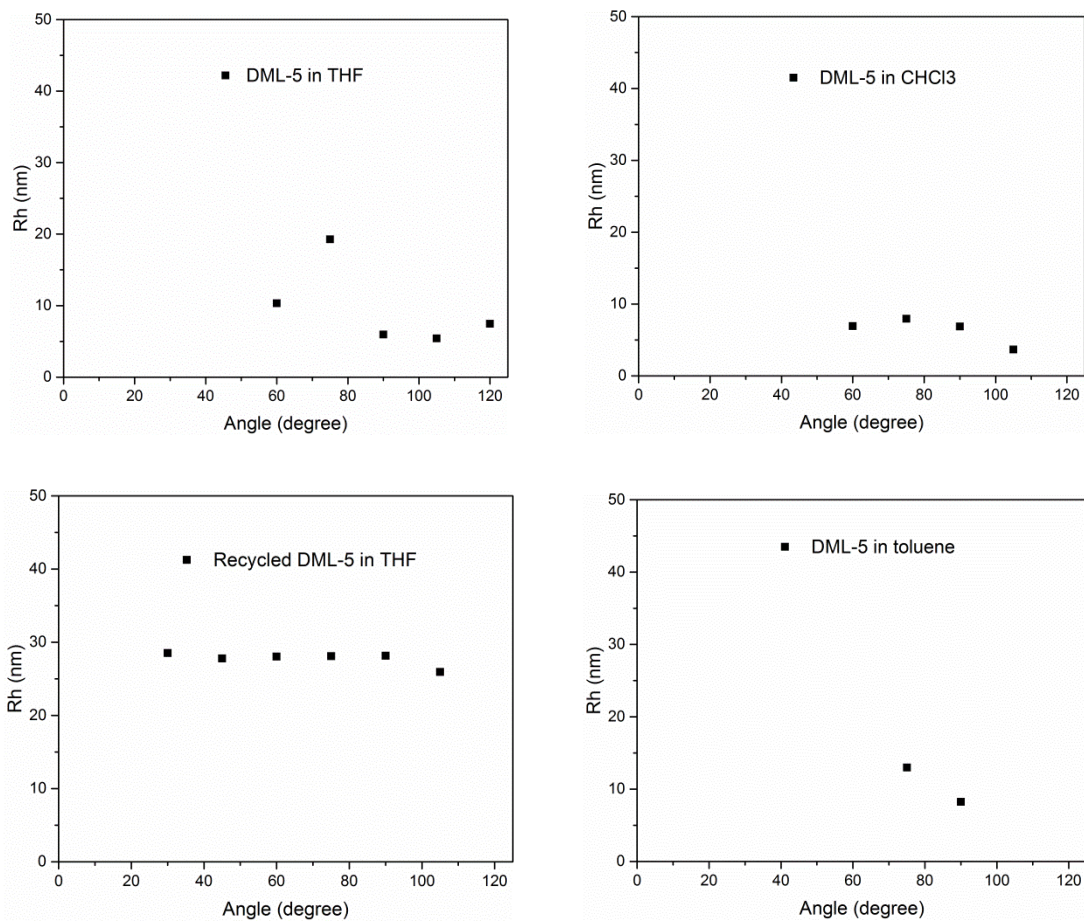


Figure 5.4: Hydrodynamic radius of DML-5 in various solvents using multiangle dynamic light scattering.

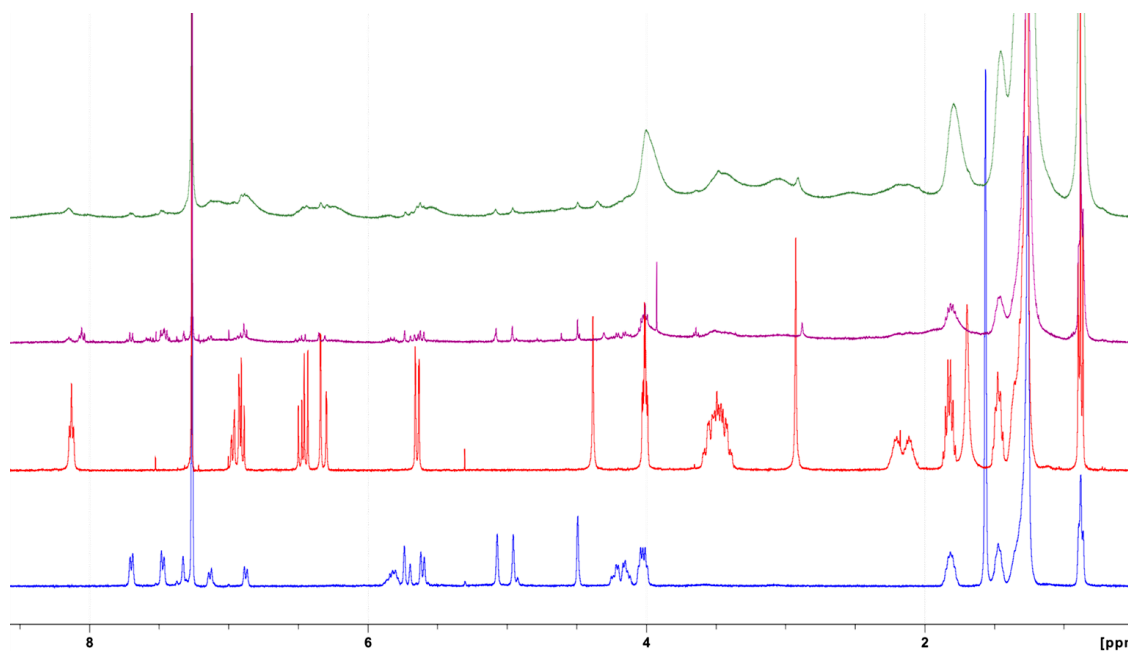


Figure 5.5: ¹H NMR spectra of surfactant A (blue) and surfact B (red) before irradiation in CDCl₃, and after irradiation to yield crude micelle (purple). After the micelle is formed, the solvent is removed by rotary evaporation and washed with cold MeOH, providing pure micelle (green).

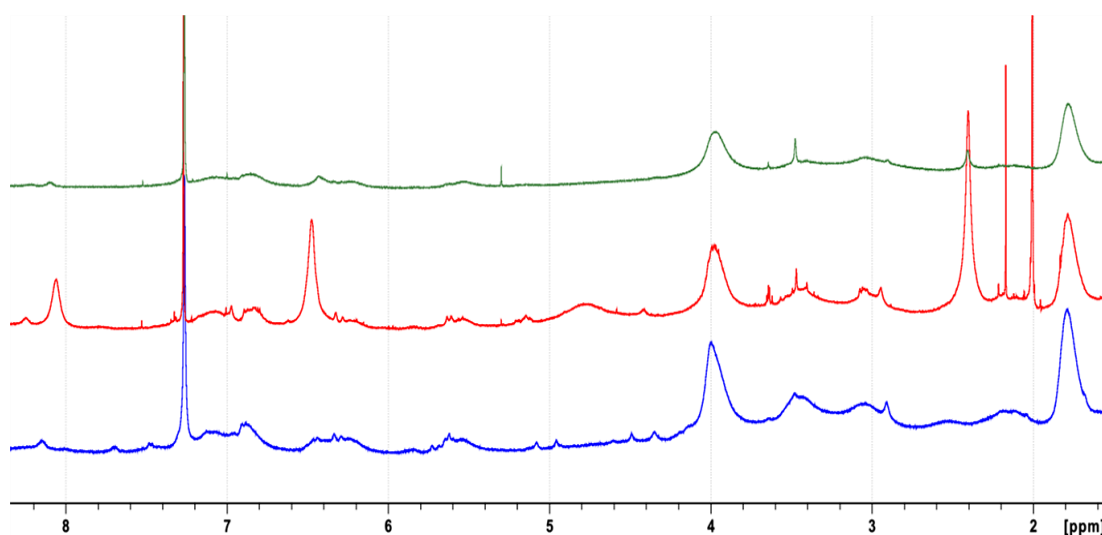


Figure 5.6: ¹H NMR spectra of ligand immobilization within micelle core. Micelle DM in CDCl₃ before ligand immobilization (blue). Next, ligand is immobilized leading to crude DML (red), and further washed with cold MeOH and pure DML is obtained (green).

Table 5.4: Elemental analysis of fresh and resued DML-5

Entry	N wt%	Pd wt%
Before 1 st monoarylation	5.27	0
Table 5.8 , entry 3	3.63	3.63
Table 5.8 , entry 5	3.63	4.77
Table 5.8 , entry 7	1.37	3.25

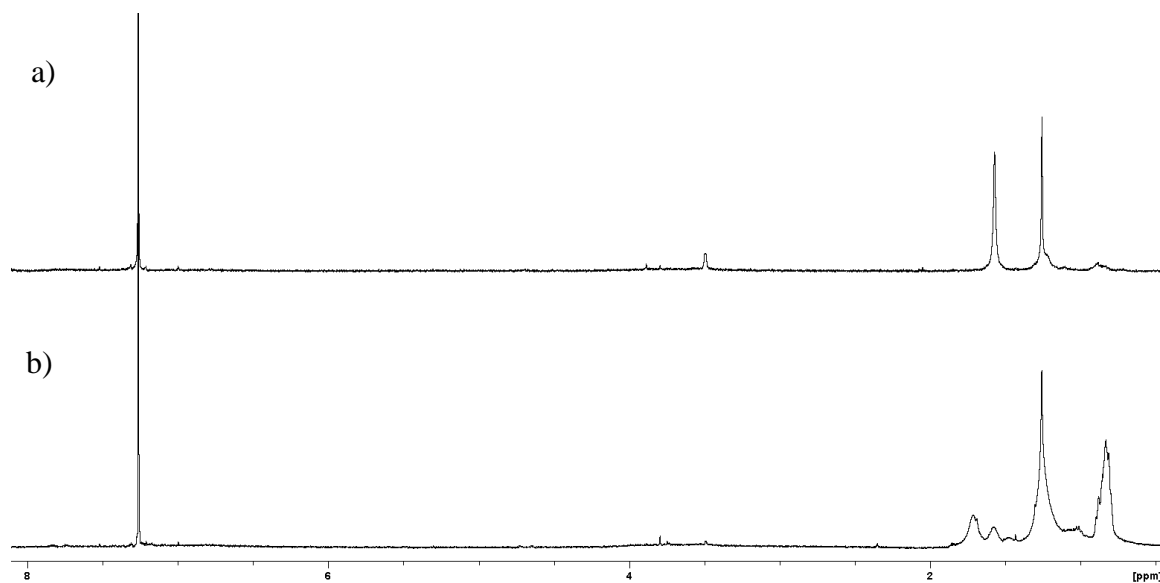


Figure 5.7: ¹H NMR (in CDCl₃) of a) recycled and b) fresh DML-5 from first run Pd-catalyzed C(sp³) – H monoarylation.

5.3 Results and Discussion

5.3.1 Micelle Design and Effects on C(sp³)-H Monoarylation

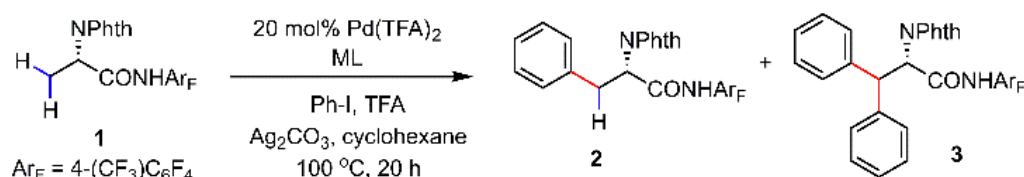


Figure 5.8: Pd-Catalyzed C(sp³)-H Monoarylation.

The design of the catalytic micelle began with identification of key properties to tune, such as the alkyl density of surfactant tails,^{122,273} size of the hydrophilic core,¹²² and ligand functionalization within that core. After exploiting the hydrophilic head group and hydrophobic alkyl tail, the resulting micelles were interfacially cross-linked to provide thermal stability,²⁶⁹ necessary for the Pd-catalyzed C(sp³)-H monoarylation shown above in Figure 5.8. In classic micelles, there is dynamic mixing of surfactant and internal contents of the core, whereas the cross-linked core of our micelles restricts the internal catalytic core and support from mixing contents, and helps retain the ligand and palladium for future reuse.

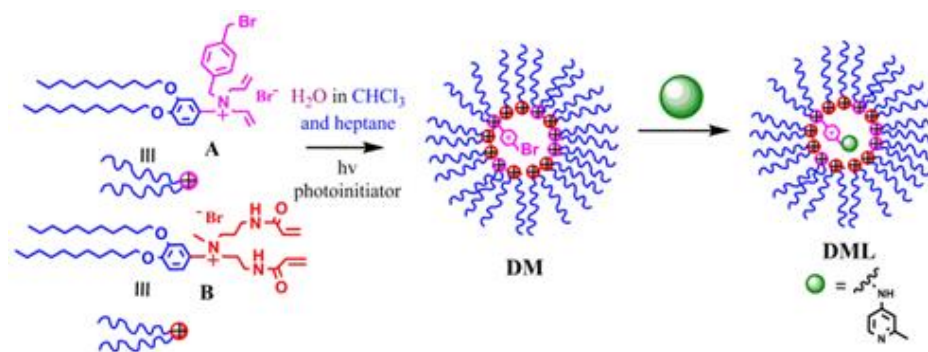


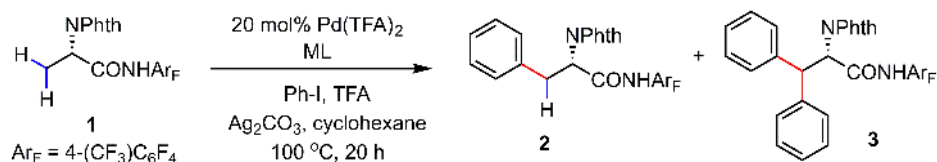
Figure 5.9: General preparation of cross-linked micelle-supported ligand.

As seen above in Figure 5.9, polymerizable surfactant **B** with functionalizable double-tail surfactant **A**, or (not pictured) a functionalizable triple tail analogue were dissolved in a 1:5 ratio of **A**:**B**. This ratio allows the surfactants to cross-link on their own, rather than add any additional crosslinker, and ensures surfactant **A** and **B** polymerize together, limiting the self-polymerization of surfactant **B**, which would occur if the ratio were larger. Surfactant **A** was designed and synthesized to contain a benzyl bromide functional handle within the core for further substitution with 4-amino 2-methylpyridine used as the ligand in the C(sp³)-H monoarylation. The micelles then self-assembled in H₂O and heptane, and were cross-linked using a photoinitiator at 365 nm to create DM, the double-tail micelle. The functionalizable benzyl bromide was substituted with amine containing ligand moieties to form the double-tail micelle with ligand (DML) and further coordinated in situ with a palladium precursor to yield the precatalyst. Next, optimization of the reaction conditions with various amounts of DML (Table 5.1), palladium and aryl iodide was completed (Table 5.2).

The first generation of the cross-linked micelle provided a tunable platform for catalyst design, and the first example of micelle-supported Pd(II)-catalyzed C(sp³)-H

monoarylation. The initial tunable property of the micelle explored was the surfactant-alkyl density of surfactant **B**. The alkyl density played a significant role in the catalytic activity of the micelle,²⁷³ altering the number of hydrophobic tails covalently bound to a hydrophilic head group between two and three. The second property of the micelle to be evaluated was the size of the catalytic core. In the synthesis of the catalytic micelle, various amounts of water were introduced in the first step of Figure 5.9 to vary the size of the micelle core, known as W_0 . The combination of assorted W_0 values paired with different numbers of alkyl hydrophobic tails potentially allows for size selectivity as well as creation of a diffusive barrier for substrates and products.

Table 5.5: Micelle-supported ligands with various W_0 and micelle shell in Pd-catalyzed $C(sp^3) - H$ arylation^{a,b}



Entry	Micelle-Ligand	W_0	Yield (%)	2:3	Selectivity (%)
1	DML	0	20	20:0	100
2	DML	2	24	24:0	100
3	DML	5	99	83:17	83
4	DML	10	76	66:10	87
5	TML	2	24	24:0	100
6	TML	5	55	51:4	93
7	TML	10	52	49:3	94
8	TML (48h)	10	65	61:4	94

^a)Reaction conditions: substrate (0.05 mmol), $Pd(TFA)_2$ [palladium(II) trifluoroacetate] (0.01 mmol), DML/TML (10 mg), Ag_2CO_3 (0.075 mmol), TFA (0.01 mmol), iodobenzene (0.15 mmol), and cyclohexane (0.3 mL) were added. The reaction vessel was sealed and the mixture was stirred at room temperature for 10 min and then heated to 100 °C for 20 h with vigorous stirring. ^b)The yield percentage and ratios of **2** and **3** were determined by 1H NMR using CH_2Br_2 as the internal standard.

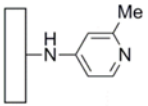
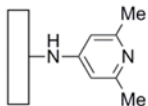
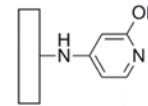
Table 5.5 displays the catalytic results highlighting the optimized micelle shell and core structure, which is comprised of a 1:5 ratio of surfactant **A** and **B** with differing core diameters, denoted W_0 . The double tail micelle supported ligand (DML) maintained the proper amphiphilic characteristics to form the initial dynamic micelle in solution, and further provided a stable reverse cross-linked micelle. Entries 1, 2, and 5 all had small W_0 , and corresponding low yields of monoarylated product **2**. A larger core, with $W_0 = 5$

or 10, appeared to allow for an increase in conversion of starting material, displaying the necessity for a core large enough to accommodate starting materials and product. There was not a large difference in selectivity with core sizes 5 or larger, which was unexpected. We anticipated with the larger core, product 2 would have the opportunity to interact with the palladium catalyst and convert to the diarylated product 3 more readily; however, this was not observed.

The triple tail micelle supported ligand (TML) displayed lower yields across various W_0 , with a higher selectivity. Unfortunately, TML $W_0 = 10$ with extended reaction time did not display significantly increased yield. This may be associated with the thick hydrophobic shell the TML possessed, while increased yield was demonstrated with the DML. The thick shell imparted a restriction on transport properties of substrates into the core, highlighted with the extended reaction time needed to allow for diffusion into the core (Table 5.5 below, entries 7 and 8), but no appreciable increased yield was observed after 48 hours. The DML hydrophobic shell is less crowded, with double tails compared to triple, and therefore we hypothesize it presented a more penetrable barrier to the active micelle core. After the examination of both the micelle core size and hydrophobicity of the micelle shell, the DML micelle with $W_0 = 5$ was carried through for further exploration in the C(sp³)-H monoarylation.

5.3.2 Micelle-Ligand structure and impact on C(sp³)-H Monoarylation

Table 5.6: Micelles with various pyridine-based ligands in Pd-catalyzed C(sp³)-H arylation^{a,b}

<div style="display: flex; justify-content: space-around; align-items: center;"> <div style="text-align: center;">  <p>DML</p> </div> <div style="text-align: center;">  <p>DML'</p> </div> <div style="text-align: center;">  <p>DML''</p> </div> </div>					
Entry	Micelle-Ligand	W ₀	Yield (%)	2:3	Selectivity (%)
1	DML	5	99	83:17	83
2	DML'	5	55	50:5	91
3	DML'(48h)	5	73	64:9	88
4	DML''	5	26	26:0	100

^a)Reaction conditions: substrate (0.05 mmol), Pd(TFA)₂ [palladium(II) trifluoroacetate] (0.01 mmol), DML/DML'/DML'' (10 mg), Ag₂CO₃ (0.075 mmol), TFA (0.01 mmol), iodobenzene (0.15 mmol), and cyclohexane (0.3 mL) were added. The reaction vessel was sealed and the mixture was stirred at room temperature for 10 min and then heated to 100 °C for 20 h with vigorous stirring. ^b)The yield percentage and ratios of **2** and **3** were determined by ¹H NMR using CH₂Br₂ as the internal standard.

In previous studies, the ligand in DML (Table 5.5) was used to carry out the C(sp³)-H arylation homogeneously,¹⁶⁹ and selectivity trends for product **2** relative to **3** were also studied with a linear polymer supported ligand, which provided a platform for improvement.²⁶³ The DML micelle with W₀ = 5 produced a selectivity of 84% for the monoarylated product after 20 h; however, incorporation of a different ligand in the micelle core could further improve the selectivity. Ligand DML' was chosen because of its similar electronic structure to the original ligand DML, but also providing added steric constraints inside the core. With a slightly bulkier ligand in the core, we hypothesized

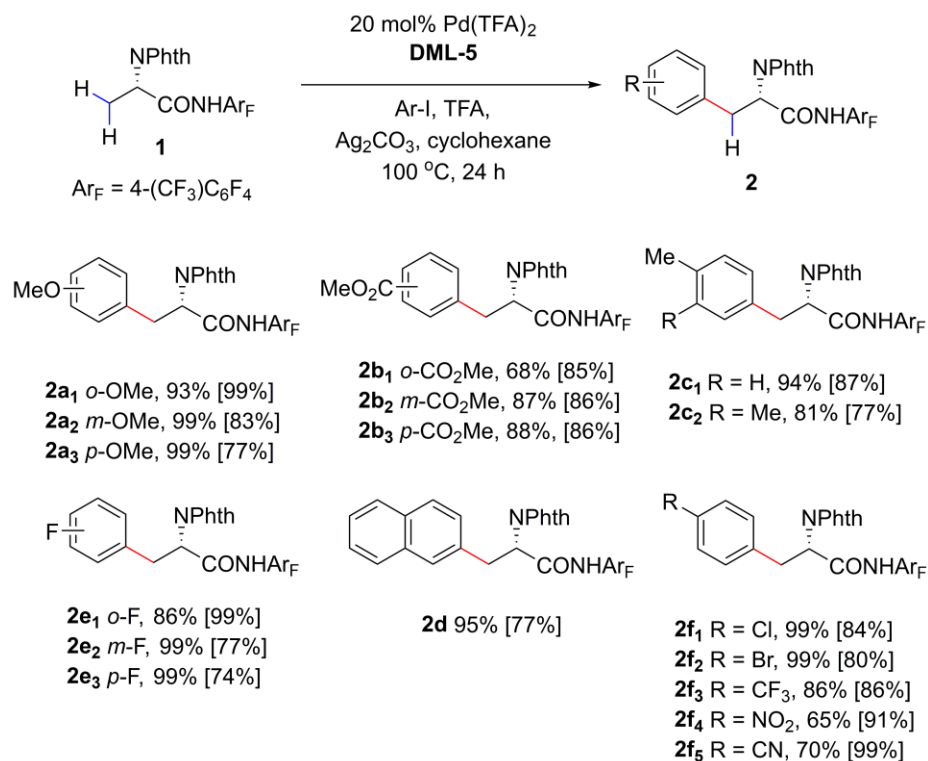
this would help force the newly formed product **2** out of the core, leading to increased selectivity for monoarylation. As has been seen with previous reports,¹⁶⁹ the activity for C(sp³)–H monoarylation is highly sensitive to the ligand, and decreased yield of product **2** was observed with the sterically more hindered ligand DML'. DML'' was also selected to probe the effect of different electronics around the pyridine ligand, incorporating a strong electron donating group *ortho*- to the pyridine nitrogen, while maintaining a similar steric influence to DML. The additional electron density in DML'' dramatically reduced yield, and correspondingly high selectivity was observed. In contrast to the homogeneous case, the incorporation of all ligand cases did not increase the amount of diarylated product **3**,¹⁶⁹ supporting the benefit of a spatially constrained catalytic pocket for improved selectivity by elimination of bulkier products. To this end, it appears the micelle core provided a valuable steric limitation for the prevention of the formation of the diarylated product. Previously, an optimal balance of sterics and electronics for the ligand-controlled C(sp³)–H arylation was demonstrated through the evaluation of multiple ligands, varying both sterics or electronics.^{169,254,274,275} This particular C(sp³)–H arylation was exceptionally sensitive to the ligand present, as seen in the homogeneous case, so the decreased yield for non-optimal ligands was not entirely unexpected.^{169,263}

5.3.3 Substrate Scope of Pd-Catalyzed C(sp³)–H arylation using DML-5

Having identified a suitable micelle catalyst structure with (i) two alkyl tails and a core size large enough to accommodate both starting material and product, and (ii) the proper ligand to promote monoarylation, which produced encouraging activity with the model substrate, further investigation of substrate substituent effects was conducted. The catalytic micelle showed excellent activity and selectivity with both electron donating

and withdrawing substituents present on the iodobenzene partner at the *ortho*-, *meta*-, and *para*-positions, as presented below in Table 5.7.

Table 5.7: Substrate scope of the Pd-catalyzed C(sp³)-H arylation using DML-5^{a,b}



^a)Reaction conditions: substrate (0.05 mmol) Pd(TFA)₂ [palladium(II) trifluoroacetate] (0.01 mmol), DML-5 (10 mg), Ag₂CO₃ (0.075 mmol), TFA (0.01 mmol), iodobenzene (0.15 mmol), and cyclohexane (0.3 mL) were added. The reaction vessel was sealed and the mixture was stirred at room temperature for 10 min and then heated to 100 °C for 20 h with vigorous stirring. ^b)The yield percentage and ratios of **2** and **3** were determined by ¹H NMR using CH₂Br₂ as the internal standard.

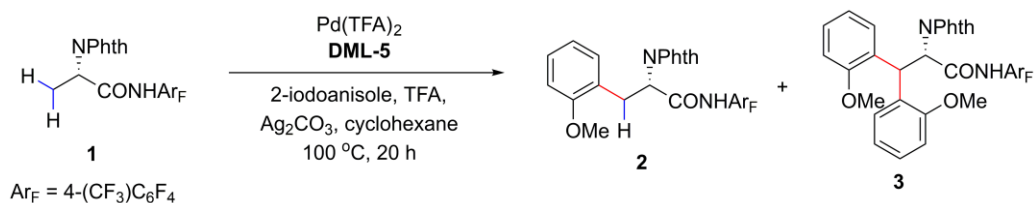
The monoarylation proceeded in high yields and selectivities for both electron-withdrawing and electron-donating substituents on the aryl iodide with the micelle-supported ligand and palladium. The selectivity can be highlighted in

products **2a1** and **2e1** (as seen in Table 5.7). These two coupling partners have second substitutions *ortho*- to the active iodo group, imparting an increase in selectivity. Notably, the same selectivity is not seen with the *para*- substituted compounds **2a3** and **2e3** that are electronically similar. Interestingly, this selectivity pattern has not been observed with other Pd-catalyzed monoarylation reactions; in fact, conversely, the yield is typically decreased with *ortho*- substitutions due to steric hinderance.²⁷⁶ Both **2a3** and **2e3** had excellent yields of 99% and similarly decreased selectivities of 77 and 74%. The high reactivity of both the *para*- and *meta*-substituted aryl iodides contributed to the decreased selectivity toward monoarylation. This selectivity at the *ortho*-position is hypothesized to be an electronically-influenced steric effect within the micelle core. A previously reported heterogeneous polymer support²⁶³ incorporated a polar, hydrogen-bonding amide backbone to increase the concentration of polar substrates in the nonpolar solvent, and we can extrapolate similar activity trends within the polar, cross-linked micelle core. The reduced freedom of movement for the ligands within the micelle core is hypothesized to create an active catalytic pocket, filled with potential hydrogen-bonding partners. Hypothesized within the active pocket, the coordinated palladium complex is sterically encouraged to interact with the starting materials and coupling partners. The substrates that participate in hydrogen-bonding within the core, such as **2a** and **2e**, have increased selectivity for *ortho*-substituted aryl halides, presumably due to hydrogen-bonding capability near the active substitution, drawing the starting material toward the Pd active site. These substitutions are electronically favored at the *ortho*-/*para*- positions because

of the electron donating behavior of the methoxy, as well as slight electron withdrawing but *ortho*-/para- activation for the fluoro-substituted starting material, such that we speculate facilitation of reactivity near the active site of substitution. Alternatively hypothesized, the micelle core concentration is high and the *ortho*-substitution encumber the stacking of molecules more so compared to the *para*-substituted aryl iodides, thus accommodating the smaller space and increased diarylated product. Similar activity is not observed for **2b** compounds, because the carbonyl group can weakly coordinate to Pd(II), which promotes the second C–H insertion to give more diarylated product. Therefore, similar selectivity trends are not seen with methyl ester aryl iodides. Generally, stronger electron-withdrawing functionality added to the substrate decreased the yield slightly; however the selectivity remains high, as seen in compound **2f**. This tolerance for many functional handles on the starting materials, paired with excellent yields, has the potential to be exploited in the future with C–H activation. Overall, this micelle-supported palladium catalyst showed high tolerance for both electron withdrawing and donating groups, as well as selectivity toward monoarylated products in all cases.

5.3.4 Recycling Studies of DML-5

Table 5.8: Recycling DML-5 in Pd-Catalyzed C(sp³)-H arylation^{a,b,c}



Entry	Micelle	Pd(TFA) ₂ (mol%)	Yield (%) ^b	Selectivity (%) ^b
1	DM-5	0	68	>99
2	DML-5	20	N.R. ^c	N.D. ^d
3	DML-5	0	93	>99
4	Recycled DML-5 from entry 3	20	11	>99
5	Recycled DML-5 from entry 3	0	77	>99
6	Recycled DML-5 from entry 4	20	N.R.	N.D.
7	Recycled DML-5 from entry 5	0	52	>99

^a) Reaction conditions: substrate (0.4 mmol) Pd(TFA)₂ [palladium(II) trifluoroacetate] (0.08 mmol), DML-5 (80 mg), Ag₂CO₃ (0.6 mmol), TFA (0.08 mmol), 2-iodoanisole (1.2 mmol), and cyclohexane (2.4 mL) were added. The reaction vessel was sealed and the mixture was stirred at room temperature for 10 min and then heated to 100 °C for 20 h with vigorous stirring. ^b) The yield percentage and selectivity in brackets were determined by ¹H NMR using CH₂Br₂ as the internal standard. ^c) NR = no reaction. ^d) ND = not determined.

Realizing the micelle-supported Pd has a high compatibility and selectivity with multiple functional handles similar to the homogeneous reaction, recycled micelle was explored for catalytic activity as one way to enhance the total TON. The micelle-support alone (without added ligand L), showed activity, reaching 68% yield of monoarylated product, which is expected due to the potential for Pd coordination with the amide groups of the cross-linked core. Next, the micelle with immobilized ligand (DML-5) was run

under standard reaction conditions, and subsequently recycled as seen in Table 5.8, entries 5 and 7. The micelle catalyst was successfully reused from ^1H NMR (Figure 5.7) in its as-recovered form, as well as with fresh palladium added, which yielded dramatically different results. Recycled micelle with no added palladium showed drastically reduced activity, producing 11 % of product **2**, while with fresh Pd added it yielded 77%. This demonstrated that the supported ligand was successfully recycled, albeit not robustly after multiple runs (Table 5.8, entries 6 and 7). Elemental analysis of the recycled micelle (Table 5.8, entry 4) showed residual palladium, and the UV/vis spectrum of used DML-5 has characteristics of both the micelle and palladium present²⁶⁹ (Figure 5.1), but only at a 1.5 mol% loading, which explains its very low productivity in as-recovered form. Also from elemental analysis (Table 5.4), there was a decrease in nitrogen content over multiple cycles, which was likely due to the displacement of the initial bromide counter ions in the amide cross-linked core with free iodide ions from excess aryl iodide in solution, causing the micelle core to become more crowded with larger counter ions present. The recycle of the micelle demonstrates the ability to reuse the ligand, without the metal, which is not unexpected with a weakly coordinated monodentate ligand and fixed micelle core. For entry 5 in Table 5.8, there is a notable decrease of yield, giving similar performance to entry 1 in Table 5.8. A possible explanation for this observation is the spatial constraints and limited mobility of the ligand within the micelle core could reduce the capability for bidentate coordination of Pd with two ligands, thus forcing the Pd to coordinate weakly with the amide cross-linkages, thereby reducing the probability for metal recycle. Another possible explanation is that the monodentate ligand allows for coordination of other species in reaction

solution with the ligand, and as the reaction progresses and starting materials are consumed, other reactants take the place of the previously coordinated starting material or metal.²⁷⁷

5.4 Conclusion

The present work demonstrated a micelle-supported ligand used for Pd-catalyzed C(sp³)-H monoarylation. The micelle was designed and synthesized with tunable properties that can be further enhanced for future use with C-H activation, as well as other reactions that benefit from spatial constraints of a catalytic pocket. Specifically, one can imagine creation of active pockets with multiple functional sites operating congruently. The micelle-supported ligand imparted a selectivity unseen by previous polymer-supported Pd-catalyzed C(sp³)-H arylation reactions, and was reused a second time. Enhanced recyclability is expected using systems that exploit multidentate ligands, reducing loss of metal from the designed microenvironments.

CHAPTER 6.

SUMMARY AND FUTURE DIRECTIONS

6.1 Summary

A summary of this dissertation with the main conclusions is broken down by chapters and presented below:

Chapter 1

An introduction into various polymer architectures was discussed, with the applications varying widely. The focus of this thesis on catalytic polymers was addressed in concert with the benefits to using these materials as catalyst supports. Key aspects of each reaction studied in this work, along with the corresponding polymer designs, were discussed. The current state of research within each of the topical areas was discussed.

Chapter 2

Cooperative catalysis of the aldol condensation with 4-nitrobenzaldehyde and acetone was demonstrated with a linear polymer backbone synthesized from weakly acidic and basic monomer units in a controlled polymerization. Using various sequences incorporating the weak acid and base monomers displayed an optimized ratio of acid and base units which was 1:1. As well, when a block copolymer structure was synthesized, the site isolation of each catalytic moiety depressed activity as expected. The system was

optimized in cosolvents to assist solubilization of the polymer, though the polymer in unprotected form was insoluble under most conditions. As a result, only some of the active sites were displayed to the solution, and when these sites were quantified, it was determined that the catalyst was as active as the benchmark mesoporous silica materials. As a first generation of polymer supported cooperative catalyst, the key features addressed were spatial placement of acid and base species, the strength of cooperative partners on single polymer chains, as well as the overall polymer structure as a platform for the next generation of catalysts, which should seek to improve the polymer solubility.

Chapter 3

A solid acid polymer catalyst was utilized for the hydroboration of substituted alkynes using pinacolborane as the first known demonstration of a polymer organocatalyst applied for this chemistry. Kinetic isotope effect studies alluded to a rehybridization of the alkyne as being involved in the rate limiting step, and a reaction order analysis using the initial rates method displayed first-order dependence on the catalyst concentration and interestingly, inverse first-order dependence on both starting materials. ^{11}B NMR studies found evidence of a boron-acid structure formed over time, inhibiting the availability of active sites, while the phenylacetylene may sterically encumber the catalyst upon polarization by the acidic proton of the acid catalyst. With these pieces of data, a proposed mechanistic pathway of a polarized alkyne coordinating with a free HBPIn to form 2-styryl-BPin in a concerted 4-membered transition state was hypothesized. The catalyst provided robust activity with a variety of substituted alkynes, and was reused 3 times without loss of product yields.

Chapter 4

A polymer brush structure has been utilized to perform a 2-step cascade reaction with the proposal of a 3rd step. Three support structures were tested for activity in the acid-base cascade: MCM-SO₃H-pyrrol gt, MCM-SO₃H-pyrrol gf, and MCM-SO₃H-pyrrol m. “Gt” and “gf” represent “grafted to” and “grafted from” approaches to synthesizing polymer brush structures, and “m” represents the molecular base functionalized on the exterior surface. “Grafting to” approach allows for complete chains to be functionalized on the surface, however lower grafting densities are seen due to the sterics of the chains, while “grafting from” allows for a higher density of polymer chains on the exterior because a small propagating agent/initiator grafted first. RAFT polymerization was employed to polymerize the basic monomer, and the molecular support has an analogous structure to the monomer. The cascade reaction is an acid-catalyzed deacetalization of 4-nitrobenzaldehyde dimethylacetal and a base-catalyzed Knoevenagel condensation to yield benzylidenemalononitrile. The design of the material incorporated an acid co-condensed in the pores of the mesoporous silica support, with basic moieties polymerized in chains on the exterior of the support to accommodate a smaller product from the acid-deprotection, which was performed in the pores in the center of the catalyst particle, to a larger product in the brush layer on the outer portion of the catalyst.

Chapter 5

C–H functionalization research has grown exponentially over the past two decades as a tool in organic synthesis. Using expensive homogenous catalysts is one

drawback to the current chemistry, and demonstrating a supported metal complex could ease the cost and viability of these chemistries in industry if the ligand and/or the metal could be recovered and recycled. In this study, a reverse cross-linked polymer micelle was functionalized with an amine ligand in the core and loaded with palladium to perform a C(sp³)-H monoarylation of an unnatural amino acid with substituted aryl iodides. The micelle support imparted a selectivity toward *ortho*-substituted aryl iodides, with high yields for most substrates. The micelle was reused and recycled two times. However, it needed additional palladium for the subsequent reactions to run with high efficiency. While the catalytic improvement was modest, this was the first application of a micelle support for C-H functionalization and provides a tunable platform for future applications.

6.2 Future Directions

6.2.1 Polymeric Cooperative catalysts

Results from the second chapter of this dissertation demonstrated that a polymer with a soluble backbone might benefit the cooperativity, and require a lower catalyst loading. The polymer catalyst synthesized in this work was highly functionalized, with a functional group on each monomer, which likely reduced solubility due to hydrogen-bonding. A future catalyst design could incorporate a spacing unit to potentially decrease the likelihood of hydrogen-bonding interactions among monomers and polymer chains. It is hypothesized that the less dense packing of these polymer chains would hopefully address the solubility problem as well. Lastly, the weak acid monomer unit used in this work is prone to oxidation.¹⁷⁸ The reduction of acidity once the oxidation has occurred

deactivates the catalyst and reuse is no longer possible. As discussed in chapter 2, the ideal acidity for cooperativity mimics the acidity of surface silanols.¹⁵⁷ A monomer synthesis that maintains the acidity of the weak acid, but does not oxidize would be ideal for future generations of cooperative polymers.

6.2.2 *Extending Polymer Brush Catalysts for 3-Step Cascade Reactions*

The extension of the cascade to incorporate three steps would improve the efficacy of such complex catalysts, which require extraordinary justification for their synthesis and use. The tandem acid-base cascade employed in this work has been demonstrated on various support structures,²⁷⁸ and the extension to include the synthesis of a larger molecule would extend this concept. The incorporation of a third step requires an added level of design to be considered. For the polymer brush structure, the chains were synthesized so that excess basic active sites would be accessible to perform a second and third transformation. From the success of the two-step cascade, it is suspected that the additional third step is viable, and can be achieved with additional work and testing.

These brush materials not only serve as platforms for organocatalytic cascades, but the incorporation of supported metal catalysts to perform organometallic cascades and variations of both organic and metal-catalyzed transformations. Such cascades should incorporate steric considerations for starting materials versus products, and the hydrophobicity and hydrophilicity of the reactants.¹²⁵ As more work is done and as effective multi-compartment cascade catalysts are developed, design principles for such structures might be achieved. Such design principles with cascade catalysis would be of

immense importance, and the polymer brush platform has the tunable properties needed to address the complex system requirements.

APPENDIX A. KINETIC EXPERIMENTS WITH POP-COOH IN HYDROBORATION OF PHENYLACETYLENE WITH PINACOLBORANE

A.1 Background on Porous Organic Polymers

For background on POPs, please see Chapter 2.

A.1.1 Porous Organic Polymer synthesis

The synthesis of this POP is similar to Chapter 2:

In a 250 mL pressure tube, DVB (2.0 g), benzoic acid monomer (7.68 mmol), 50 mL THF, AIBN (0.20 mg) and 1 mL deionized water were stirred vigorously for 24 h at 100 °C. The resulting solid was washed with copious amounts of THF, and dried overnight at 100 °C under reduced pressure. The resulting porous organic polymer was characterized by nitrogen physisorption, XPS, and elemental analysis.

A.1.2 Porous Organic Polymer Characterization

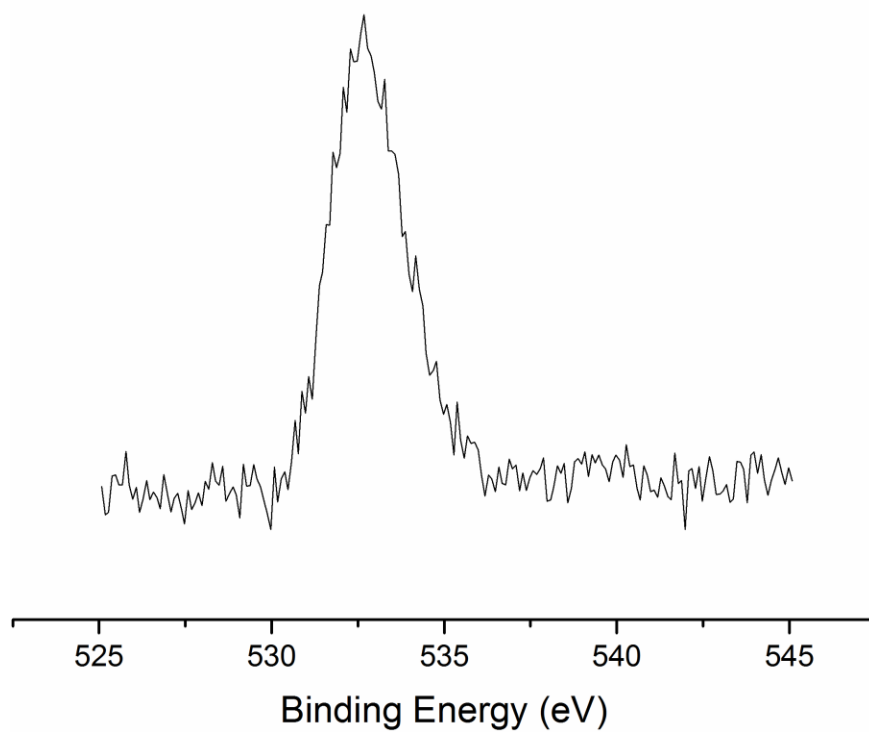


Figure A.1: XPS O1s scan of COOH-POP.

From XPS oxygen scans, there was about 3 mol % oxygen detected in the sample.

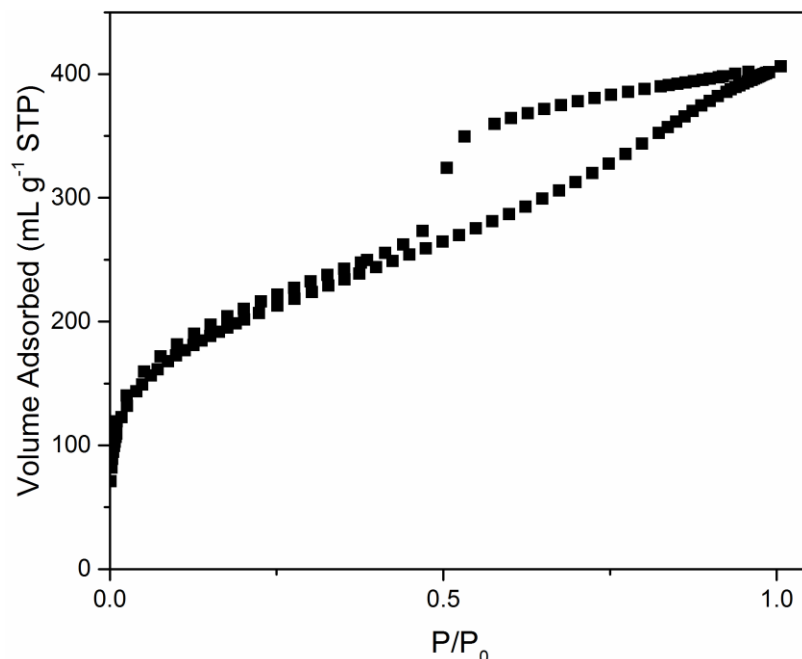


Figure A.2: Nitrogen physisorption isotherm of POP-COOH.

BET Surface area recorded was 640 m²/g_{POP} with a pore volume of 0.7 cm³/g

A.1.3 Porous Organic Polymer Catalyst Performance

Table A.1: Catalytic Activity of the POP-COOH catalyst in the hydroboration of phenylacetylene with HBPi^{a,b}

Catalyst	Yield % ^b
POP-COOH	70

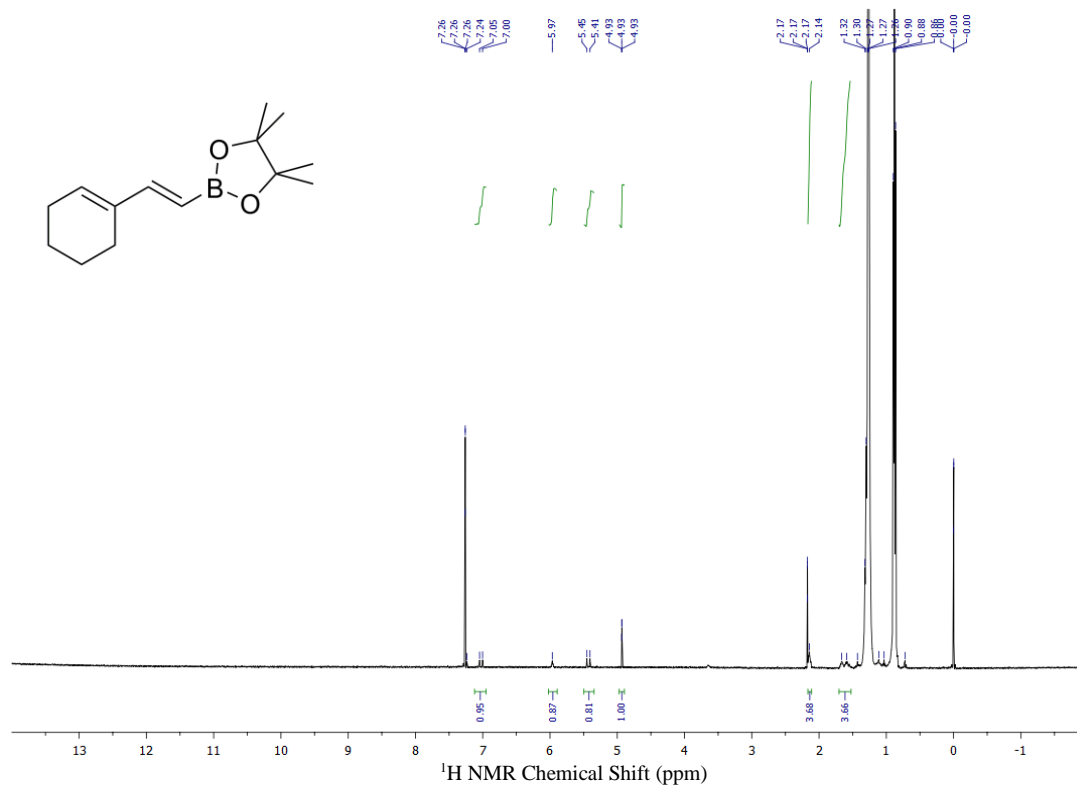
^a) Reaction conditions: Under an inert atmosphere of N₂, phenylacetylene (0.4 mmol), HBPi (1.2 mmol, 3 eq.), and 5 mol% catalyst were added to a 3.5 mL vial with octane (1 mL) and CH₂Br₂ as the internal standard at 30 °C stirring vigorously for 16 h. ^b) All yields were determined by crude ¹H NMR analysis.

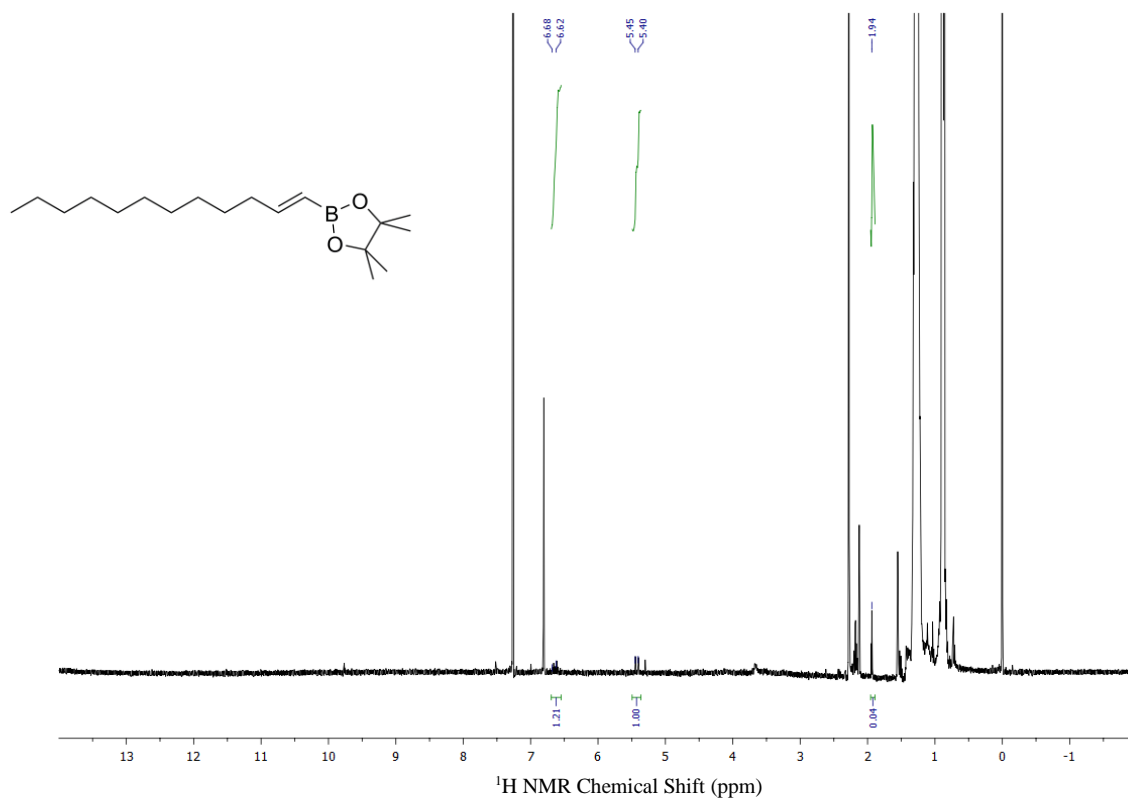
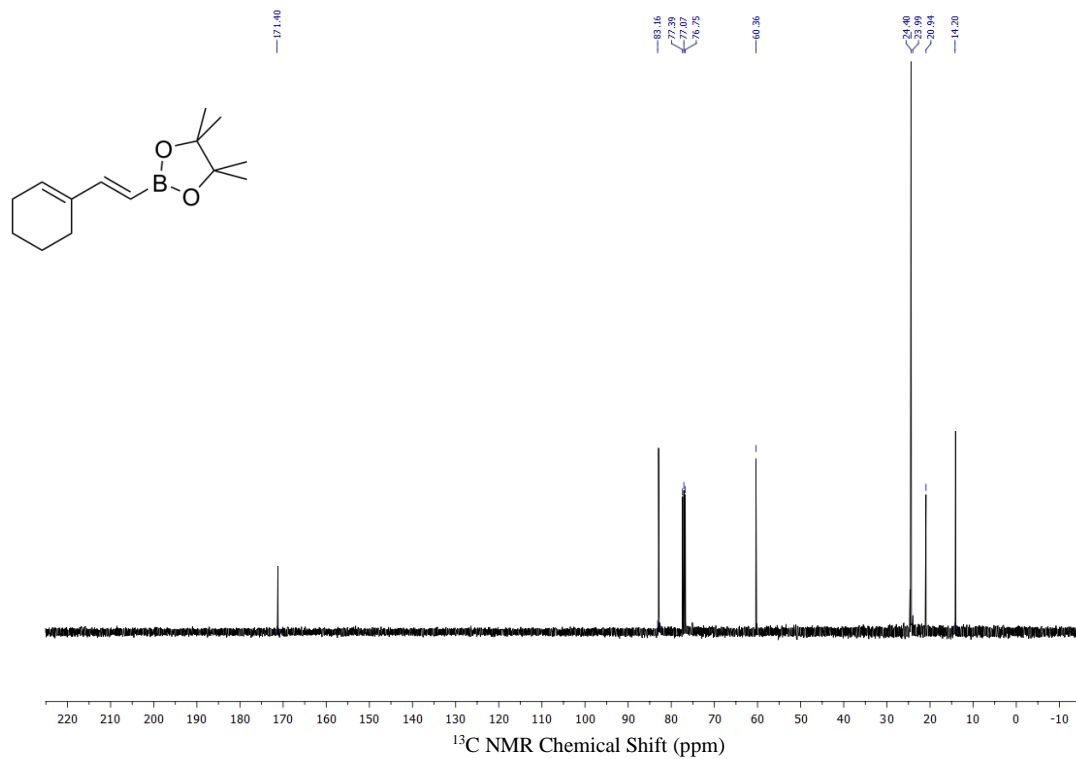
Applying this solid catalyst to the hydroboration of phenylacetylene with pinacolborane, there was a noticeable decrease in product yield compared to the other catalysts, at 70 % over the course of 16 h. The kinetics of this catalyst compared to both the poly(vba) and homogeneous case were much slower. Due to the fixed support structure, we have attributed the depressed activity to the side product formations being more prevalent with a surface structure that allows for more accessible sites.

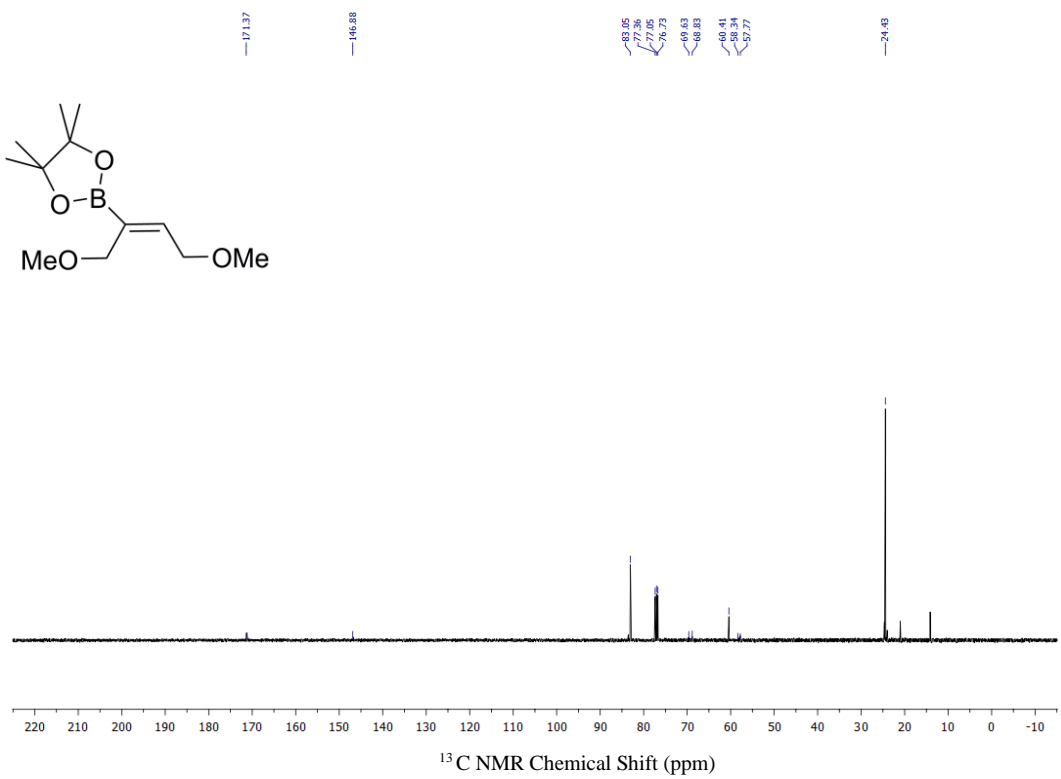
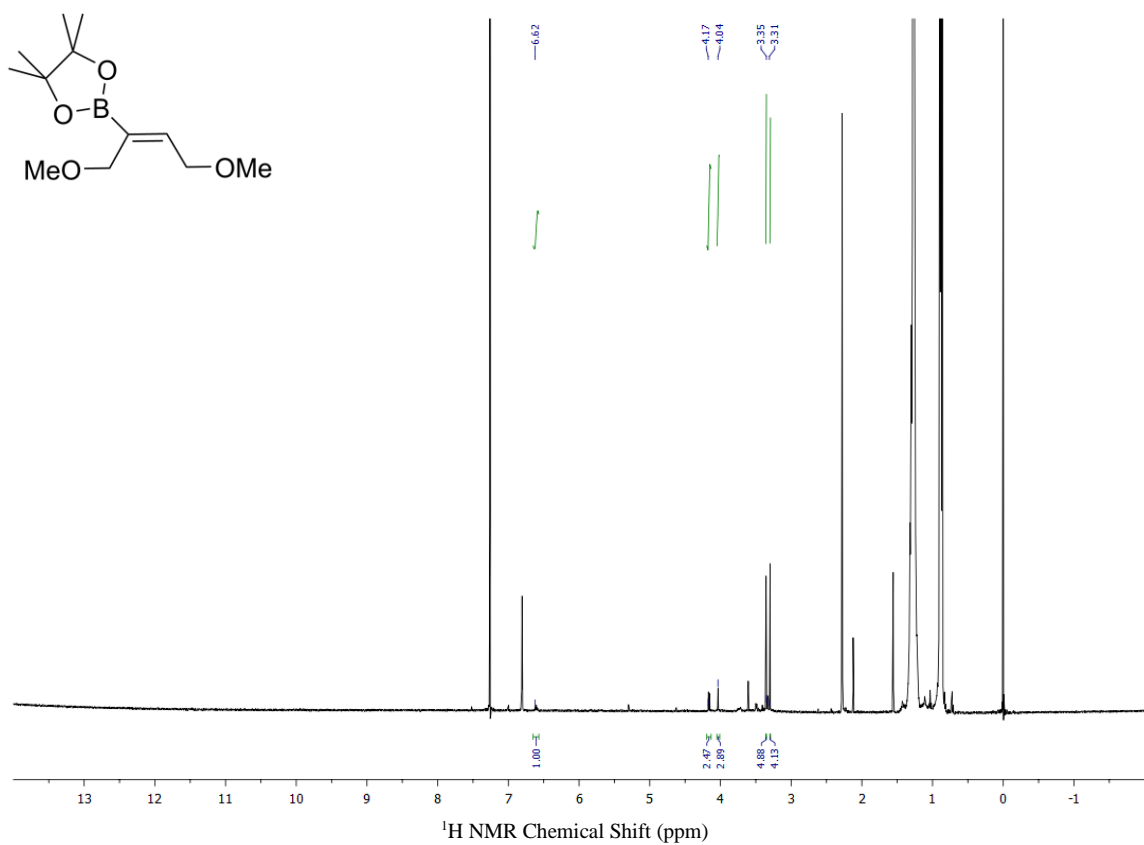
APPENDIX B. CRUDE ^1H AND ^{13}C SPECTRA FOR TABLE 3.7

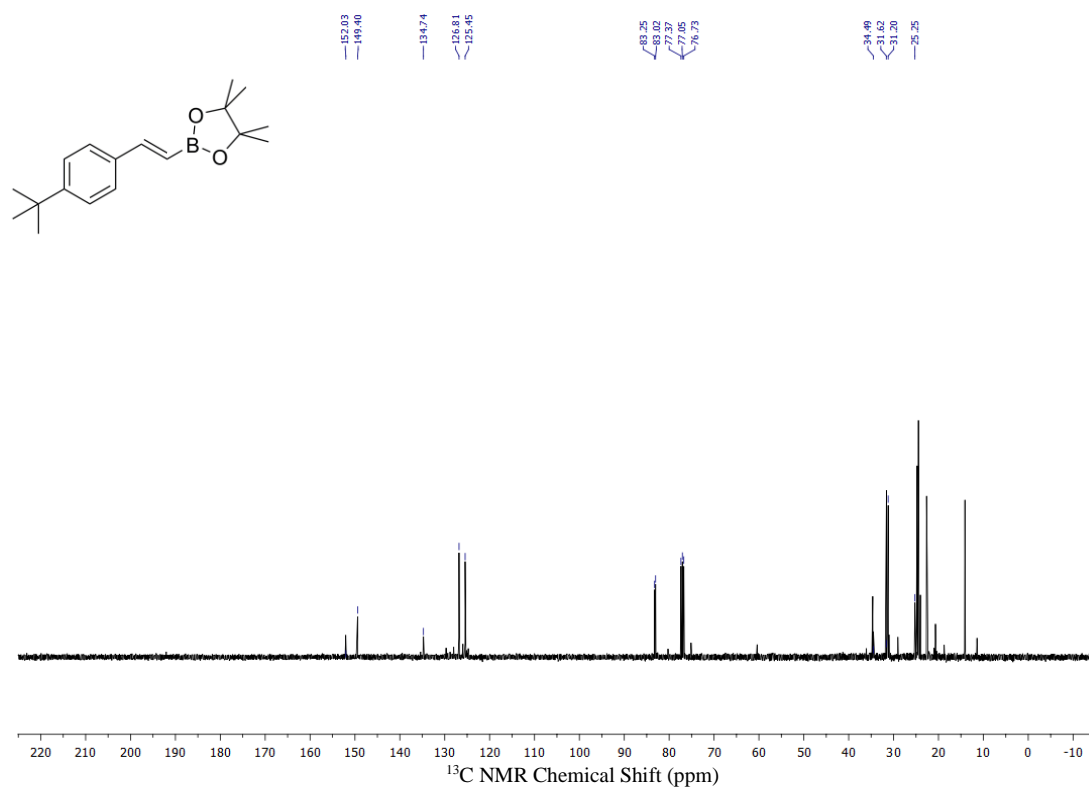
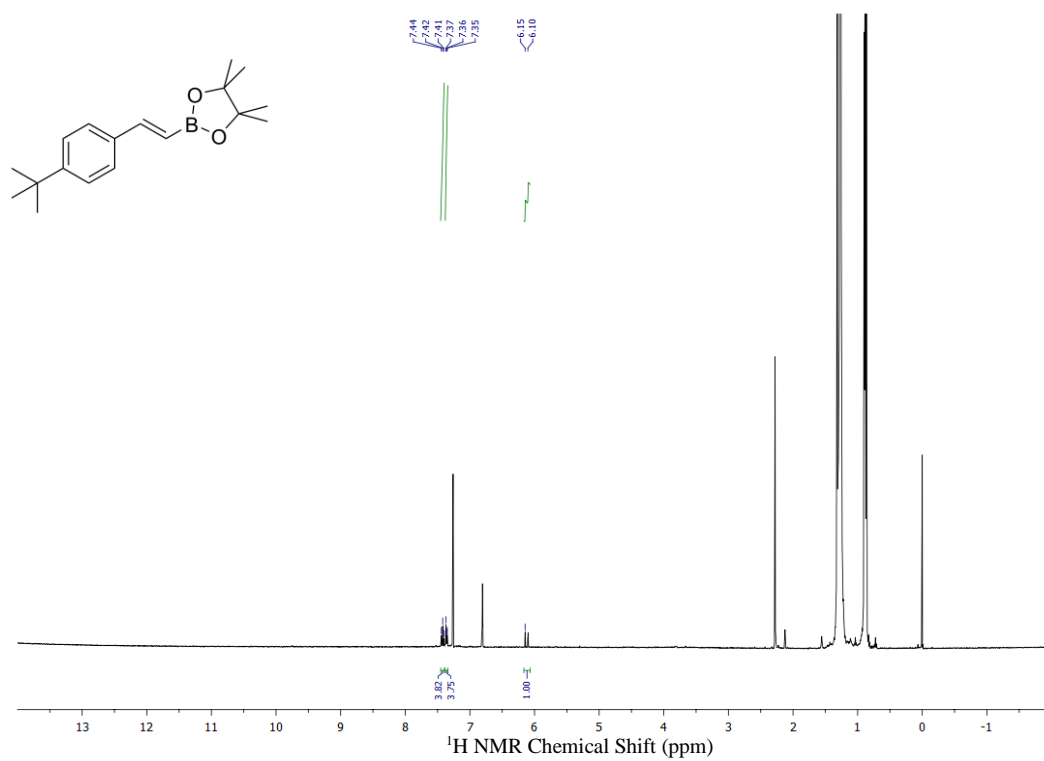
SUBSTRATE SCOPE OF HYDROBORATION OF SUBSTITUTED

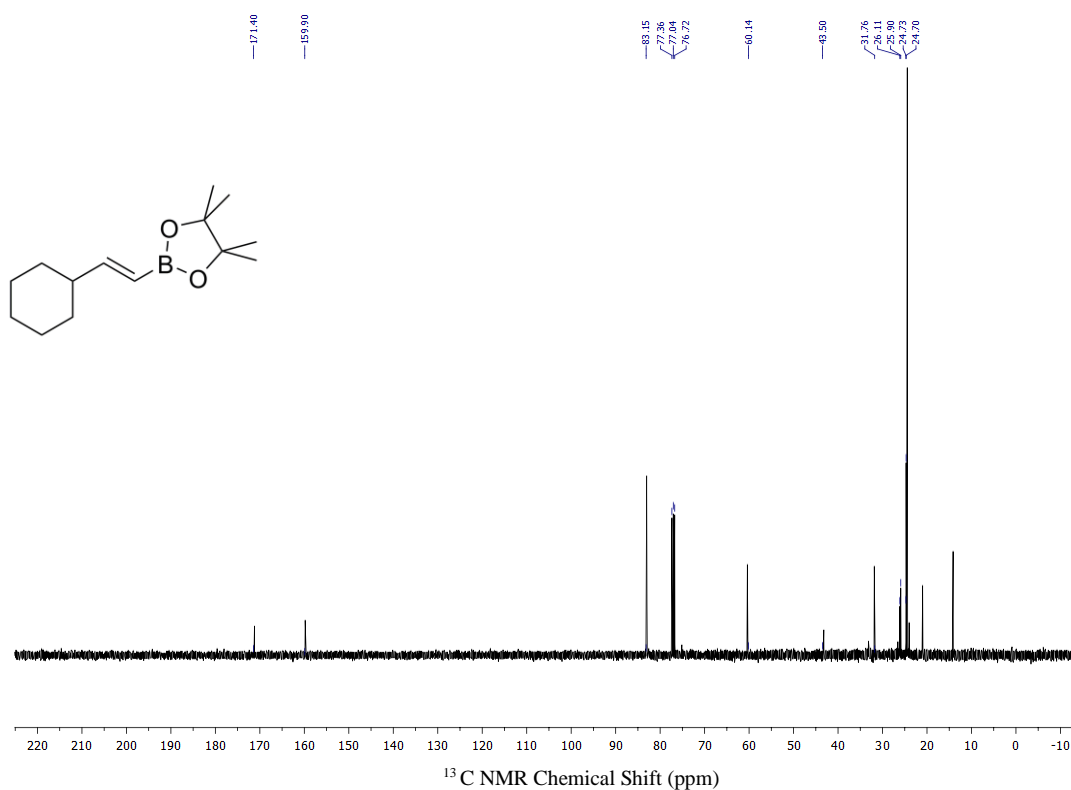
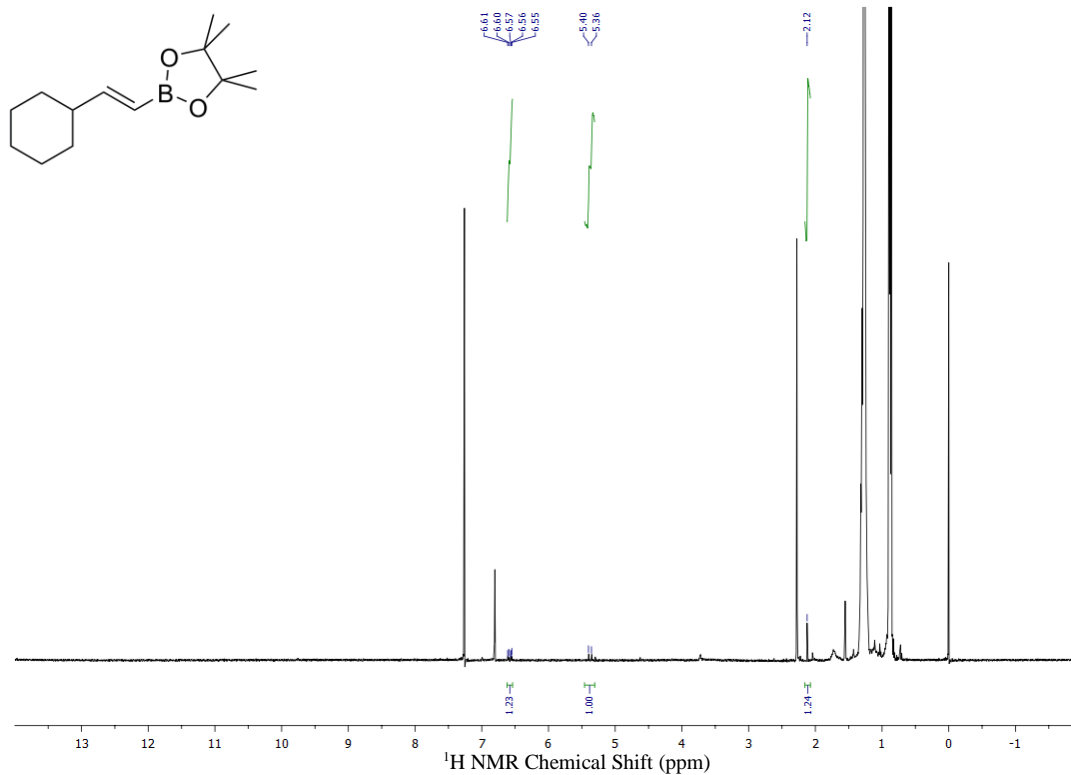
ALKYNES USING PINACOLBORANE

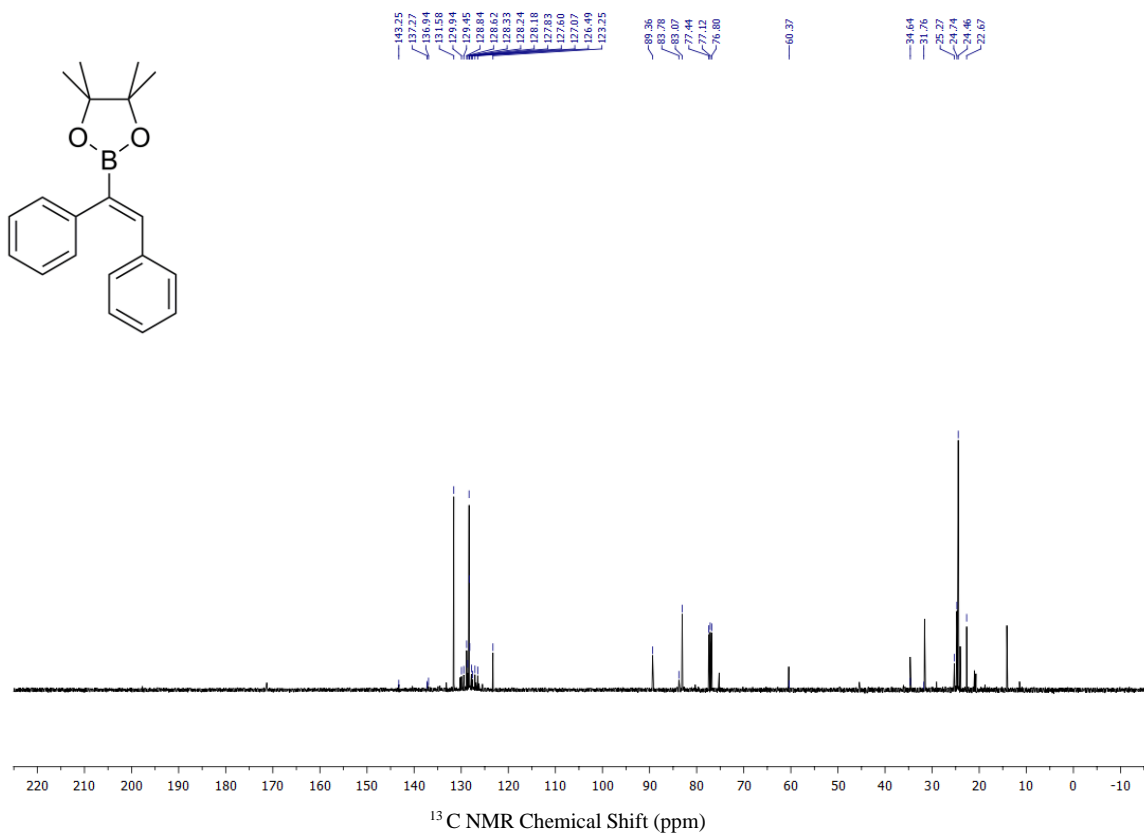
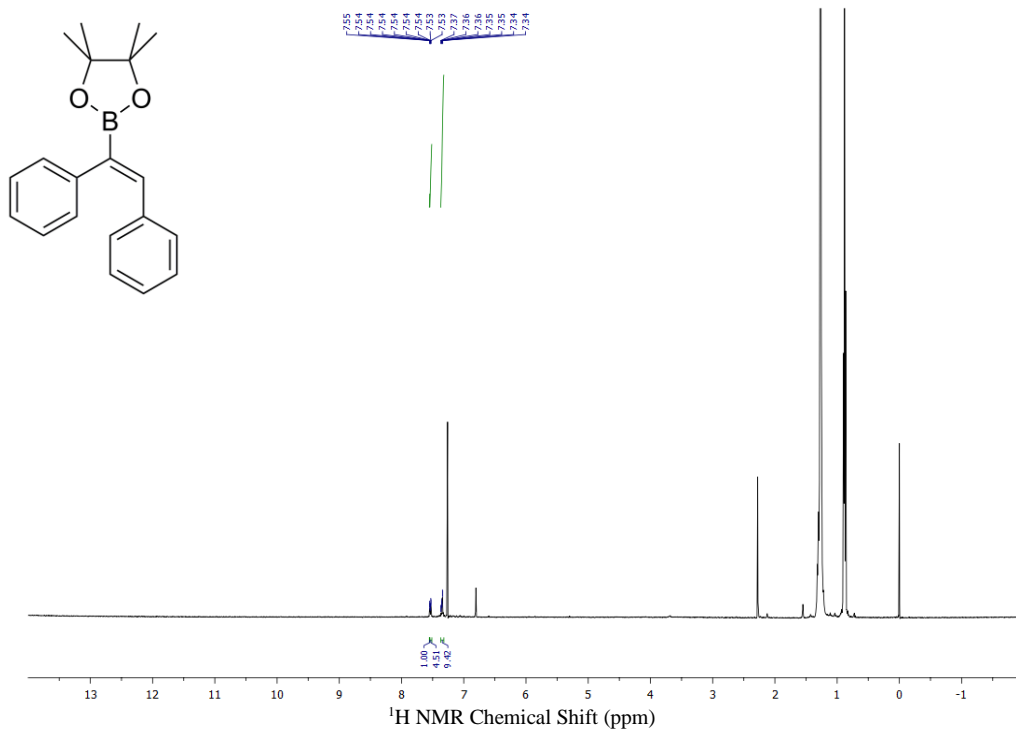


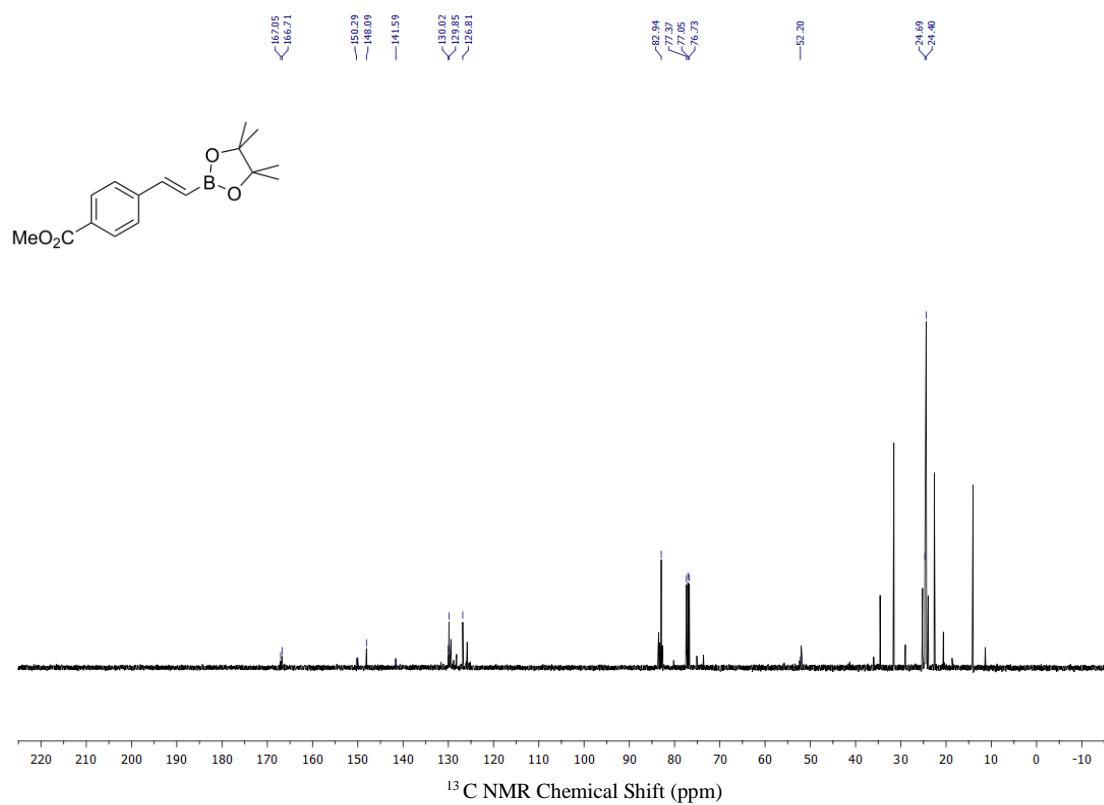
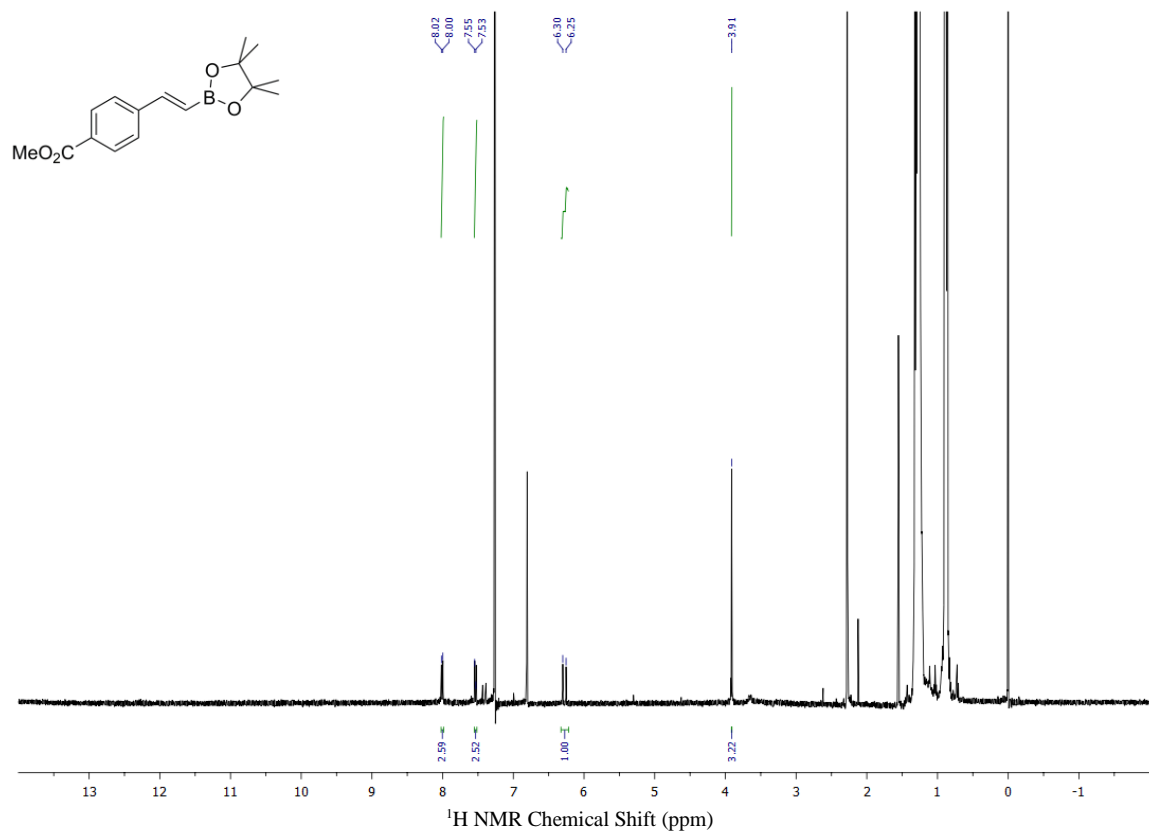


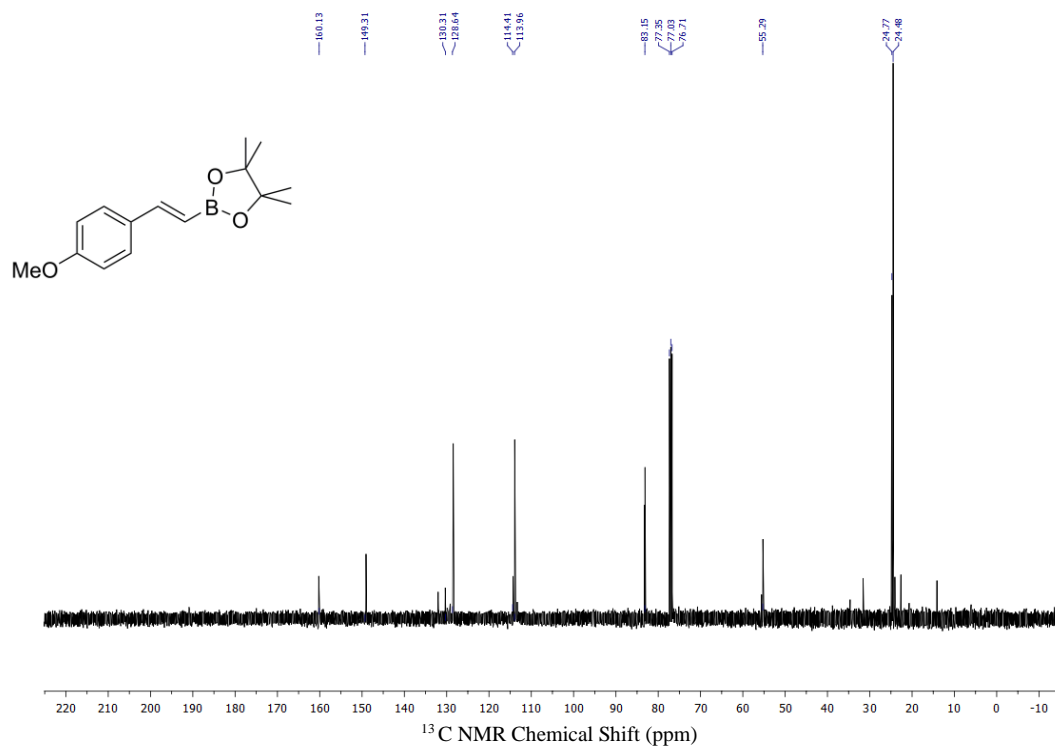
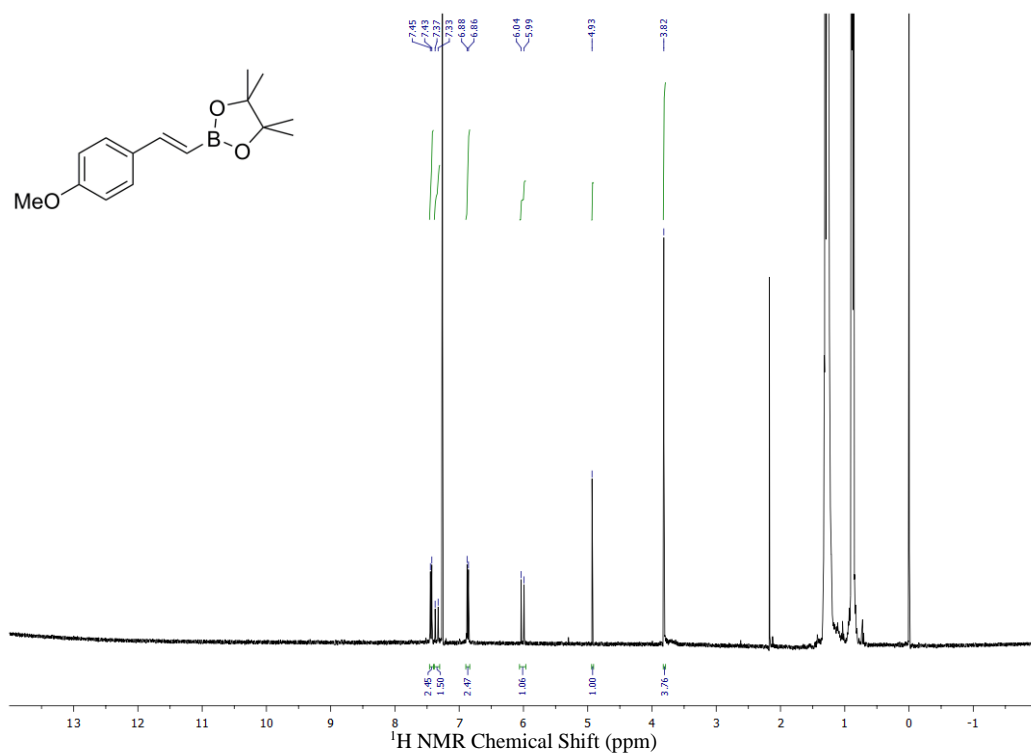


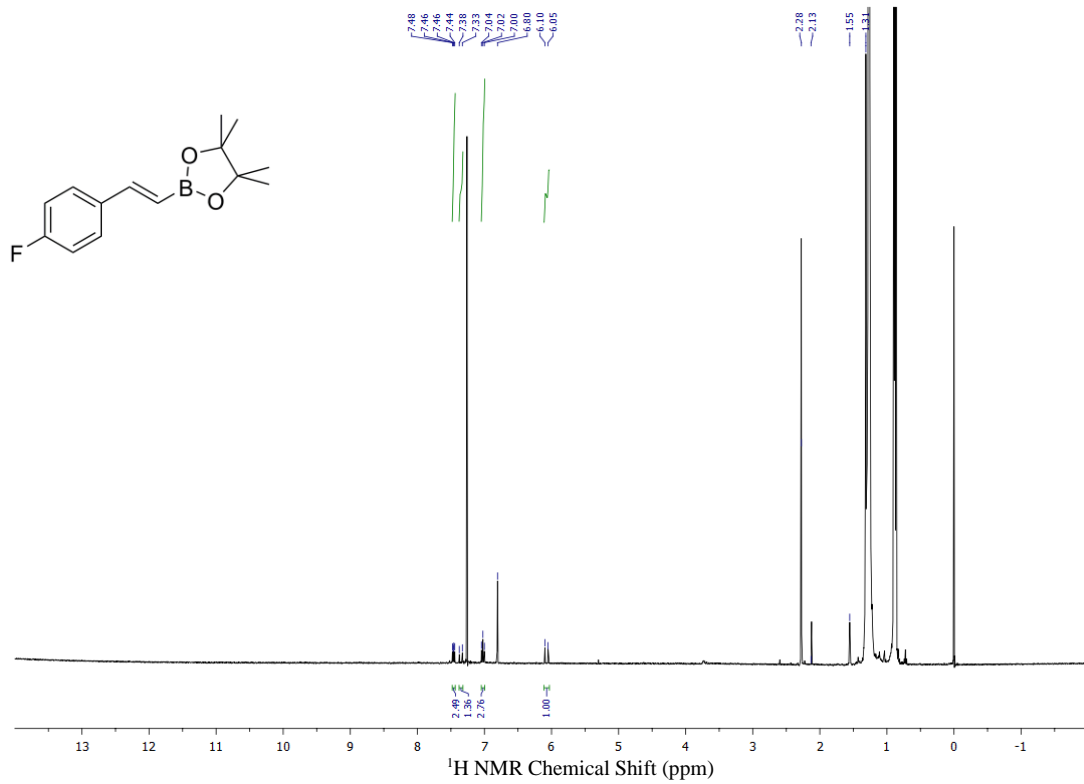
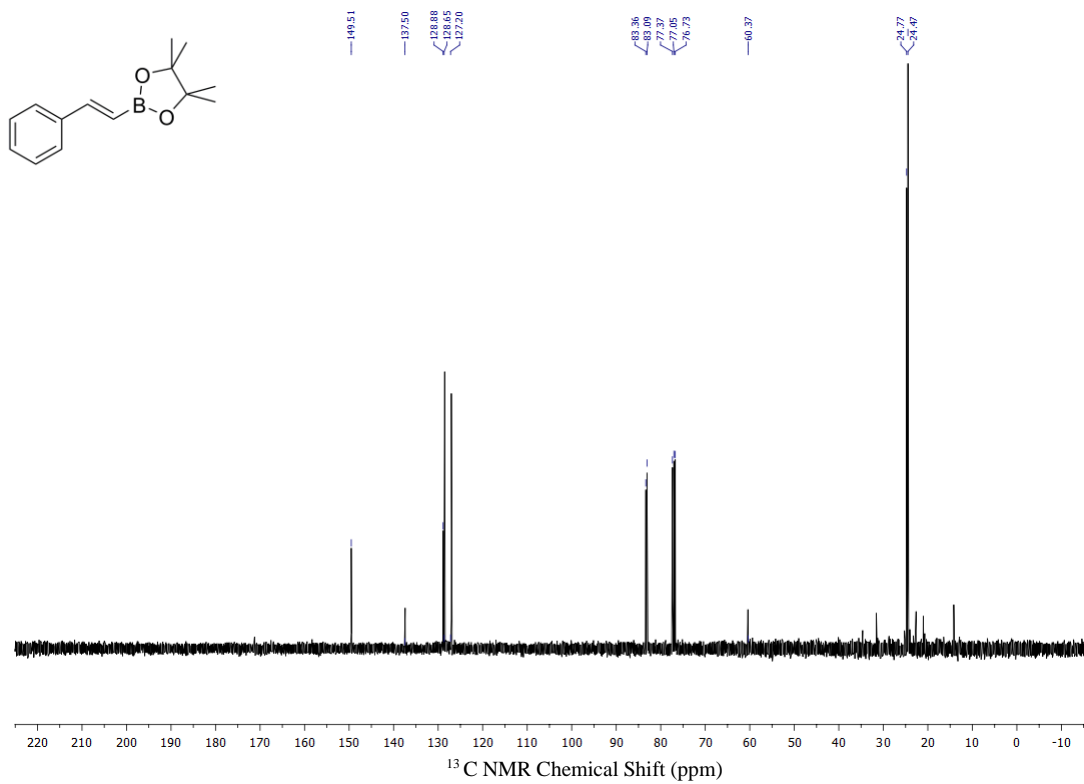


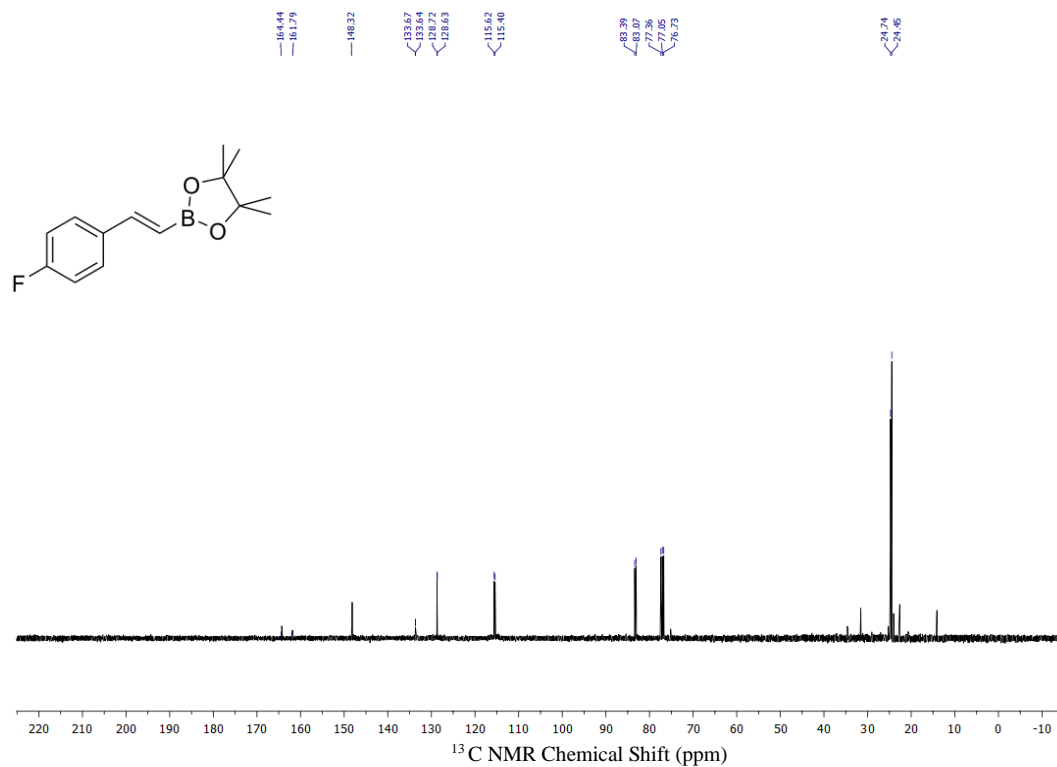












REFERENCES

- (1) Bell, A. T.; Gates, B. C.; Ray, D. *Basic Research Needs: Catalysis for Energy*; 2007.
- (2) Hübner, S.; de Vries, J. G.; Farina, V. *Adv. Synth. Catal.* **2016**, 358 (1), 3–25.
- (3) Gladysz, J. A. *Chem. Rev.* **2002**, 102, 3215–3216.
- (4) Toy, P. H. *Pure Appl. Chem.* **2014**, 86 (11), 1651–1661.
- (5) Rossi, L. M.; Costa, N. J. S.; Silva, F. P.; Wojcieszak, R. *Green Chem.* **2014**, 16 (6), 2906–2933.
- (6) De Vos, D. E.; Dams, M.; Sels, B. F.; Jacobs, P. A. *Chem. Rev.* **2002**, 102, 3615–3640.
- (7) Bianchini, C.; Giambastiani, G.; Luconi, L.; Meli, A. *Coord. Chem. Rev.* **2010**, 254, 431–455.
- (8) Youk, S. H.; Oh, S. H.; Rho, H. S.; Lee, J. E.; Lee, J. W.; Song, C. E. *Chem. Commun.* **2009**, 16, 2220–2222.
- (9) Tuchman-Shukron, L.; Miller, S. J.; Portnoy, M. *Chem. - A Eur. J.* **2012**, 18 (8), 2290–2296.
- (10) Tebben, L.; Studer, A. *Angew. Chemie Int. Ed.* **2011**, 50 (22), 5034–5068.
- (11) Advincula, R. In *Advances in Polymer Science*; Springer-Verlag: Berlin/Heidelberg, 2006; pp 107–136.
- (12) Barbey, R.; Lavanant, L.; Paripovic, D.; Schüwer, N.; Sugnaux, C.; Tugulu, S.; Klok, H.-A. *Chem. Rev.* **2009**, 109 (11), 5437–5527.
- (13) Ye, R.; Zhukhovitskiy, A. V.; Deraedt, C. V.; Toste, F. D.; Somorjai, G. A. *Acc. Chem. Res.* **2017**, 50, 1894–1901.
- (14) Wang, D.; Deraedt, C.; Ruiz, J.; Astruc, D. *Acc. Chem. Res.* **2015**, 48, 1871–1880.
- (15) Buurma, N. J. *Annu. Reports Sect. "B" (Organic Chem.* **2012**, 108 (0), 316–333.
- (16) Bernal, E.; Marchena, M.; Sánchez, F. *Molecules* **2010**, 15 (7), 4815–4874.
- (17) Beletskaya, I.; Tyurin, V. *Molecules* **2010**, 15 (7), 4792–4814.

- (18) Akay, G.; Kennedy, J. F.; Jenkins, A. D. *Macromolecular Chemistry : Volume 3*; London, 1984.
- (19) Catherine A. McNamara; Mark J. Dixon, A.; Bradley*, M. *Chem. Rev.* **2002**, *102*, 3275–3300.
- (20) Dickerson, T. J.; Reed, N. N.; Janda, K. D. *Chem. Rev.* **2002**, *102*, 3325–3344.
- (21) Patel, M. M. *Rubber News* **1967**, *6*, 22–30.
- (22) Raemaenen, H.; Lassila, H.; Lensu, A.; Lahti, M.; Oikari, A. *J. Soils Sediments* **2010**, *10* (3), 349–358.
- (23) Gao, C.; Wang, L.; Li, X.; Wang, H. *Polym. Chem.* **2014**, *5* (18), 5200–5210.
- (24) Gao, Y.; Liu, M.; Zhang, Y.; Liu, Z.; Yang, Y.; Zhao, L. *Polymers (Basel)*. **2017**, *9* (39), 1–42.
- (25) Hu, Z.; Zhang, K.; Huang, F.; Cao, Y. *Chem. Commun.* **2015**, *51* (26), 5572–5585.
- (26) Huo, L.; Hou, J. *Polym. Chem.* **2011**, *2* (11), 2453.
- (27) Pai, R. K.; T. N., A.; B., H. *RSC Adv.* **2016**, *6* (28), 23760–23774.
- (28) Boeva, Z. A.; Sergeyev, V. G. *Polym. Sci. Ser. C* **2014**, *56* (1), 144–153.
- (29) Antolini, E.; Gonzalez, E. R. *Appl. Catal. A Gen.* **2009**, *365* (1), 1–19.
- (30) Agnieszka, I.; Malinowski, M.; Grzegorz, P. *Renew. Sustain. Energy Rev.* **2015**, *49*, 954–967.
- (31) Nie, M.; Zhang, L. Y.; Jiang, C. Y.; Tian, X. H.; Li, Q.; Liu, X. W.; Du, S. J.; Lu, S.; Lei, D.; Wang, X. H.; Yuan, J. H.; Zhao, Z. Z.; Wu, M. Z. *Plast. Rubber Compos.* **2016**, *45* (1), 31–42.
- (32) von Hauff, E. *Semicond. Semimetals* **2011**, *85*, 231–260.
- (33) Schulz, G. L.; Ludwigs, S. *Adv. Funct. Mater.* **2017**, *27* (1), 1603083.
- (34) Chiechi, R. C.; Hummelen, J. C. *ACS Macro Lett.* **2012**, *1* (10), 1180–1183.
- (35) Huang, C.-F. *Polym. J.* **2016**, *48* (4), 341–350.
- (36) Khabibullin, A.; Mastan, E.; Matyjaszewski, K.; Zhu, S. Springer, Cham, 2015; pp 29–76.
- (37) Hui, M.; Pietrasik, J.; Schmitt, M.; Mahoney, C.; Choi, J.; Bockstaller, M. R.; Matyjaszewski, K. *Chem. Mater.* **2014**, *26* (1), 745–762.

- (38) Ohno, K.; Ma, Y.; Huang, Y.; Mori, C.; Yahata, Y.; Tsujii, Y.; Maschmeyer, T.; Moraes, J.; Perrier, S. *Macromolecules* **2011**, *44* (22), 8944–8953.
- (39) Rungta, A.; Natarajan, B.; Neely, T.; Dukes, D.; Schadler, L. S.; Benicewicz, B. C. *Macromolecules* **2012**, *45* (23), 9303–9311.
- (40) Yang, Y.; Yang, Z.; Zhao, Q.; Cheng, X.; Tjong, S. C.; Li, R. K. Y.; Wang, X.; Xie, X. *J. Polym. Sci. Part A Polym. Chem.* **2009**, *47* (2), 467–484.
- (41) Phan, T. N. T.; Jestin, J.; Gimes, D. In *Controlled Radical Polymerizations at and from Solid Surfaces*; Springer, Cham, 2015; pp 1–27.
- (42) Billon, L. *Surface-initiated nitroxide-mediated polymerization*; RSC Polymer Chemistry Series, 2016.
- (43) Bünsow, J.; Kelby, T. S.; Huck, W. T. S. *Acc. Chem. Res.* **2010**, *43* (3), 466–474.
- (44) Cayre, O. J.; Chagneux, N.; Biggs, S. *Soft Matter* **2011**, *7* (6), 2211–2234.
- (45) Yu, Q.; Ista, L. K.; Gu, R.; Zauscher, S.; López, G. P. *Nanoscale* **2016**, *8* (2), 680–700.
- (46) Gill, C. S.; Long, W.; Jones, C. W. *Catal. Letters* **2009**, *131*, 425–431.
- (47) Xiong, L.; Zhang, H.; Zhong, A.; He, Z.; Huang, K.; Drechsler, M.; Muller, A. H. E.; Muller, A. H. E. *Chem. Commun.* **2014**, *50* (94), 14778–14781.
- (48) Gill, C. S.; Venkatasubbaiah, K.; Phan, N. T. S.; Weck, M.; Jones, C. W. *Chem. - A Eur. J.* **2008**, *14* (24), 7306–7313.
- (49) Mou, J.; Gao, G.; Chen, C.; Liu, J.; Gao, J.; Liu, Y.; Pei, D. *RSC Adv.* **2017**, *7* (23), 13868–13875.
- (50) Liao, X.-H.; Liu, Y.; Peng, X.; Mi, C.; Meng, X.-G. *Catal. Letters* **2016**, *146* (7), 1249–1255.
- (51) Mukherjee, M.; Mahapatra, A. *Colloids Surfaces A Physicochem. Eng. Asp.* **2013**, *430*, 13–20.
- (52) Janib, S. M.; Moses, A. S.; MacKay, J. A. *Adv. Drug Deliv. Rev.* **2010**, *62* (11), 1052–1063.
- (53) Khan, D. R.; Favela, S. J.; Muniz, A. E.; Blakeman, A. A. *Recent Patents Nanomed.* **2013**, *3*, 21–25.
- (54) Zaera, F. *Chem. Soc. Rev.* **2013**, *42*, 2746–2762.
- (55) Thanneeru, S.; Duay, S. S.; Jin, L.; Fu, Y.; Angeles-Boza, A. M.; He, J. *ACS Macro Lett.* **2017**, *6* (7), 652–656.

- (56) Potier, J.; Menuel, S.; Fournier, D.; Fourmentin, S.; Woisel, P.; Monflier, E.; Hapiot, F. *ACS Catal.* **2012**, 2 (7), 1417–1420.
- (57) Margelefsky, E. L.; Zeidan, R. K.; Davis, M. E. *Chem. Soc. Rev.* **2008**, 37 (6), 1118–1126.
- (58) Chen, D. F.; Han, Z. Y.; Zhou, X. Le; Gong, L. Z. *Acc. Chem. Res.* **2014**, 47 (8), 2365–2377.
- (59) Brunelli, N. A.; Jones, C. W. *J. Catal.* **2013**, 308, 60–72.
- (60) Kuwamura, N.; Kurioka, Y.; Konno, T. *Chem. Commun.* **2017**, 53 (5), 846–849.
- (61) Chiola, V.; Ritsko, J. E.; Vanderpool, C. D. Process for Producing Low-Bulk Density Silica. 3,556,725, 1971.
- (62) Beck, J. S.; Chu, C. T.-W.; Johnson, I. D.; Kresge, C. T.; Leonowicz, M. E.; Roth, W. J.; Vartuli, J. C. Synthetic Porous Crystalline Material, It's Preparation, and Use. WO9111390, 1991.
- (63) Di Renzo, F.; Cambon, H.; Dutartre, R. *Microporous Mater.* **1997**, 10, 283–286.
- (64) Burkett, S. L.; Sims, S. D.; Mann, S.; Thomas, J. M.; Beck, J. S. *Chem. Commun.* **1996**, 4 (11), 1367–1368.
- (65) Bukhryakov, K. V.; Desyatkin, V. G.; Rodionov, V. O. *Chem. Commun.* **2016**, 52 (48), 7576–7579.
- (66) Du, J.; Tao, M.; Zhang, W. *ACS Sustain. Chem. Eng.* **2016**, 4, 4296–4304.
- (67) Peng, Y.; Wang, J.; Long, J.; Liu, G. *Catal. Commun.* **2011**, 15, 10–14.
- (68) Zeidan, R. K.; Davis, M. E. *J. Catal.* **2007**, 247 (2), 379–382.
- (69) Brunelli, N. a.; Venkatasubbaiah, K.; Jones, C. W. *Chem. Mater.* **2012**, 24 (13), 2433–2442.
- (70) Brunelli, N. a.; Didas, S. a.; Venkatasubbaiah, K.; Jones, C. W. *J. Am. Chem. Soc.* **2012**, 134 (34), 13950–13953.
- (71) Brown, H. C.; Murray, K. *J. Am. Chem. Soc.* **1959**, 81 (15), 4108–4109.
- (72) Xue, C.; Kung, S.-H.; Wu, J.-Z.; Luo, F.-T. *Tetrahedron* **2008**, 64 (1), 248–254.
- (73) Miyaura, N.; Suzuki, A. *Chem. Rev.* **1995**, 95 (7), 2457–2483.
- (74) Brown, C. A.; Coleman, R. A. *J. Org. Chem.* **1979**, 44 (13), 2328–2329.
- (75) Brown, H. C.; Gupta, S. K. *J. Am. Chem. Soc.* **1975**, 97 (18), 5249–5255.

- (76) Brown, H. C.; Gupta, S. K. *J. Am. Chem. Soc.* **1972**, *94* (12), 4370–4371.
- (77) Gorgas, N.; Alves, L. G.; Stö, B.; Martins, A. M.; Veiros, L. F.; Kirchner, K. *J. Am. Chem. Soc.* **2017**, *139* (24), 8130–8133.
- (78) John Wiley & Sons. *E-EROS encyclopedia of reagents for organic synthesis*; 2014.
- (79) He, X.; Hartwig, J. F. *J. Am. Chem. Soc.* **1996**, *118* (7), 1696–1702.
- (80) Pereira, S.; Srebnik, M. *Organometallics* **1995**, *14* (7), 3127–3128.
- (81) Pereira, S.; Srebnik, M. *Tetrahedron Lett.* **1996**, *37* (19), 3283–3286.
- (82) Xu, S.; Zhang, Y.; Li, B.; Liu, S.-Y. *J. Am. Chem. Soc.* **2016**, *138* (44), 14566–144569.
- (83) Ojha, D. P.; Prabhu, K. R. *Org. Lett.* **2016**, *18* (3), 432–435.
- (84) Beletskaya, I.; Pelter, A. *Tetrahedron* **1997**, *53* (14), 4957–5026.
- (85) Irvine, G. J.; Lesley, M. J. G.; Marder, T. B.; Norman, N. C.; Rice, C. R.; Robins, E. G.; Roper, W. R.; Whittell, G. R.; Wright, L. J. *Chem. Rev.* **1998**, *98*, 2685–2722.
- (86) Li, Z.; Wang, Z.; Zhu, L.; Tan, X.; Li, C. *J. Am. Chem. Soc.* **2014**, *136* (46), 16439–16443.
- (87) Gunanathan, C.; Hölscher, M.; Pan, F.; Leitner, W. *J. Am. Chem. Soc.* **2012**, *134* (35), 14349–14352.
- (88) Ohmura, T.; Yamamoto, Y.; Miyaura, N. *J. Am. Chem. Soc.* **1988**, *8* (1268), 703–749.
- (89) Semba, K.; Fujihara, T.; Terao, J.; Tsuji, Y. *Chem. - A Eur. J.* **2012**, *18* (14), 4179–4184.
- (90) Sundararaju, B.; Fürstner, A. *Angew. Chemie Int. Ed.* **2013**, *52* (52), 14050–14054.
- (91) Haberberger, M.; Enthaler, S. *Chem. - An Asian J.* **2013**, *8* (1), 50–54.
- (92) Wu, J. Y.; Moreau, B.; Ritter, T. *J. Am. Chem. Soc.* **2009**, *131* (36), 12915–12917.
- (93) Obligacion, J. V.; Chirik, P. J. *ACS Catal.* **2017**, *7*, 4366–4371.
- (94) Krautwald, S.; Bezdek, M.; Chirik, P. J. *J. Am. Chem. Soc.* **2017**, *139*, 3868–3875.
- (95) Obligacion, J. V.; Semproni, S. P.; Pappas, I.; Chirik, P. J. *J. Am. Chem. Soc.* **2016**, *138* (33), 10645–10653.

- (96) Peng, J.; Docherty, J. H.; Dominey, A. P.; Thomas, S. P.; Ito, S.; Nakamura, E.; Nakamura, N. *Chem. Commun.* **2017**, 53 (34), 4726–4729.
- (97) Kim, H. R.; Yun, J.; Sabat, M.; Ingallina, P.; Lee, E. S.; Yun, J.; Son, S. U.; Fernández, E.; Wright, L. J. *Chem. Commun.* **2011**, 47 (10), 2943–2945.
- (98) Romero, E. A.; Jazzar, R.; Bertrand, G. J. *Organomet. Chem.* **2017**, 829, 11–13.
- (99) Woo, H.; Park, J.; Kim, J.; Park, S.; Park, K. H. *Catal. Commun.* **2017**, 100, 52–56.
- (100) Xu, P.; Li, B.; Wang, L.; Qin, C.; Zhu, L. *Catal. Commun.* **2016**, 86, 23–26.
- (101) Zhao, J.; Niu, Z.; Fu, H.; Li, Y. *Chem. Commun. Chem. Commun* **2014**, 50, 2058–2060.
- (102) Huang, Z.; Liu, D.; Camacho-Bunquin, J.; Zhang, G.; Yang, D.; Loez-Encarnacio, J. M.; Xu, Y.; Ferrandon, M. S.; Niklas, J.; Poluektov, O. G.; Jellinek, J.; Lei, A.; Bunel, E. E.; Delferro, M. *Organometallics* **2017**, 36, 3921–3930.
- (103) Manna, K.; Ji, P.; Greene, F. X.; Lin, W. *J. Am. Chem. Soc.* **2016**, 138, 7488–7491.
- (104) Taylor, R. A.; Santora, B. P.; Gagné, M. R. *Org. Lett.* **2000**, 2 (12), 1781–1783.
- (105) Geier, M.; Geier, S.; Vogels, C.; Béland, F.; Westcott, S. *Synlett* **2009**, No. 3, 477–481.
- (106) Eedugurala, N.; Wang, Z.; Chaudhary, U.; Nelson, N.; Kandel, K.; Kobayashi, T.; Slowing, I. I.; Pruski, M.; Sadow, A. D. *ACS Catal.* **2015**, 5 (12), 7399–7414.
- (107) Barbey, R.; Lavanant, L.; Paripovic, D.; Schüwer, N.; Sugnaux, C.; Tugulu, S.; Klok, H.-A. *Chem. Rev.* **2009**, 109 (11), 5437–5527.
- (108) Liang Li, G.; Qun Xu, L.; Neoh, K. G.; Kang, E. T. *Macromolecules* **2011**, 44, 2365–2370.
- (109) Liu, B.; Zhang, D.; Wang, J.; Chen, C.; Yang, X.; Li, C. *J. Phys. Chem. C* **2013**, 117, 6363–6372.
- (110) Koenig, M.; Simon, F.; Formanek, P.; Müller, M.; Gupta, S.; Stamm, M.; Uhlmann, P. *Macromol. Chem. Phys.* **2013**, 214 (20), 2301–2311.
- (111) Fernandes, A. E.; Ye, Q.; Collard, L.; Le Duff, C.; d’Haese, C.; Deumer, G.; Haufroid, V.; Nysten, B.; Riant, O.; Jonas, A. M. *ChemCatChem* **2015**, 7 (5), 856–864.
- (112) Hoyt, C. B.; Lee, L.-C.; Cohen, A. E.; Weck, M.; Jones, C. W. *ChemCatChem* **2017**, 9 (1), 137–143.

- (113) Wang, K.; Jia, Z.; Yang, X.; Wang, L.; Gu, Y.; Tan, B. *J. Catal.* **2017**, *348*, 168–176.
- (114) Li, H.; Pan, Q.; Ma, Y.; Guan, X.; Xue, M.; Fang, Q.; Yan, Y.; Valtchev, V.; Qiu, S. *J. Am. Chem. Soc.* **2016**, *138*, 14783–14788.
- (115) Dhakshinamoorthy, A.; Garcia, H. *ChemSusChem* **2014**, *7* (9), 2392–2410.
- (116) Helms, B.; Guillaudeu, S. J.; Xie, Y.; McMurdo, M.; Hawker, C. J.; Fréchet, J. M. *J. Angew. Chemie - Int. Ed.* **2005**, *44* (39), 6384–6387.
- (117) Mou, J.; Gao, G.; Chen, C.; Liu, J.; Gao, J.; Liu, Y.; Pei, D. *RSC Adv.* **2017**, *7*, 13868–13875.
- (118) Arigoni, D.; Sagner, S.; Latzel, C.; Eisenreich, W.; Bacher, A.; Zenk, M. H. *Proc. Natl. Acad. Sci. U. S. A.* **1997**, *94* (20), 10600–16005.
- (119) Agapakis, C. M.; Boyle, P. M.; Silver, P. A. *Nat. Chem. Biol.* **2012**, *8*, 527–5.
- (120) Fletcher, P. D. *Curr. Opin. Colloid Interface Sci.* **1996**, *1* (1), 101–106.
- (121) Owen, T.; Butler, A. *Coord. Chem. Rev.* **2011**, *255*, 678–687.
- (122) Zhang, S.; Zhao, Y. *ACS Nano* **2011**, *5* (4), 2637–2646.
- (123) Li, S.; Yi, J.; Li, W.; Wang, L.; Wang, Z. *J. Mater. Sci.* **2017**, *52*, 12593–12607.
- (124) Liu, Y.; Wang, Y.; Wang, Y.; Lu, J.; Pi~ N On, V.; Weck, M. *J. Am. Chem. Soc.* **2011**, *133*, 14260–14263.
- (125) Lu, J.; Dimroth, J.; Weck, M. *J. Am. Chem. Soc.* **2015**, *137* (40), 12984–12989.
- (126) Lempke, L.; Ernst, A.; Kahl, F.; Weberskirch, R.; Krause, N. *Adv. Synth. Catal.* **2016**, *358* (9), 1491–1499.
- (127) Joumaa, A.; Chen, S.; Vincendeau, S.; Gayet, F.; Poli, R.; Manoury, E. *Mol. Catal.* **2017**, *438*, 267–271.
- (128) Gerola, A. P.; Wanderlind, E. H.; Gomes, Y. S.; Giusti, L. A.; García-Río, L.; Nome, R.; Kirby, A. J.; Fiedler, H. D.; Nome, F. *ACS Catal.* **2017**, *7*, 2230–2239.
- (129) Hoyt, C. B.; Lee, L.-C.; He, J.; Yu, J.-Q.; Jones, C. W. *Adv. Synth. Catal.* **2017**.
- (130) Kramer, S.; Kim, K. O.; Zentel, R. *Macromol. Chem. Phys.* **2017**, *218* (19), 1700113–1700122.
- (131) Soleymani Abyaneh, H.; Reza Vakili, M.; Shafaati, A.; Lavasanifar, A. *Mol. Pharm.* **2017**, *14*, 2487–2502.

- (132) Lebouille, J. G. J. L.; Leermakers, F. A. M.; Cohen Stuart, M. A.; Tuinier, R. *Phys. Rev. E* **2016**, *94*, 1–15.
- (133) Tritschler, U.; Pearce, S.; Gwyther, J.; Whittell, G. R.; Manners, I. *Macromolecules* **2017**, *50*, 3439–3463.
- (134) Fan, X.; Li, Z.; Loh, X. J. *Polym. Chem.* **2016**, *7*, 5898–5919.
- (135) Yuan, H.; Yoo, W.-J.; Miyamura, H.; Kobayashi, S. *J. Am. Chem. Soc.* **2012**, No. 134, 13970–13973.
- (136) Souillart, L.; Cramer, N. *Chem. Rev.* **2015**, *115* (17), 9410–9464.
- (137) Khusnutdinova, J. R.; Milstein, D. *Angew. Chemie - Int. Ed.* **2015**, *54* (42), 12236–12273.
- (138) Li, M. Q.; Zhang, J. X.; Huang, X. F.; Wu, B.; Liu, Z. M.; Chen, J.; Li, X. D.; Wang, X. W. *European J. Org. Chem.* **2011**, No. 27, 5237–5241.
- (139) Miyaji, R.; Asano, K.; Matsubara, S. *J. Am. Chem. Soc.* **2015**, *137* (21), 6766–6769.
- (140) Sohtome, Y.; Nagasawa, K. *Chem. Commun.* **2012**, 48 (63), 7777.
- (141) Jindal, G.; Kisan, H. K.; Sunoj, R. B. *ACS Catal.* **2015**, *5* (2), 480–503.
- (142) Scheffler, U.; Mahrwald, R. *Chem. - A Eur. J.* **2013**, *19* (43), 14346–14396.
- (143) Maruoka, K.; List, B.; Yamamoto, H.; Gong, L.-Z. *Chem. Commun.* **2012**, 48, 10703.
- (144) List, Benjamin; Yang, J. W. *Science* (80-.). **2006**, *313* (September), 1583–1584.
- (145) Choudary, B. M.; Kantam, M. L.; Sreekanth, P.; Bandopadhyay, T.; Figueras, F.; Tuel, A. *J. Mol. Catal. A Chem.* **1999**, *142* (3), 361–365.
- (146) Bass, J. D.; Solovyov, A.; Pascall, A. J.; Katz, A. *J. Am. Chem. Soc.* **2006**, *128* (19), 3737–3747.
- (147) An, Z.; Guo, Y.; Zhao, L.; Li, Z.; He, J. *ACS Catal. Catal.* **2014**, *4*, 2566–2576.
- (148) Motokura, K.; Tanaka, S.; Tada, M.; Iwasawa, Y. *Chem. - A Eur. J.* **2009**, *15* (41), 10871–10879.
- (149) Motokura, K.; Tada, M.; Iwasawa, Y. *Angew. Chemie - Int. Ed.* **2008**, *47* (48), 9230–9235.
- (150) Lauwaert, J.; De Canck, E.; Esquivel, D.; Van Der Voort, P.; Thybaut, J. W.; Marin, G. B. *Catal. Today* **2015**, *246*, 35–45.

- (151) Kubota, Y.; Yamaguchi, H.; Yamada, T.; Inagaki, S.; Sugi, Y.; Tatsumi, T. *Top. Catal.* **2010**, *53* (7–10), 492–499.
- (152) Lauwaert, J.; Moschetta, E. G.; Van Der Voort, P.; Thybaut, J. W.; Jones, C. W.; Marin, G. B. *J. Catal.* **2015**, *325*, 19–25.
- (153) Hruby, S. L.; Shanks, B. H. *J. Catal.* **2009**, *263* (1), 181–188.
- (154) Hicks, J. C.; Dabestani, R.; Buchanan, a. C.; Jones, C. W. *Chem. Mater.* **2006**, *18* (21), 5022–5032.
- (155) Hicks, J. C.; Jones, C. W. *Langmuir* **2006**, *22* (6), 2676–2681.
- (156) Umr, L.; Mitterrand, B. F.; Maupertuis, B. *J. Chem. Theory Comput.* **2012**, *8*, 1037–1047.
- (157) Hair, M. L.; Hertl, W. *J. Phys. Chem.* **1970**, *74* (1), 91–94.
- (158) Kubota, Y.; Goto, K.; Miyata, S.; Goto, Y.; Fukushima, Y.; Sugi, Y. *Chem. Lett.* **2003**, *32* (3), 234–235.
- (159) Motokura, K.; Tada, M.; Iwasawa, Y. *J. Am. Chem. Soc.* **2009**, *131* (23), 7944–7945.
- (160) Motokura, K.; Viswanadham, N.; Dhar, G. M.; Iwasawa, Y. *Catal. Today* **2009**, *141* (1–2), 19–24.
- (161) Moschetta, E. G.; Brunelli, N. A.; Jones, C. W. *Appl. Catal. A Gen.* **2015**, *504*, 429–439.
- (162) Brummelhuis, N. Ten; Weck, M. *J. Polym. Sci. Part A Polym. Chem.* **2014**, *52*, 1555–1559.
- (163) Hanková, L.; Holub, L.; Meng, X.; Xiao, F.-S.; Jeřábek, K. *J. Appl. Polym. Sci.* **2014**, *131* (23), 41198/1–41198/7.
- (164) Zeidan, R. K.; Hwang, S. J.; Davis, M. E. *Angew. Chemie - Int. Ed.* **2006**, *45* (38), 6332–6335.
- (165) Solin, N.; Han, L.; Che, S.; Terasaki, O. *Catal. Commun.* **2009**, *10* (10), 1386–1389.
- (166) Kandel, K.; Althaus, S. M.; Peeraphatdit, C.; Kobayashi, T.; Trewyn, B. G.; Pruski, M.; Slowing, I. I. *J. Catal.* **2012**, *291*, 63–68.
- (167) Nicolaou, K. C.; Lister, T.; Denton, R. M.; Gelin, C. F. *Tetrahedron* **2008**, *64* (21), 4736–4757.

- (168) Emer, E.; Pfeifer, L.; Brown, J. M.; Gouverneur, V. *Angew. Chem. Int. Ed. Engl.* **2014**, *53* (16), 4181–4185.
- (169) He, J.; Li, S.; Deng, Y.; Fu, H.; Laforteza, B. N.; Spangler, J. E.; Homs, A.; Yu, J.-Q. *Science* **2014**, *343* (6176), 1216–1220.
- (170) Hill, M. R.; Carmean, R. N.; Sumerlin, B. S. *Macromolecules* **2015**, *48* (16), 150728155954001.
- (171) Walling, C.; Briggs, E. R.; Wolfstirn, K. B.; Mayo, F. R. *J. Am. Chem. Soc.* **1948**, *70* (14), 1537–1542.
- (172) Packirisamy, S.; Hirao, Akira; Nakahama, S. *J. Polym. Sci. Part A Polym. Chem.* **1989**, *27*, 2811–2814.
- (173) Nagamani, C.; Viswanathan, U.; Versek, C.; Tuominen, M. T.; Auerbach, S. M.; Thayumanavan, S. *Chem. Commun. (Camb)*. **2011**, *47* (23), 6638–6640.
- (174) Kandel, K.; Althaus, S. M.; Peeraphatdit, C.; Kobayashi, T.; Trewyn, B. G.; Pruski, M.; Slowing, I. I. *ACS Catal.* **2013**, No. 3, 265–271.
- (175) Nyberg, A. I.; Usano, A.; Pihko, P. M. *Synlett* **2004**, *11*, 1891–1896.
- (176) Pihko, P. M.; Laurikainen, K. M.; Usano, A.; Nyberg, A. I.; Kaavi, J. A. *Tetrahedron* **2006**, *62* (2–3), 317–328.
- (177) Hilal, S. H.; Bornander, L. L.; Carreira, L. A. *QSAR Comb. Sci.* **2005**, *24* (5), 631–638.
- (178) Deng, C. C.; Brooks, W. LA; Abboud, K. A.; Sumerlin, B. S.; Butler, J. *ACS Macro Lett.* **2015**, *4*, 220–224.
- (179) Herlinger, E.; Jamesonb, R. F.; Linerta, W. *J. Chem. Soc. Perkin Trans. 2* **1995**, 259–263.
- (180) Liu, F.; Zheng, A.; Noshadi, I.; Xiao, F. S. *Appl. Catal. B Environ.* **2013**, *136–137*, 193–201.
- (181) Wang, L.; Zhang, J.; Sun, J.; Zhu, L.; Zhang, H.; Liu, F.; Zheng, D.; Meng, X.; Shi, X.; Xiao, F. S. *ChemCatChem* **2013**, *5* (6), 1606–1613.
- (182) Beletskaya, I.; Moberg, C. *Chem. Rev.* **2006**, *106*, 2320–2354.
- (183) Mukherjee, D.; Osseili, H.; Spaniol, T. P.; Okuda, J. *J. Am. Chem. Soc.* **2016**, *138* (34), 10790–10793.
- (184) Mukherjee, D.; Ellern, A.; Sadow, A. D. *Chem. Sci.* **2014**, *5*, 959–964.

- (185) Eisenberger, P.; Bailey, A. M.; Crudden, C. M. *J. Am. Chem. Soc.* **2012**, *134* (42), 17384–17387.
- (186) Fan, X.; Zheng, J.; Li, Z. H.; Wang, H. *J. Am. Chem. Soc.* **2015**, *137* (15), 4916–4919.
- (187) Dureen, M. A.; Lough, A.; Gilbert, T. M.; Stephan, D. W. *Chem. Commun.* **2008**, 0, 4303–4305.
- (188) Stephan, D. W. *Acc. Chem. Res.* **2015**, *48*, 306–316.
- (189) Garrett, C. E.; Fu, G. C. *J. Org. Chem.* **1996**, *61*, 3224–3225.
- (190) Wen, K.; Chen, J.; Gao, F.; Bhadury, P. S.; Fan, E.; Sun, Z. *Org. Biomol. Chem.* **2013**, *11* (37), 6350.
- (191) Ho, H. E.; Asao, N.; Yamamoto, Y.; Jin, T. *Org. Lett.* **2014**, *16*, 4670–4673.
- (192) Barbeyron, R.; Benedetti, E.; Cossy, J.; Vasseur, J.-J.; Arseniyadis, S.; Smietana, M. *Tetrahedron* **2014**, *70*, 8431–8452.
- (193) Nakajima, K.; Kato, T.; Nishibayashi, Y. *Org. Lett.* **2017**, *19*, 4323–4326.
- (194) Reid, W. B.; Spillane, J. J.; Krause, S. B.; Watson, D. A. *J. Am. Chem. Soc.* **2016**, *138*, 5539–5542.
- (195) Morimoto, M.; Miura, T.; Murakami, M. *Angew. Chemie Int. Ed.* **2015**, *54* (43), 12659–12663.
- (196) Brown, H. C.; Murray, K. J.; Murray, L. J.; Snover, J. A.; Zweifel, G. *J. Am. Chem. Soc.* **1960**, *82* (16), 4233–4241.
- (197) Brown, H. C.; Zweifel, G. *J. Am. Chem. Soc.* **1960**, *82* (17), 4708–4712.
- (198) Lin, Y.-C.; Hatzakis, E.; McCarthy, S. M.; Reichl, K. D.; Lai, T.-Y.; Yennawar, H. P.; Radosevich, A. T. *J. Am. Chem. Soc.* **2017**, *139* (16), 6008–6016.
- (199) Fleige, M.; Möbus, J.; vom Stein, T.; Glorius, F.; Stephan, D. W. *Chem. Commun.* **2016**, *52* (72), 10830–10833.
- (200) Yin, Q.; Kemper, S.; Klare, H. F. T.; Oestreich, M. *Chem. - A Eur. J.* **2016**, *22* (39), 13840–13844.
- (201) Yin, Q.; Soltani, Y.; Melen, R. L.; Oestreich, M. *Organometallics* **2017**, *36* (13), 2381–2384.
- (202) Zhang, Z.; Jain, P.; Antilla, J. C. *Angew. Chemie Int. Ed.* **2011**, *50* (46), 10961–10964.

- (203) Fulmer, G. R.; M Miller, A. J.; Sherden, N. H.; Gottlieb, H. E.; Nudelman, A.; Stoltz, B. M.; Bercaw, J. E.; Goldberg, K. I.; Beckman, M. *Organometallics* **2010**, *29*, 2176–2179.
- (204) Bolañ, T.; Esteruelas, M. A.; Gay, M. P.; Oñ, E.; Pastor, I. M.; Yus, M. *Organometallics* **2015**, *34*, 3902–3908.
- (205) Atkins, P.; Paula, J. de. *Physical Chemistry*, 8th ed.; W. H. Freeman and Company: New York, 2002.
- (206) Poliakoff, M.; Fitzpatrick, J. M.; Anastas, P. T. *Science (80-.)*. **2002**, *297* (5582), 807–810.
- (207) Huang, H.; Denard, C. A.; Alamillo, R.; Crisci, A. J.; Miao, Y.; Dumesic, J. A.; Scott, S. L.; Zhao, H. *ACS Catal.* **2014**, *4*, 2165–2168.
- (208) Yang, Y.; Liu, X.; Li, X.; Zhao, J.; Bai, S.; Liu, J.; Yang, Q. *Angew. Chemie Int. Ed.* **2012**, *51* (36), 9164–9168.
- (209) Shi, J.; Zhang, L.; Jiang, Z. *ACS Appl. Mater. Interfaces* **2011**, *3*, 881–889.
- (210) Runge, M. B.; Mwangi, M. T.; Miller, A. L.; Perring, M.; Bowden, N. B. *Angew. Chemie Int. Ed.* **2008**, *47* (5), 935–939.
- (211) Gelman, F.; Blum, J.; Avnir, D. *J. Am. Chem. Soc.* **2002**, *124*, 14460–14463.
- (212) Gelman, F.; Blum, J.; Avnir, D. *Angew. Chemie Int. Ed.* **2001**, *40* (19), 3647.
- (213) Chi, Y.; Scroggins, S. T.; Fré, J. M. J. *J. Am. Chem. Soc.* **2008**, *130*, 6322–6323.
- (214) Pilling, A. W.; Boehmer, J.; Dixon, D. J. *Angew. Chemie Int. Ed.* **2007**, *46* (28), 5428–5430.
- (215) Peters, R. J. R. W.; Louzao, I.; Van Hest, J. C. M. *Chem. Sci.* **2012**, *3*, 335–342.
- (216) Miller, A. L.; Bowden, N. B. *Adv. Mater.* **2008**, *20* (21), 4195–4199.
- (217) Phan, N. T. S.; Gill, C. S.; Nguyen, J. V.; Zhang, Z. J.; Jones, C. W. *Angew. Chemie Int. Ed.* **2006**, *45* (14), 2209–2212.
- (218) Huang, Y.; Trewyn, B. G.; Chen, H.-T.; Lin, V. S.-Y. *New J. Chem.* **2008**, *32*, 1311–1313.
- (219) Huang, Y.; Xu, S.; Lin, V. S. Y. *Angew. Chemie - Int. Ed.* **2011**, *50* (3), 661–664.
- (220) Li, P.; Cao, C.-Y.; Liu, H.; Yu, Y.; Song, W.-G. *J. Mater. Chem. A* **2013**, *1* (41), 12804.
- (221) Peng, Y.; Wang, J.; Long, J.; Liu, G. *Catal. Commun.* **2011**, *15* (1), 10–14.

- (222) Gao, J.; Zhang, X.; Lu, Y.; Liu, S.; Liu, J. *Chem. - A Eur. J.* **2015**, *21* (20), 7403–7407.
- (223) Advincula, R. *Polymer brushes: synthesis, characterization, applications*; WILEY-VCH Verlag: Weinheim, 2004.
- (224) Fleer, G. J. *Polymer at Interfaces*, 1st ed.; Chapman & Hall: London, 1993.
- (225) Mittal, V. *Polymer brushes substrates, technologies, and properties*; Taylor & Francis: Boca Raton, FL, 2012.
- (226) Zoppe, J. O.; Ataman, N. C.; Mocny, P.; Wang, J.; Moraes, J.; Klok, H.-A. *Chem. Rev.* **2017**, *3* (117), 1105–1318.
- (227) Choi, J.; Schattling, P.; Jochum, F. D.; Pyun, J.; Char, K.; Theato, P. *J. Polym. Sci. Part A Polym. Chem.* **2012**, *50* (19), 4010–4018.
- (228) Di Carlo, G.; Damin, F.; Armelao, L.; Maccato, C.; Unlu, S.; Spuhler, P. S.; Chiari, M. *Appl. Surf. Sci.* **2011**, *258*, 3750–3756.
- (229) Duan, Z.; Qu, Z.; Hu, F.; Yang, Y.; Chen, G.; Xu, H. *Appl. Surf. Sci.* **2014**, *300*, 104–110.
- (230) Gunay, K. A.; Unay, G.; Schüwer, N.; Klok, H.-A. *Polym. Chem.* **2012**, *3*, 2186–2192.
- (231) Ohno, K.; Ma, Y.; Huang, Y.; Mori, C.; Yahata, Y.; Tsujii, Y.; Maschmeyer, T.; Moraes, J.; Perrier, S. *Macromolecules* **2011**, *44* (22), 8944–8953.
- (232) Rotzoll, R.; Nguyen, D. H.; Vana, P. *Macromol. Symp.* **2009**, *275–276* (1), 1–12.
- (233) Rotzoll, R.; Vana, P. *J. Polym. Sci. Part A Polym. Chem.* **2008**, *46* (23), 7656–7666.
- (234) Wang, L.; Benicewicz, B. C. *ACS Macro Lett.* **2013**, *2* (2), 173–176.
- (235) Cano-Serrano, E.; Campos-Martin, J. M.; Fierro, J. L. G.; Castner, D. G.; Sastre, E.; Kemner, K. M. *Chem. Commun.* **2003**, *228* (2), 246–247.
- (236) Uemukai, T.; Ishifune, M. *J. Appl. Polym. Sci.* **2013**, *129* (5), 2554–2560.
- (237) Moad, G.; Rizzardo, A. E.; Thang, S. H. *Aust. J. Chem* **2005**, *58*, 379–410.
- (238) Stenzel, M. H.; Zhang, L.; Huck, W. T. S. *Macromol. Rapid Commun.* **2006**, *27* (14), 1121–1126.
- (239) Azizi, K.; Heydari, A.; Burange, A. S.; Gawande, M. B.; Jayaram, R. V.; Sarvary, A.; Ng, S. W. *RSC Adv.* **2014**, *4* (13), 6508.

- (240) Li, C.; Benicewicz, B. C. *Macromolecules* **2005**, *38*, 5929–5936.
- (241) Noisier, A. F. M.; Brimble, M. A. *Chem. Rev.* **2014**, *114* (18), 8775–8806.
- (242) Jazzar, R.; Hitce, J.; Renaudat, A.; Sofack-Kreutzer, J.; Baudoin, O. *Chem. - A Eur. J.* **2010**, *16* (9), 2654–2672.
- (243) Reddy, C.; Bisht, N.; Parella, R.; Babu, S. A. *J. Org. Chem.* **2016**, *81* (24), 12143–12168.
- (244) Gu, Z.-Y.; Liu, C.-G.; Wang, S.-Y.; Ji, S.-J. *J. Org. Chem.* **2017**.
- (245) Jaiswal, Y.; Kumar, Y.; Thakur, R.; Pal, J.; Subramanian, R.; Kumar, A. *J. Org. Chem.* **2016**, *81* (24), 12499–12505.
- (246) Giri, R.; Maugel, N.; Li, J.; Wang, D.; Breazzano, S. P.; Saunders, L. B.; Yu, J. *J. Am. Chem. Soc.* **2007**, *129* (12), 3510–3511.
- (247) Wang, H.-L.; Shang, M.; Sun, S.-Z.; Zhou, Z.-L.; Laforteza, B. N.; Dai, H.-X.; Yu, J.-Q. *Org. Lett.* **2015**, *17* (5), 1228–1231.
- (248) Nishikata, T.; Abela, A. R.; Huang, S.; Lipshutz, B. H. *J. Am. Chem. Soc.* **2010**, *132* (14), 4978–4979.
- (249) Rouquet, G.; Chatani, N. *Angew. Chemie Int. Ed.* **2013**, *52* (45), 11726–11743.
- (250) Lyons, T. W.; Sanford, M. S. *Chem. Rev.* **2010**, *110* (2), 1147–1169.
- (251) Chen, X.; Engle, K. M.; Wang, D. H.; Jin-Quan, Y. *Angew. Chemie - Int. Ed.* **2009**, *48* (28), 5094–5115.
- (252) Wei, Y.; Tang, H.; Cong, X.; Rao, B.; Wu, C.; Zeng, X. *Org. Lett.* **2014**, *16* (8), 2248–2251.
- (253) Saikia, K.; Dutta, D. K. *J. Mol. Catal. A Chem.* **2015**, *408*, 20–25.
- (254) He, J.; Takise, R.; Fu, H.; Yu, J. Q. *J. Am. Chem. Soc.* **2015**, *137* (14), 4618–4621.
- (255) He, J.; Jiang, H.; Takise, R.; Zhu, R. Y.; Chen, G.; Dai, H. X.; Dhar, T. G. M.; Shi, J.; Zhang, H.; Cheng, P. T. W.; Yu, J. Q. *Angew. Chemie - Int. Ed.* **2016**, *55* (2), 785–789.
- (256) Bisht, R.; Chattopadhyay, B. *J. Am. Chem. Soc.* **2016**, *138* (1), 84–87.
- (257) Colby, D. A.; Bergman, R. G.; Ellman, J. A. *Chem. Rev.* **2010**, *110* (2), 624–655.
- (258) Simonetti, M.; Larrosa, I. *Nat. Chem.* **2016**, *8* (12), 1086–1088.
- (259) Daugulis, O.; Do, H.-Q.; Shabashov, D. *Acc. Chem. Res.* **2009**, *42* (8), 1074–1086.

- (260) Mkhaliid, I. A. I.; Barnard, J. H.; Marder, T. B.; Murphy, J. M.; Hartwig, J. F. *Chem. Rev.* **2010**, *110* (2), 890–931.
- (261) Sun, C.-L.; Li, B.-J.; Shi, Z.-J. et al. *Chem. Commun.* **2010**, *46* (5), 677–685.
- (262) Shabashov, D.; Daugulis, O. *Org. Lett.* **2005**, *7* (17), 3657–3659.
- (263) Lee, L. C.; He, J.; Yu, J. Q.; Jones, C. W. *ACS Catal.* **2016**, *6* (8), 5245–5250.
- (264) Pascanu, V.; Carson, F.; Solano, M. V.; Su, J.; Zou, X.; Johansson, M. J.; Martín-Matute, B. *Chem. - A Eur. J.* **2016**, *22* (11), 3729–3737.
- (265) Fei, H.; Cohen, S. M. *J. Am. Chem. Soc.* **2015**, *137* (6), 2191–2194.
- (266) Pla, D.; Gómez, M. *ACS Catal.* **2016**, *6* (6), 3537–3552.
- (267) Park, G.; Lee, S.; Son, S. J.; Shin, S. *Green Chem.* **2013**, *15* (12), 3468–3473.
- (268) Liu, J.; Xie, Y.; Zeng, W.; Lin, D.; Deng, Y.; Lu, X. *J. Org. Chem.* **2015**, No. li, 150417074907009.
- (269) Lee, L.; Zhao, Y. *Helv. Chim. Acta* **2012**, *95*, 863–871.
- (270) Liu, Y.; Yang, K.; Ge, H.; Wang, C.; Liebeskind, L. S.; He, G.; Chen, G.; Liu, C.; Zhao, X.; Chu, C.; Liu, R. *Chem. Sci.* **2016**, *7* (4), 2804–2808.
- (271) Isley, N. A.; Dobarco, S.; Lipshutz, B. H.; Slack, E. D.; Mo, S.; Orjala, J.; Mesecar, A. D.; Franzblau, S. G.; Kozikowski, A. P. *Green Chem.* **2014**, *16* (3), 1480–1488.
- (272) Duplais, C.; Krasovskiy, A.; Lipshutz, B. H. *Organometallics* **2011**, *30* (22), 6090–6097.
- (273) Lee, L.-C.; Zhao, Y. *Org. Lett.* **2012**, *14* (3), 784–787.
- (274) Guo, P.; Joo, J. M.; Rakshit, S.; Sames, D. *J. Am. Chem. Soc.* **2011**, *133* (41), 16338–16341.
- (275) Yang, K.; Li, Q.; Liu, Y.; Li, G.; Ge, H. *J. Am. Chem. Soc.* **2016**, *138* (39), 12775–12778.
- (276) Zhang, F.-L.; Hong, K.; Li, T.-J.; Park, H.; Yu, J.-Q. *Science (80-.)*. **2016**, *351* (6270), 252–256.
- (277) Xue, M.; Lü, Y.; Sun, Q.; Liu, K.; Liu, Z.; Sun, P. *Cryst. Growth Des.* **2015**, *15* (11), 5360–5367.
- (278) Wang, Y.; Lu, H.; Xu, P.-F. *Acc. Chem. Res.* **2015**, *48* (7), 1832–1844.